Universitätsklinikum Tübingen

Innere Medizin VIII

(Medizinische Onkologie und Pneumologie)

Personalized Immuno-/Virotherapy of Colorectal Carcinoma (CRC) using CRC organoids as a model

Personalisierte Immuno-/Virotherapie des Kolorektalen Karzinoms (CRC) am CRC Organoid-Modell

Inaugural-Dissertation
zur Erlangung des Doktorgrades
der Medizin

vorgelegt von

von Schimonsky, Franziska

2025

Dekan:	Professor Dr. B. Pichler
1. Berichterstatter:	Professor Dr. U. Lauer
2. Berichterstatter:	Privatdozent Dr. J. Heitmann
Tag der Disputation:	14.04.2025

Für Mamuschka und Papa

Table of Contents

1 Introduction

1.1 Colorectal Carcinoma (CRC): a major tumor burden worldwide

Medical care has improved dramatically in recent decades. Diseases that would have meant a death sentence in the past can now be treated sufficiently. This is explicitly the case for cancer research, which has seen major breakthroughs in the last years and thus contributed to a significant increase in average life expectancy, most drastically in the western world.[1] But despite the success of modern therapy strategies, cancer is still a leading cause of death worldwide,[2] with colorectal carcinoma (CRC) being one of the most common cancer types.[3] In most cases, CRC is diagnosed very late, limiting therapy to a palliative approach. From this it becomes evident that an efficient therapy, especially in advanced stages, is desperately needed and although cancer research has come very far, there is still a very long way to go.

1.1.1 Definition of CRC

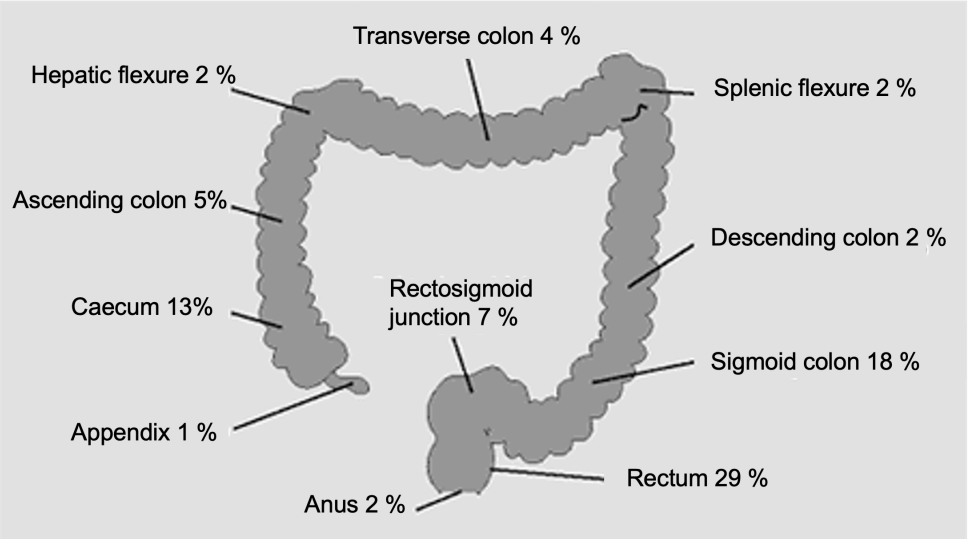

Figure 1: Graphic of the distribution of the localization of colorectal carcinomas, data is shown in percentage. Picture was created based on a graphic from ONKODIN.

Colorectal Carcinoma (CRC) is a malignant tumor of the epithelium from the large intestine which infiltrates locally and can potentially metastasize. It includes tumors of the colon (part of the intestine aboral of the ileocolic valve) and the rectum. The line between colon and rectum is defined differently and is measured by a rigid rectoscope to reliably determine the distance from the anocutaneous line (ACL)[4]: according to the International Documentation System (IDS), a rectum carcinoma is a tumor which is located less than 16 cm (< 16 cm) from the ACL.[4,5] Union international contre le cancer (UICC) further divides rectum carcinomas in tumors of the upper third (12-16 cm from the Linea anocutanea), the middle third (6-12 cm) and the lower third of the rectum (< 6 cm).[4,6]

In contrast to that, in the USA the differentiation between colon and rectal carcinomas is at 12 cm above the ACL, as recurrences tend to occur more often in tumors located under 12 cm from the Linea anocutanea, which has consequences for therapy planning.[4,7] Furthermore, colon carcinomas also show different locations within the colon: caecum, ascending colon, hepatic flexure, transverse colon, splenic flexure, descending colon and sigmoid colon (see Figure 1).[6] This has not only implications for surgical intervention but also pharmaceutical therapy approaches including therapy responses.

1.1.2 Epidemiology

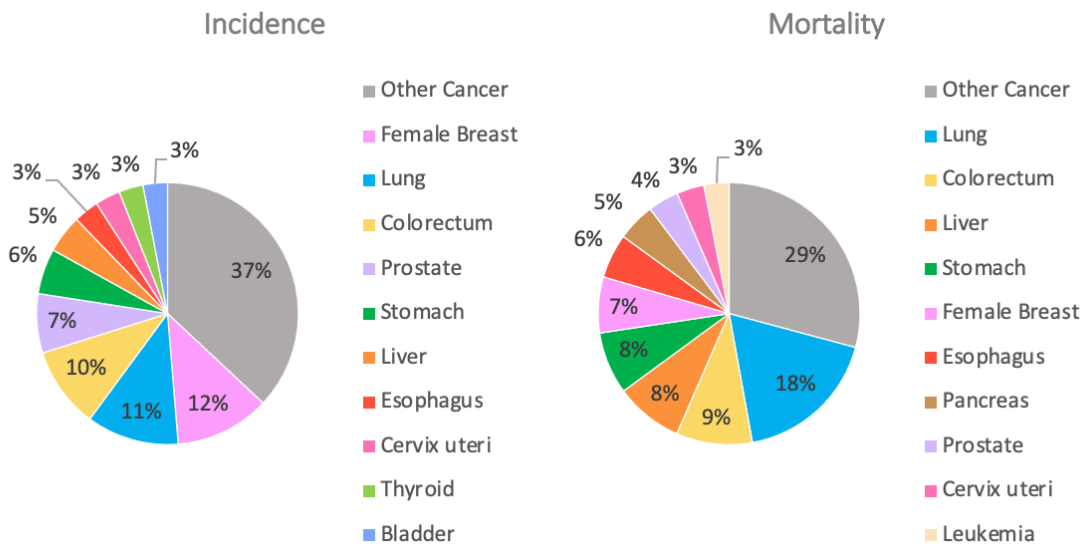

Figure 2: Incidence and mortality rates of different cancer entities of both sexes worldwide. Incidence rates are based on 19.3 million new cases per year worldwide. Mortality rates are based on 9.9 million deaths per year worldwide. Other cancers include nonmelanoma skin cancer. Source: Globocan 2020

CRCs represent one of the most frequent tumor entities worldwide. It is the third most common tumor in men and the second most common tumor in women.[8] With 1.9 million new cases and over 900.000 deaths worldwide in 2020, CRC ranks third in terms of incidence and second in terms of mortality.[8] In Germany, CRC even represents one in eight cancer cases, with over 60.000 new cases and over 24.000 deaths in 2018.[9] This higher incidence in Germany is in line with the higher occurrence of CRC in countries with a high development index (HDI).[10,11] CRC is a tumor entity which mostly appears in older patients: average age of onset is 75 in women and 72 in men, with only 10% of CRC cases appearing before the age of 55.[9] In Germany, incidence rates have been decreasing over the last twenty years: age-standardized incidence rate in men by 2 %, in women by 2.2 %.[12] Nonetheless, the number of new cases stays relatively constant, as the population grows older and CRC occurs more often in older patients. 5-year survival rates are in the middle range of tumor diseases with 54% of men and 59% of women living after five years.[12] This data shows, that CRC represents a major tumor burden, not only worldwide but especially in developed countries with ever growing older population structures and thus even higher numbers of new cases in the future.[13]

1.1.3 Pathogenesis and risk factors of CRC

The pathogenesis of CRC encompasses very heterogenous pathways and complex interactions. It is mainly driven by a progressive accumulation of genetic and epigenetic alterations, which was firstly described as the adenoma-carcinoma sequence by Fearon and Vogelstein in 1990. The so called “Vogelgram” is still a widely used model to describe the transformation of normal colon epithelium to adenomatous polyps and finally carcinomas in sporadic CRCs.[14] This sequence is defined by multiple steps, in which every histological alteration is caused by some kind of molecular dysregulation that subsequently leads to an accumulation of mutations in tumor suppressor and oncogenes.[14,15] Since then, this model was superseded by pathway models, that are characterized by specific precursor lesions and distinct molecular dysregulations, namely the conventional/ traditional (which derived from the “Vogelgram”) and the serrated pathway.[16] Pancione et al. also describe a third, the alternative pathway, which is yet to be further characterized and much more heterogenous than the other ones.[16] These developmental pathways have different molecular features characterized by three major groups of alterations: chromosomal instability (CIN), microsatellite instability (MSI) and the CpG-island methylation phenotype (CIMP). Different multistep associations of these alterations lead to the above mentioned three distinct developmental pathways.[17] With the exception of the alternative pathway, both the conventional and the serrated pathway have relatively distinct molecular characteristics which rarely overlap.[18] In most cases (70-80%) CRCs occur sporadically, emerging from somatic mutations in specific genes. In 5 % of the cases, CRC can occur in patients with highly penetrant germ-line mutations that cause well-defined hereditary diseases such as Hereditary Non-Polyposis Colorectal Carcinoma (HNPCC) or Familial Adenomatous Polyposis (FAP). The rest of CRC cases (20%) have a family history of CRC but without any obvious cancer syndromes attributed to. Additionally, environmental factors, gut microbiome, chronic inflammatory bowel diseases and lifestyle factors have an impact on CRC pathogenesis as well.[19]

1.1.3.1 Molecular alterations and tumor progression

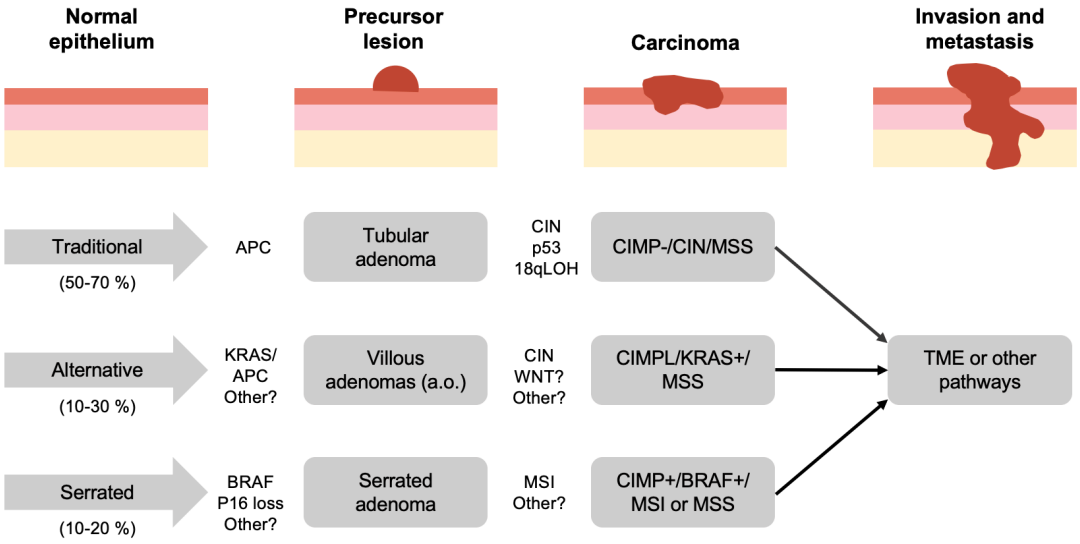

Figure 3: Molecular alterations and genetic mutations occurring during tumorigenesis in CRC. Illustration of traditional, alternative, and serrated pathway. APC = Adenomatous polyposis coli, BRAF = proto-oncogene B-Raf, CIMP = CpG-island methylator phenotype, CIN = Chromosomal instability, KRAS = Kirsten rat sarcoma virus, LOH = Loss of heterozygosity, MSI = Microsatellite instability, MSS = Microsatellite stable, TME = tumor microenvironment, WNT = Wnt signaling pathway. Graphic was created using a graphic from Pancione et al[16].

As mentioned before, there are three developmental pathways which are associated with at least three major groups of molecular alterations. These alterations can cause normal colon or rectal epithelium to progress to adenomatous polyps and finally carcinoma.[19] CRCs can present one particular kind of molecular alteration but can also have features from several different ones. These alterations can both occur in CRCs with a sporadic or hereditary background.[20–23]

The most frequent molecular alteration is chromosomal instability (CIN): 70-80% of CRC cases arise from this transmutation.[19] It is characterized by chromosomal aberrations such as aneuploidy, chromosomal rearrangements and a loss of heterozygosity (LOH) at gene loci for tumor suppressor genes.[21] CIN is typically present in CRCs deriving from the conventional pathway but can also be found in the alternative pathway. Frequently, mutation of the Adenomatous polyposis coli (APC) gene represents the initiating event: normal colon epithelium transforms to an early adenoma by inactivation of APC. This mutation occurs in 80% of sporadic CRC cases and is also responsible for Familial Adenomatous Polyposis (FAP) when mutated in germ line.[24]

Important for immunogenicity and thus therapy approaches is microsatellite-instability (MSI): MSI is associated with genetic hypermutability and represents another molecular alteration through which tumorigenesis in colon epithelium occurs. Microsatellites, also called short tandem repeats or simple sequence repeats, are short, non-coding DNA-sequences which are spread throughout the human genome. They are highly repetitive and subsequently very prone to transcription errors. In this case, a mismatch repair system (MMR) ensures that these errors are detected and repaired. MMR is composed of different proteins, which act as heterodimers (namely MSH2, MSH3, MSH6, MLH1 and PMS2).[25] If this MMR-system is deficient (dMMR) due to mutations in genes that code for these proteins, MSI occurs.[26] This faulty MMR system can either cause point or even frame-shift mutations causing a downstream nonsense mutation, which leads to the production of a non-functional protein, usually a tumor suppressor protein.[27] Tumors are further subclassified into high (MSI-H), low (MSI-L) and stable (MSS), depending on the number of mutated microsatellites.[28] MSI occurs in 15% of all CRCs, 12% of these are sporadic and are caused by hypermethylation of the promoter of the MLH1 gene. The other 3% are associated with Lynch syndrome, which is caused by a germline mutation in one of the four key MMR genes: MLH1, MSH2, MSH6 or PMS2.[29]

1.1.3.2 The tumor microenvironment as an important factor for prognosis

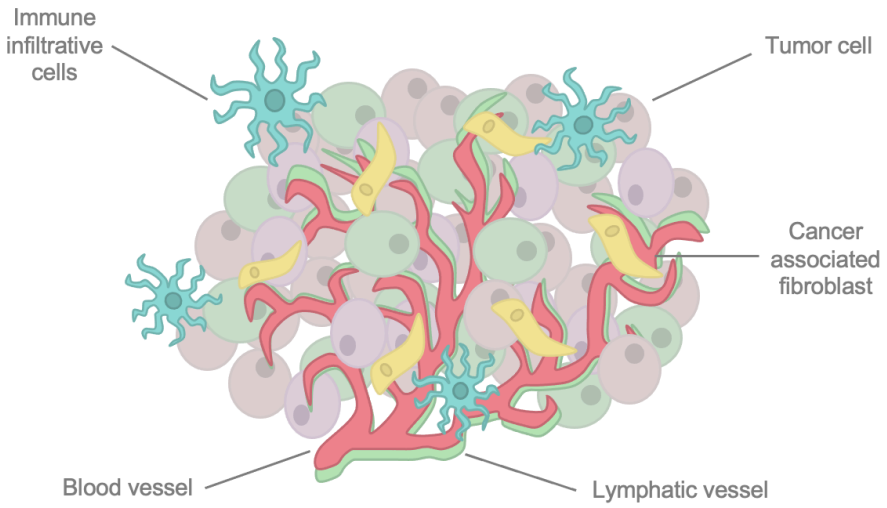

Figure 4: Depiction of the tumor microenvironment (TME) consisting of tumor cells surrounded by immune infiltrative cells and cancer associated fibroblasts (CAFs), nourished by a vascular network consisting of blood vessels and lymphatic vessels. The graphic was created using a graphic from Schmitt, M. & Greten, F. R.[19].

A crucial component of TME are immune cells: as cancer cells express neoantigens on their surface membrane as a consequence of their mutational load, they can be recognized by T-lymphocytes.[30] This makes clear, why especially tumor infiltrating immune cells have a major impact on prognosis: presence of T_{H1}-cells, cytotoxic T-cells and memory T-cells correlate with a positive prognosis compared to immunologically "cold" tumors, which merely show an infiltration of these cells. This goes as far as immunogenic features of the tumor, defined by an "Immunoscore" is more important for the evaluation of prognosis than the AJCC/UICC TNM classification.[19,31]

Another cell type which contributes significantly to TME composition and thus tumor prognosis are CAFs.[32] In contrast to normal fibroblasts, which help to produce components of the ECM, CAFs secrete growth factors (e.g. Vascular Endothelial Growth Factor, VEGF),[33] hence supporting vascularization and thus tumor growth.[34,35] Additionally, CAFs also contribute to drug resistance in cancer cells.[34]

The third major cell type encompassing the TME are endothelial cells, which branch out from pre-existing vessels or derive from endothelial progenitor cells.[36] They support tumor growth and development through nutrition provision.[37]

Furthermore, some studies implicate, that nerve cells also have an impact on the development of neoplasia[38–40], e.g. via mechanical aspects (nerve fibers as a guidance for tumor growth) or excretion of neurotransmitters influencing local vascularization and cell migration.[38,41,42] In the case of intestinal cells, there are numerous studies which suggest participation of nerve cells in the regulation of the stem cell niche.[39,42–44]

All these aspects of the TME composition and its implications on tumorigenesis highlight the importance of a more integrated approach in cancer treatment development.

1.1.4 Current therapy standards

The therapy of CRCs is highly dependent on the localization and the stadium of the tumor. Precursor lesions and localized tumors which haven't crossed the border of the mucosa yet can be removed by endoscopic resection.[45] This is often the case during a screening checkup, which is recommended (in Germany) every nine years for men starting at the age of 50 and for women at the age of 55.[4]

Unfortunately, in most cases CRCs are more advanced and surgery is first in line regarding therapy options. Especially differentiation of colon and rectum tumors is essential for determination of the resection line and selection of the surgical method.[4] After surgery, adjuvant chemotherapy is recommended for patients with advanced colon tumors which have a microsatellite stable (MSS) genetic profile (as adjuvant chemotherapy in MSI-H CRCs seems to present a disadvantage in overall survival).[46] This therapy approach is also performed in rectum carcinomas of the upper third. In contrast to that, CRCs of the middle and lower third of the rectum receive neoadjuvant radiochemotherapy.[47]

5-Fluorouracil (5-FU), a fluoropyrimidine, presents the basis of adjuvant chemotherapy in CRCs. 5-FU can be given as monotherapy in patients with UICC stadium II and which have certain risk factors, but is not a general recommendation.

In UICC stadium III, patients receive combination regimens including 5-FU, Oxaliplatin (platin derivate), Leucovorin (folinic acid), Capecitabine (prodrug which is metabolized to 5-FU) and/or the topoisomerase I inhibitor Irinotecan.[4] Patients with a metastatic disease also receive monoclonal antibodies, either epidermal growth factor receptor (EGFR) or vascular endothelial growth factor (VEGF) antibodies, dependent on their mutational status.[4]

1.1.4.1 Molecular diagnostics are essential for first-line therapy

Molecular features of CRCs play an important role in deciding which treatment modality is appropriate for each individual patient, especially in patients with metastatic disease. For this purpose, all patients which are planned to receive a systemic therapy receive molecular testing for mutations in ras genes (e.g., KRAS and NRAS), BRAF-gene and status of microsatellite stability.[4]

First, KRAS is tested: patients with a mutation in this gene do not profit from a combination of chemotherapy with anti-EGFR-inhibitors (e.g. Cetuximab) compared to patients with wildtype KRAS tumors which showed a significant improvement in progression-free and overall survival.[48]

Interestingly, a KRAS and BRAF mutation almost never occur simultaneously, so a BRAF mutation is only tested if a KRAS wildtype has been found.[49] Mutation of the BRAF V600 gene comes with a bad prognosis.[50] Hence, if this mutation is detected, an earlier and more aggressive systemic therapy approach is chosen.

1.1.4.2 Immunotherapy as a new therapeutic approach in patients with CRC

Especially in patients with a metastatic disease, new therapy approaches are in dire need. Immunotherapy, which has become one of the major pillars in cancer therapy in recent years, could present a promising approach. Over the past decades, the importance of immunological factors for tumorigenesis, tumor progression and consequently prognosis have finally found acknowledgement.

Scientists have discovered cancer cells which have acquired different modalities to evade immune recognition and hence eradication, such as upregulation of immunosuppressive pathways, faulty antigen presentation and recruitment of immunosuppressive cells.

To overcome these evasion mechanisms different therapy approaches have been developed: cytokine therapies, adoptive cell transfer, cancer vaccination, immune checkpoint inhibition and oncolytic virotherapy as well.

Immunotherapy is not yet part of guideline therapy in Germany, but two immune checkpoint inhibitors, namely programmed cell death 1 (PD-1) blocking antibodies nivolumab and pembrolizumab have been granted accelerated FDA approval for metastatic MSI-H CRCs in 2017.[51]

1.2 Oncolytic virotherapy as a novel approach to treat immunological "cold" tumors

Oncolytic virotherapy utilizes both naturally occurring and genetically altered viruses, which selectively replicate in and lyse cancer cells without destroying normal cells in the process.[52] As a part of immunotherapy, this principle of action is also used to activate the host immune system and consequently lead to an immune response which further destroys cancer cells. To this date, only one oncolytic viral agent has been approved both by FDA and EMA for clinical use: T-VEC (Talimogene laherparepvec, Imlygic©) is a recombinant herpes simplex virus and is currently used for the therapy of high-grade non-operable melanoma[53]. There is a Phase-II study which suggests that T-VEC also represents a promising approach in neoadjuvant therapy of melanomas, with a significant increase of two year relapse-free survival.[54] Another oncolytic virus, which was approved by FDA for the treatment of BCG-refractory non-muscular invasive bladder cancer in situ is Nadofaragene Firadenovec (Adstiladrin®), a non replicable Adeonvirus.[55]
As there is still a lack of effective therapies, especially for advanced cancers, virotherapy represents a promising approach.

1.2.1 History of virotherapy

Viral agents were used as cancer therapy even before scientific research has grasped a representative concept of their viral nature.[56] The first treatment trials with viruses as a therapy option for cancer were conducted as early as the end of the 19th century.[57]

Using this biological treatment method can be ascribed to the observation that cancer patients who contracted viral infections occasionally went into clinical remission. These case reports could predominantly be led back to patients with hematological malignancies, which showed a significant immunosuppression in the first place. One of the earliest case reports was described by Dock in 1896: after a presumed influenza infection (influenza was not even determined as a viral infection yet), a 42-year-old woman with “myelogenous leukemia” went into remission. She showed a significant reduction in leukocyte platelet count and diminution of liver and spleen size to a nearly normal extent.[57]

At the beginning of the 20th century, trials with viruses as cancer treatment only occurred sporadically.[58–60]

This changed half a century later in the 1950s and 1960s with the first clinical trials to thoroughly investigate oncolytic viruses. These experiments were conducted under questionable ethical circumstances as infectious bodily fluids or tissues from infected patients were administered to cancer patients.[61,62]

The first viruses which were used in these early significant trials included Hepatitis B virus[61], Egypt 101 virus[63], adenoidal-pharyngeal-conjunctival virus[64] and Mumps virus[65]. After the initial euphoria concerning virotherapy, disillusionment followed, probably also because of the regulatory barriers which scientists have faced by using non-attenuated viral agents for anti-cancer therapy. However, researchers held on to the prospect of virotherapy as a promising treatment option and consequently focused on reducing the pathogenic potential of oncolytic viruses.[56]

In a first attempt to circumvent pathogenicity in humans, animal viruses were used, hoping to retain oncolytic potential by avoiding rapid elimination of the virus

and simultaneously control virulence. Although some animal viruses showed significant regressions and increased survival in rodent models (e.g. the “M-P” virus, a strain of lymphocytic choriomeningitis virus), these virotherapeutics failed to present the same effects in humans.[56]

Consequently, the era of manipulating oncolytic viruses by adaptation, and ultimately genetic engineering, began. Before viruses could be genetically altered, scientists used other methods to change their properties: to enhance oncolytic potency of viruses, Moore utilized successive passaging. This led to a “natural selection” of properties which were useful for infection of respective tumor.[66]

However, genetic engineering in oncolytic viruses (as we know it today) only began approximately 30 years ago. In 1991, Martuza et al. employed a thymidine-kinase deficient herpes simplex virus in glioma cells. He hypothesized that these mutant viruses, which selectively replicate in dividing cells, would only lyse glioma cells.[67] This was the start of engineering tumor-specific viral agents for oncolytic virotherapy as we know it today.

1.2.2 Principles of oncolytic virotherapy

As mentioned before, an oncolytic virus selectively infects, replicates in and kills cancer cells.[68] This is achieved by characteristics of the virus itself, both naturally given and genetically manufactured, as well as immune responses triggered by consequent lysis of cancer cells. These mechanisms as well as genetic alterations, specifically the introduction of suicide gene therapy enhancing lysis in the first place, are further explained below.

1.2.2.1 Mechanisms of oncolytic virus mediated tumor cell death

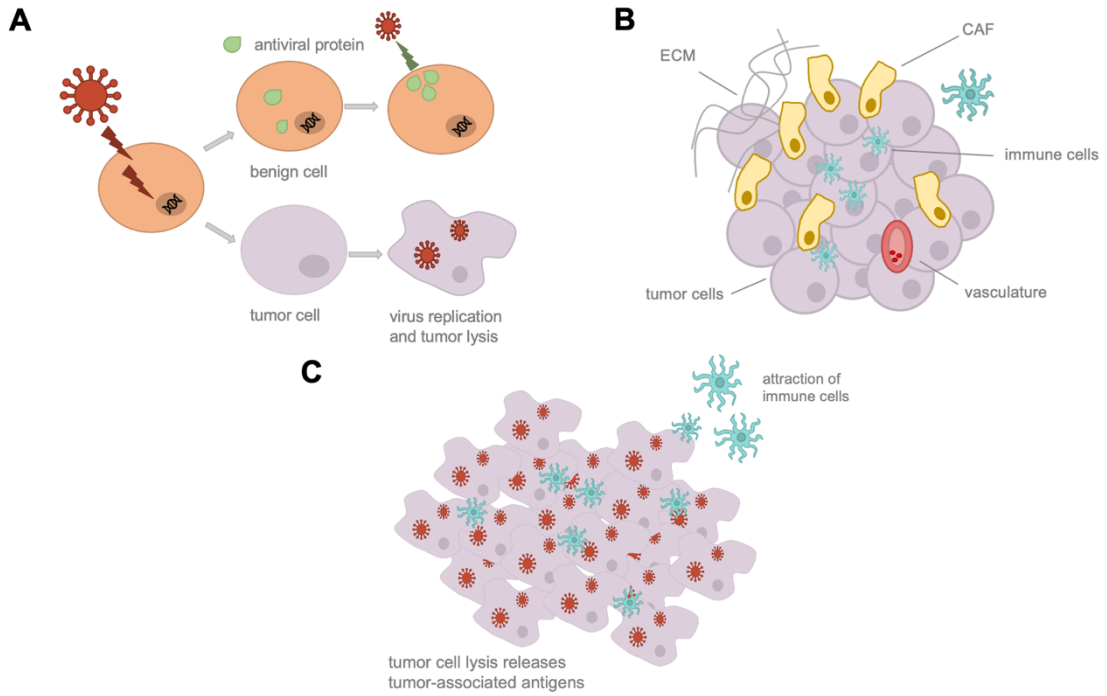

Figure 5: Main principles of oncolytic viruses. (A) Selectivity of oncolytic viruses for malignant cells, (B) manipulation of tumor microenvironment by oncolytic viruses, (C) attraction of immune cells through release of tumor-associated antigens. Graphic was created by using [69].

The main principles of oncolytic virotherapy are shown above: oncolytic viruses (OVs) selectively infect and replicate in tumor cells (A), OVs influence the tumor microenvironment, including vasculature, CAFs and immune cells (B) and the following tumor lysis leads to release of tumor-associated antigens which attract immune cells (C).[69]

Tumor cells harbor many genetic and epigenetic mutations that help them to evade the immune system, circumvent apoptosis and lead to uncontrolled cell proliferation. As helpful these characteristics may be for exponential cell growth, they are dramatically inconvenient in the face of a viral infection.[70] On the one hand, mutations in tumor cells lead to the expression of features which enhance tumor tropism in oncolytic viruses: overexpression of entry receptors, abnormal antiviral mechanisms such as downregulation of antiviral signaling as well as downregulation of antiproliferative signaling.[69,71] On the other hand, mechanisms which lead to apoptosis and hence limitation of viral spreading in normal cells are faulty in tumor cells and consequently present an advantage in replication for oncolytic viruses. In contrast to normal tissue, tumor cells represent an ideal host

cell for viruses to maximally exploit cellular resources for the synthesis and assembly of new viral particles.[72]

Next to the direct lysis of tumor cells, OVs also influence the TME, which is crucial in the genesis, maintenance and therapy response of tumors, as explained above.[73] Based on immune phenotypes, in other words presence of distinct immune cells, TMEs can be roughly categorized into two groups: immune-inflamed and non-inflamed tumors.[74] Inflamed tumors present a variety of immune cells in proximity to the tumor, including CD_4- and CD_8-expressing T-cells, myeloid cells and monocytic cells.[74–76] Additionally, proinflammatory cytokines such as IFN-γ as well as genomic instability can be found in these tumors as well.[74,77] Non-inflamed tumors on the other hand express immunosuppressive cytokines and exhibit cell types associated with immunosuppression and a low mutational burden.[74] These tumors either present inflammation associated cells located in the tumoral stroma but not the tumor itself,[74,78,79] or a very low number or rather no immune cells at all, neither in the tumor itself nor the surrounding stroma.[74] This lack of immune response which is vital not only for the control of the tumor by the host himself but also for immunotherapy presents a big hurdle to overcome for an efficient immunotherapy. Here, OVs come into play: by lysing cancer cells and consequently releasing tumor antigens as well as danger signals to the TME, they could activate local immunogenic cells and create an inflammatory environment, thus turning an immunological “cold” tumor “hot”.

Finally, OVs have a systemic effect on tumor immunity as well and can function as an “in situ vaccine” specifically targeted at the tumor.[69,80] Cancer cell oncolysis induced by OVs leads to a release of tumor-specific antigens and allows dendritic cells (DCs) to cross-prime a CD_8-response which is tumor specific. This mechanism can also further enhance a possible immune checkpoint-inhibition and may play a vital role in complementing immunotherapy for cancer in the future.[81]

1.2.2.2 Enhancing oncolytic efficacy by genetically introducing a suicide gene

As mentioned above, to enhance selectivity and boost virulence in malignant cells, scientists began to genetically modify OVs. One way of doing so was the introduction of suicide gene therapy (SGT), which was firstly discovered in 1986 by Moolten: he exposed neoplastic BALB/c-murine cells bearing the herpes simplex thymidine kinase gene to the thymidine kinase specific substrate 9-([2-hydroxy-1-(hydroxymethyl)-ethoxy]methyl)guanine, which led to the ablation of clonogenic potential and consequently regression of tumors in BALB/c bearing mice.[82,83] This finding demonstrates the concept of SGT: a malignant cell is infected with a (genetically modified) OV which bears the gene for an enzyme. This enzyme is expressed by the infected cell and can now convert an administered, harmless pro-drug into the effective chemotherapeutic. Ideally, thanks to the selectivity of OVs to cancer cells, this only happens in malignant cells and normal cells are spared of the toxic metabolite.

In this thesis we used measles virus (MeV-SCD) as well as vaccinia virus (GLV-1h94) equipped with a suicide gene. In GLV-1h94 and MeV-SCD, the suicide gene FCU-1 was used, which is a fusion gene derived from the phosphoribosyltransferase gene FUR1 and the Saccharomyces cerevisiae cytosine deaminase gene FCY1.[84,85] It encodes for the enzyme super cytosine deaminase (SCD), which can deaminate the non-toxic pro-drug 5-fluorocytosine (5-FC) to the toxic antimetabolite 5-fluorouracil (5-FU) and facilitate further conversion into 5-fluorouridine monophosphate (5-FUMP).[82,86] Cellular enzymes further phosphorylate the metabolite to an active triphosphate compound, which interferes with DNA repair and inhibits RNA and DNA-synthesis, consequently leading to cell death.[82,84]

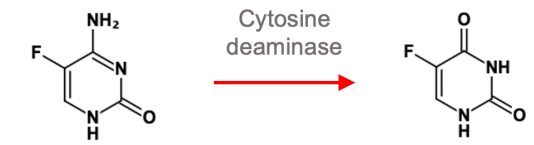

5-Fluorocytosine 5-Fluorouracil

Figure 6: Conversion of 5-fluorocytosine to the toxic metabolite 5-fluorouracil by cytosine deaminase cloned from E. coli. The chemical structures were adapted from PubChem.

1.2.3 Characteristics of viral agents used in this thesis

1.2.3.1 Measles Virus

1.2.3.1.1 Properties of wild type Measles virus

Measles virus (MeV) belongs to the family of Paramyxoviridae, genus Morbillivirus and is a negative-sensed, non-segmented RNA virus. Its genome encodes for six structural and two non-structural proteins and is approximately 16kb long.[87] There are two transmembrane glycoproteins on the surface of the virus: hemagglutinin (H) and the fusion protein (F), which are both responsible for fusion with a host cell. Other structural proteins include the nucleocapsid (N) which encapsulates the genome and forms the ribonucleotide protein (RNP) complex together with the viral polymerase, also known as the large protein (L) and its cofactor phospho protein (P). They are connected to the viral envelope via the matrix protein (M).[88]

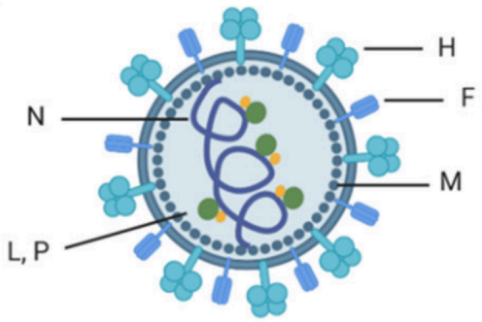

Figure 7: Schematic structure of a measles virus. Transmembrane glycoproteins include haemagglutinin (H) and fusion protein (F). The nucleocapsid protein (N) encapsulated the genome. The phospho protein (P) is a cofactor of the large protein (L). Together with (N) they are connected to the matrix protein (M). Picture is taken with permission from Engeland, C. E. & Ungerechts, G.[87].

1.2.3.1.2 Construction of recombinant MeV-GFP and MeV-SCD

Recombinant MeV was constructed by inserting respective gene into the empty additional transcription unit (ATU) in genome position one in a commercially available monovalent vaccine batch of measles virus strain Mérieux (Sanofi-Pasteur, Leimen, Germany) (Figure 8).

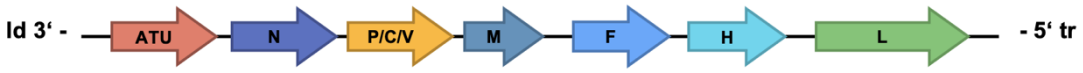

Figure 8: Schematic representation of measles virus genome and the localization of the genes encoding for their respective protein. The second gene encodes for three proteins: one structural (phospho protein) and two non-structural (C and V) protein. The additional transcription unit is in position one and can be utilized to insert recombinant genes. Graphic was created using [89].

By inserting a gene encoding green fluorescent protein (GFP) into the ATU, MeV-GFP was created. Similarly, MeV-SCD was created by inserting a gene encoding for Supercytosine deaminase (SCD) as described above.

1.2.3.2 Vaccinia Virus

Vaccinia virus (VACV) is an enveloped, double stranded (ds) DNA virus with a 190 kb long genome which encodes for ap. 250 genes translating to 223 proteins. As a part of the Poxvirus family, genus Orthopoxviridae (which also includes cowpox, variola and monkeypox virus) it represents one of the largest DNA viruses and forms the basis for the smallpox vaccine. Interestingly, Vaccinia viruses do not replicate in the nucleus but only in the cytosol of the host cell, which is a unique characteristic regarding DNA viruses.[90]

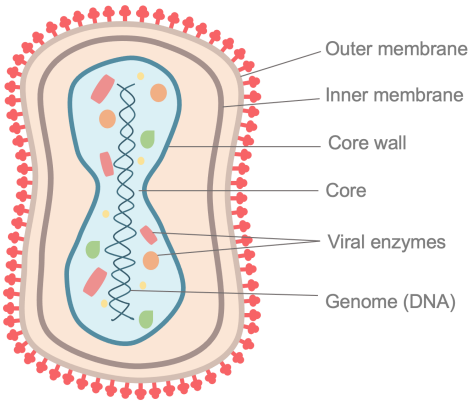

Figure 9: Structure of a Vaccinia virus, representative for enveloped DNA-viruses. Graphic was created using a picture taken from [91].

All the mentioned recombinant Vaccinia viruses were created by modifying them at three different gene loci, including F41.5, J2R (which encodes for thymidine kinase) and A56R (which encodes for hemagglutinin).

1.2.3.2.1 GLV-0b347

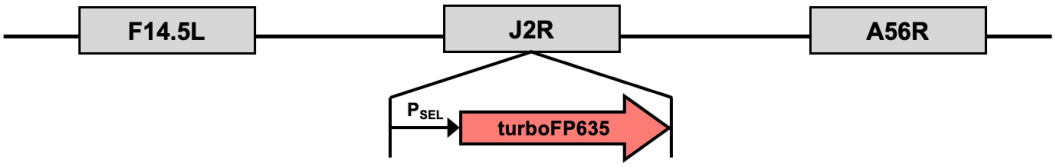

Figure 10: Schematic structure of VACV GLV-0b347 with indication of the gene loci F14.5L, J2R and A56R. At the gene locus J2R turboFP635 (far-red mutant of the red fluorescent protein from sea anemone Entacmaea quadricolor) under the control of the promoter P_{SEL} (synthetic early/late promoter) was inserted. Information on this genome originates from the oral abstract at SITC 27th Annual Meeting 2012: Chen et al.

GLV-0b437 is a recombinant Vaccinia virus derived from the *Western Reserve* Strain (which originated from the New York City Board of Health strain by repeated passaging in mouse brains)[92] with several modifications at the J2R gene locus. This gene normally encodes for a non-essential thymidine kinase. In GLV-0b347 this gene is replaced with a synthetic early/late promoter (P_{SEL})[93] and the turboFP635 marker gene, which encodes for a red marker protein and thus visualizes infected cells.[94] Furthermore, deletion of the thymidine kinase and thus disruption of the J2R locus leads to a reduced virulence.[93,95]

1.2.3.2.2 GLV-1h68

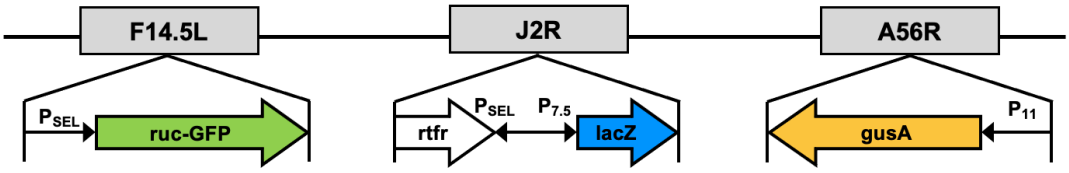

Figure 11: Schematic structure of VACV GLV-1h68 with indication of the gene loci F14.5L, J2R and A56R. Genes inserted at these loci include ruc-GFP = Renilla luciferase - Aequorea green fluorescent protein, rtfr = reverse human transferrin receptor, lacZ = β-galactosidase (β-gal), gusA = β-glucuronidase (β-gluc). Promoters include P_{SEL}= synthetic early/late promoter, $P_{7.5}$ = early/late promoter, P_{11} = late promoter. This VACV was created using the lister strain. Zhang et al. 2007.[96]

GLV-1h68 was created by using the Vaccinia virus Lister strain LIVP (Lister strain from the Institute for Research on Viral Preparations, Moscow, Russia) as a backbone.[95] This strain was modified by homologous recombination of foreign genes into three expression cassettes mentioned above: at the F14.5L gene locus the Renilla luciferase and Aequorea green fluorescent protein (ruc-GFP) fusion gene was inserted, again using the early/late promoter (P_{SEL}) as a control.[96] At the J2R locus the lacZ (LacZ) gene (encoding for the E.coli enzyme β-galactosidase) under the control of the Vaccinia early/late promoter $P_{7.5}$[97] and reverse gene encoding for a human transferrin receptor (rtfr) which serves as a control .[96,98] Furthermore, viral hemagglutinin at the A56R locus was replaced with the E.coli gene for β-glucuronidase (gusA) and is controlled by the promoter P_{11}.[99]

1.2.3.2.3 GLV-1h94

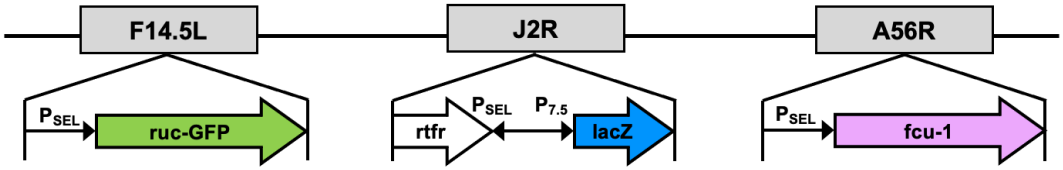

Figure 12: Schematic structure of VACV GLV-1h94 with indication of the gene loci F14.5L, J2R and A56R. Genes inserted at these loci include ruc-GFP = Renilla luciferase - Aequorea green fluorescent protein, rtfr = reverse human transferrin receptor, lacZ = β-galactosidase (β-gal), fcu-1 = a fusion suicide gene 1. Promoters include P_{SEL}= synthetic early/late promoter, $P_{7.5}$ = early /late promoter. This VACV was created using the lister strain.

GLV-1h94 is a derivate of the viral construct GLV-1h68 described above. GLV-1h94 was constructed using the Vaccinia virus Lister strain LIVP and modifying the three gene loci according to GLV-1h68 except for A56R: instead of the gene gusA, the suicide gene fcu1 under the control of P_{SEL} was inserted. As mentioned earlier, expression of the converting enzyme cytosine deaminase enables the conversion of 5-FC to 5-FU resulting in an inhibition of DNA synthesis.

1.2.3.2.4 GLV-1h254

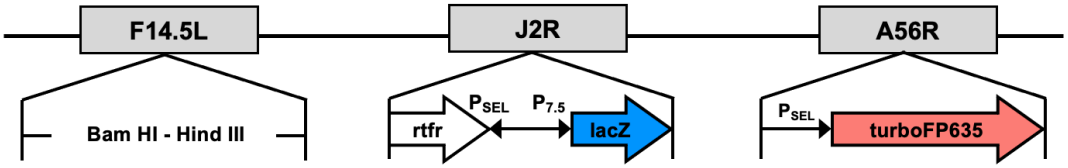

Figure 13: Schematic structure of VACV GLV-1h254 with indication of the gene loci F14.5L, J2R and A56R. Genes inserted at these loci include rtfr = reverse human transferrin receptor, lacZ = β-galactosidase (β-gal) and turboFP635 (far-red mutant of the red fluorescent protein from sea anemone Entacmaea quadricolor). Promoters include P_{SEL}= synthetic early/late promoter, $P_{7.5}$ = early/late promoter. This VACV was created using the lister strain.

GLV-1h254 was constructed using the viral construct GLV-1h71, which is a ruc-GFP deficient version of GLV-1h68. Using GLV-1h71 as a template, GLV-1h254 was created by replacing gusA in the A56R gene locus with the gene for the red-light emitting fluorescent protein turboFP635, resulting in a viral genome as shown in Figure 13.

1.2.3.2.5 GLV-4h463

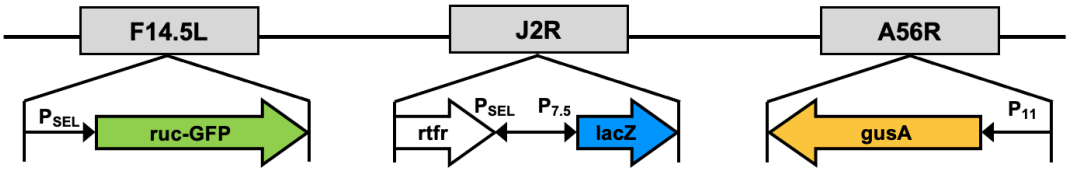

Figure 14: Schematic structure of VACV GLV-4h463 with indication of the gene loci F14.5L, J2R and A56R. Genes inserted at these loci include ruc-GFP = Renilla luciferase - Aequorea green fluorescent protein, rtfr = reverse human transferrin receptor, lacZ = β-galactosidase (β-gal), gusA = β-glucuronidase (β-gluc). Promoters include P_{SEL}= synthetic early/late promoter, $P_{7.5}$ = early /late promoter, P_{11} = late promoter. Information on this viral construct was kindly provided by Genelux company.

GLV-4h463 was created using the Vaccinia virus *Copenhagen* strain. It has the same gene insertions as GLV-1h68: at the F14.5L locus ruc-gfp was inserted, also controlled by the early/late promoter P_{SEL}. At the J2R locus lacZ under the control of the P7.5 promoter and rtfr under the control of P_{SEL} were inserted. Finally, gusA under the control of P11 was inserted into the A56R gene locus.

1.2.3.3 Herpes Virus: T-VEC

Herpes simplex virus 1 (HSV-1) is an enveloped, double stranded (ds) DNA virus with a 152 kb long genome. HSV-1 particles are complex structures and consist of three distinct layers: a 125 nm diameter capsid which encapsules a single copy of the dsDNA, an envelope consisting of a lipid bilayer and between them the so called tegument, comprising a multitude of proteins.[100]

T-VEC (Talimogene Laherparepvec; Imlygic) is a recombinant HSV-1 with several genetic modifications. The ICP34.5 gene is a viral pathogenicity gene, its deletion ensures a reduced neurovirulence[101] and leads to selective replication of the virus in tumor cells.[53] In T-VEC, this deleted neurovirulence factor was replaced by a coding sequence for human Granulocyte-Macrophage-Colony-Stimulating factor (GM-CSF) which leads to a local increase of immunogenic cells, activation of dendritic cells and thus a systemic anti-tumor response.[53] Additionally, the deletion of the ICP47 gene leads to a reduced suppression of antigen presenting cells as well as an increased expression of the US11 gene. This gene ensures a promotion of viral growth in the host cell without impairing its tumor selectivity.[53] T-VEC was approved for the treatment of stage III and IV M1a melanoma by the European medicines agency and for the treatment of advanced melanoma by the FDA and is consequently the first OV to be officially approved in clinical practice.[102,103] The here used version of Talimogene Laherparepvec was kindly provided by Amgen Inc. (Thousand Oaks, CA, USA).

1.3 Organoids as a novel approach to personalized medicine

1.3.1 From reaggregation to self-organization - the evolving definition of organoids

Using the term “organoid” to describe a certain kind of cell culture implies that their characteristics “resemble an organ”. This modern definition based on these implications was not always applied: in fact, the history of organoids is very complex and started before the term was even established.

The history of organoids started before the term was even introduced: in 1907 Wilson was able to demonstrate that sponge cells, which were dissociated beforehand, were able to rearrange themselves and even build functioning organs again.[104] This potential of self-aggregation and organ functionality will later be a crucial part of organoid description. The term “organoid” on the other hand was firstly introduced in 1946 by Smith and Cochrane. It did not describe a self-organizing cell structure but rather a cystic teratoma in a 4-year old boy.[105,106] It was not until the 1960s to 1980s that the term “organoid” defined organo-typic cell cultures in vitro and gained more wide-spread recognition: several experiments in the field of developmental biology demonstrated the reorganization potential of various tissues which were dissociated beforehand.[107,108] To elucidate this observation, Steinberg proposed the differential adhesion hypothesis: self-organization capacity is driven by the differentiation in cell adherence properties of respective cells which lead to the most thermodynamic stable state.[109]

All of experiments described above used synthetical 2D matrices which inherently lacked the possibility of studying cell behavior linked to a 3D setting.[110] Barcellos-Hoff et al. were the first to use three-dimensional laminin-rich matrices attempting to culture the morphogenesis of structures derived from the mammary gland.[111]

But it was not until human pluripotent stem cells (PSCs) were first isolated in 1998 when organoid research started to thrive. Back then, scientists believed only PSCs were able to be established into organoids. Therefore, Sato et al. provided a major breakthrough in 2009: by culturing adult stem cells (ASCs) in conditions which met the growth requirements, they managed to establish organoids from healthy and malignant patient colon tissue without having a mesenchymal

niche.[112] This breakthrough presents the birth of patient derived organoids (PDOs) and patient derived tumor organoids (PDTOs).

Finally, Lancaster and Knoblich provided our modern definition of an organoid as an “organ-like” cell collection. This definition implies a multitude of characteristics: firstly, an organoid must harbor multiple organ-specific cell types, which are organized in a three-dimensional manner, similar to the organ and hence are capable of some kind of specific function of respective organ.[108] These organoids originate from stem cells and further differentiate into functional cell types that form “mini-organs” resembling the histological architecture of respective organ in vivo.[113] This differentiation and also self-organization happens by sorting of cells and eventually commitment of respective cells to their final lineage.[108] All these mechanisms are enabled by specific culture conditions and addition of crucial growth factors, which is further described below for the case of gut organoids.

1.3.2 Gut organoids - a long route to differentiation

Organoids can be cultured in-vitro by using progenitor or stem cells and are capable of long-term growth, preservation of individual characteristics and cellular diversity.[114] These abilities are enabled by the defining characteristics of stem cells: their capacity to self-renewal and differentiation into various different tissues.[115] In general, these stem cells can be divided into two major categories: (I) pluripotent stem cells (PSCs) and (II) adult stem cells (ASCs).[106] PSCs are either embryonic stem cells (ESCs) or induced pluripotent stem cells (iPSC), which originate from adult somatic cells and are reprogrammed to an embryonic stem cell-like state. ASCs on the other hand are organ specific and found in adult organisms, like in this case with colonic or rectal organoids at the bottom of a crypt. [106]

First and foremost, an extracellular matrix that mimics the basement membrane and allows the cells to grow three dimensionally has to be employed: in our case Matrigel, an extract of soluble basement proteins with specific characteristics. Matrigel is derived from the Engelbreth-Holm-Swarm tumor (EHS), a chondrosarcoma which provides a basement membrane resembling tumor matrix.[116] Next, specific niche factors have to be added which are essential for both human and

mouse derived intestinal organoids. Epidermal growth factor (EGF) is indispensable for signaling of mitogenic effects on stem cells.[112,117] It represents one of several signaling pathways controlling crypt stem cells. Another factor is R-spondin1, an agonist of the Wnt-pathway, which is crucial for crypt proliferation, including stem cell proliferation and maintenance of stem cell fate.[118] Next, Noggin, a bone morphogenic protein (BMP) inhibitor, which expands the number of crypts, is added as well.[112,119]

To further optimize culturing conditions, Sato et al. examined other factors to add to the medium as well: A83-01, a small molecule inhibitor of activin like kinase (alk) 4/5/7, improves plating efficiency. Furthermore, addition of Nicotinamide and gastrin enhances culture efficiency.[117,118]

As colon organoids, in contrast to small intestine organoids[120], produce insufficient amount of Wnt-3a, pivotal for maintenance and proliferation of intestinal stem cells (ISCs), Wnt-3a is supplemented.[118,120] To suppress anoikis (detachment induced cell death) of ISCs, the Rho-associated kinase (ROCK) inhibitor Y-27632 is added to the culture medium.[112,117,121]

This multitude of culture conditions and growth factors added to the medium of intestinal organoids, specifically hindgut organoids, demonstrates the complexity of in-vivo tissue and consequently the importance for a more representative culture method.

1.3.3 Organoids employed in oncolytic virotherapy research

Though virotherapy as well as organoid methods have significantly improved in recent years, using organoids as a culture vessel to test oncolytic viruses is still not a widely spread technique.

One of the first works that made use of organoids to test oncolytic viruses was in 2016 by Del Bufalo et al.: they generated organoids by culturing lung adenocarcinoma cells in PEG-fibrin hydrogel systems and infected them with oncolytic adenovirus.[122]

Organoids as a culture method to investigate oncolytic virotherapy is predominantly used in the field of glioblastoma (GBM) research. In 2017, Zhu et al. examined the neural tropism of Zika Virus (ZIKV) employed in glioblastoma cells. After observing a much lower rate of viral spreading in differentiated glioma cells (DGCs) than in glioblastoma stem cells (GSCs) they wanted to test the specificity of ZIKV in a heterogenous cell environment using organoids, as it is more representative of the actual pathophysiological conditions. And indeed: ZIKV infected and consequently lysed predominantly cells expressing the GSC marker SOX2. This resulted in a relative increase in DGCs.[123] Zhu et al. further demonstrated the SOX2-dependent infection of GSCs in 2020. To mimic tumor growth, they implanted GBM tumors in mature brain cortical organoids (BCOs) from human pluripotent stem cells. Infection with ZIKV preferentially reduced GFP-labeled GSCs and not normal BCO cells, which express SOX2 at a much lower rate.[124] Farreira et al. proved tropism of ZIKV to tumor cells by co-culturing brain organoids with embryonal CNS tumor cells: even though normal cells were SOX2 positive, ZIKV would only infect tumor cells.[125]

Other tumors which were examined for oncolytic virotherapy using organoids included pancreas[126], breast[93], bladder[127] as well as and renal cell carcinoma.[128] In 2022, Harryvan et. al. were the first to infect co-cultured GI-fibroblasts and organoids with reovirus and showed, that co-culturing had a massive impact on infection.[129]

1.4 Objective

Thanks to demographic changes such as low birthrates as well as a higher life expectancy, our society grows older. As a consequence, conditions which are associated with advanced age are becoming more relevant for the health of society. This includes not only cardiovascular diseases but cancer entities as well. Especially colorectal cancer (CRC) represents a cancer entity, which becomes more prevalent with an older age.

Cancer therapy on the other hand becomes increasingly individualized. As cancer research moves forward, it becomes evident that cancer is a highly heterogenous disease regarding aspects like genetic mutations, tumor microenvironment as well as spreading behavior and therapy response. Immunotherapy, including oncolytic virotherapy takes all these aspects into consideration.

The aim of this dissertation was to use a novel cell model, namely patient derived tumor organoids (PDTOs), as a more representative preclinical approach to examine the efficacy of different oncolytic viruses on CRC tumor cells to generate a personalized “virogram” (analogous to an antibiogram) for each patient tested and finally find the most efficient therapy option.

First, the most important question was whether treatment with oncolytic viruses as well as the prodrug 5-FC was feasible in PDTOs of CRC origin. To elucidate this question, we were able to culture four PDTOs, treated them with a selection of oncolytic viruses and observed them for a time period of 96 hours. Within these 96 hours, we took photos via phase contrast as well as fluorescent microscopy. This allowed us to observe morphological changes as well as infection through the detection of a fluorescent signal. At the end of the observation period, we conducted a viability assay to further objectify oncolysis.

After observing the feasibility of infection in CRC PDTOs, experiments to further characterize replication behavior were conducted. This was done by virus growth curves for each organoid with different viruses from each species, respectively. Here we could observe different virus replication behaviors and compared them with morphological changes at respective time points.

These experiments lead to the generation of a personalized “virogram” for each tested PDTO and thus each patient, suggesting which of the employed OVs may be the most effective in each of them also in a clinical setting.

2 Material and Methods

2.1 Material

All cited materials have been used in the highest achievable purity. Materials were purchased in a sterile state from the companies listed below. All other matter was sterilized by autoclaving at 2 bar pressure and 121 °C for 20 minutes. If water was used for experiments, it had always been deionized and filtered, unless described in any other way.

2.1.1 Characteristics of viruses

Virus	Strain	Gene disruptions	Gene insertions	Source
MeV-GFP	Mérieux	/	eGFP	provided by[130]
MeV-SCD	Mérieux	/	SCD[131]	
T-VEC	JS-1	ICP 34.5, ICP 47	GM-CSF	Amgen Inc.
GLV-0b347	Western Reserve	F14.5L, J2R, A56R	turboFP635	Genelux Corporation
GLV-1h94	Lister (derivate of GLV-1h68)	F14.5L, J2R, A56R	ruc-GFP, lacZ, fcu1	Genelux Corporation
GLV-1h254	Lister (derivate of GLV-1h68)	F14.5L, J2R, A56R	rTfr + lacZ, turboFP635	Genelux Corporation
GLV-4h463	Copenhagen	F14.5L, J2R, A56R	ruc-GFP, rTfr + lacZ, gusA	Genelux Corporation
GLV-1h68	Lister	F14.5L, J2R, A56R	ruc-GFP, lacZ, gusA	Genelux Corporation

Table 1: Characteristics of viruses used in experiments.
Abbreviations: eGFP (enhanced green fluorescent protein), SCD (super cytosine deaminase), GM-CSF (Granulocyte-macrophage colony-stimulating-factor), turboFP635 (Far-red fluorescent protein turbo FP635), ruc-GFP (Renilla luciferase - Aequorea green-fluorescent-protein), lacZ (encodes for β-galactosidase), fcu1 (fusion suicide gene, encodes for a fusion protein of cytosine deaminase and uracil phosphoribosyltransferase which catalyzes the conversion of 5-FC to 5-FU and 5-FUMP)[132], rTfr (reverse transferrin receptor gene), gusA (gene encoding for β-glucuronidase).

2.1.2 Chemicals

Chemical	Manufacturer	Location
Descosept	Dr. Schuhmacher GmbH	Malsfeld-Beisewörth, Germany
5-Fluorocytosine	Hoffmann-La Roche AG	Basel, Switzerland
5-Fluorouracil	Pharmaceutical Department, Tuebingen University Hospital	Tübingen, Germany
Isopropanol (70%)	SAV Liquid Production GmbH	Flintsbach, Germany
Cell Titer Reagent	Promega Corporation	Madison, USA
Trypan Blue	Sigma-Aldrich	St. Louis, USA

Table 2: Chemicals used in experiments with specification of the manufacturer and its location.

2.1.3 Media, sera and buffer

Product	Manufacturer	Location
adDMEM/F-12 (Advanced Dulbecco's Modified Eagle's Medium/F-12)	Gibco, Thermo Fisher Scientific	Waltham, USA
DMEM (Dulbecco's Modified Eagle's Medium)	Sigma-Aldrich	St. Louis, USA
FCS (Fetal Calf Serum)	Gibco, Thermo Fisher Scientific	Waltham, USA
Recovery™ Cell Culture Freezing Medium	Thermo Fisher Scientific	Waltham, USA
GlutaMAX™	Thermo Fisher Scientific	Waltham, USA
Hepes	Thermo Fisher Scientific	Waltham, USA
Matrigel© Matrix	Corning, Inc.	Corning, USA

PBS (Phosphate-Buffered Saline)	Sigma-Aldrich	St. Louis, USA
Penicillin-Streptomycin	Thermo Fisher Scientific	Waltham, USA
TrypLE Express	Gibco, Thermo Fisher Scientific	Waltham, USA
Trypsin EDTA	Gibco, Thermo Fisher Scientific	Waltham, USA
Tumor dissociation kit, human (enzymes H, R and A, respectively)	Miltenyi Biotec B.V. & Co. KG	Bergisch Gladbach, Germany

Table 3: Media, sera and buffers used in experiments with specification of the manufacturer and its location.

2.1.4 Self-made solutions

Several solutions which were necessary for experiments, had to be manufactured individually and were prepared as described below.

2.1.4.1 Organoid growth medium

Growth medium was mixed in 500 ml advanced DMEM/F12 with addition of 5 ml GlutaMAX™ Supplement, 5 ml Hepes (1 M) and 5 ml Penicillin-Streptomycin (10,000 µg/mL) (splitting medium). Using 19 ml of this medium, organoid growth medium was prepared according to the table below. Wnt-3a was added right before medium change in a 1:1000 proportion. Y27632 had to be added after isolation of cells, thawing or after passaging of organoids.

Stock	Volume	Final concentration	Stock concentration	Producer/country of origin
Growth/Splitting medium	19 ml	/	/	
B27 Supplement (50x)	400 µl	1x		Thermo Fisher Scientific; USA
N2 Supplement (100x)	200 µl	1x		Thermo Fisher Scientific; USA

Nicotinamide (100x)	200 µl	10 mM	1 M	Sigma Aldrich; USA
N-Acetylcysteine (400x)	50 µl	1.25 mM	500 mM	Sigma Aldrich; USA
A83-01 (1000x)	20 µl	0.5 µM	0.5 mM	TOCRIS; UK
GastrinI (1000x)	20 µl	10 nM	10 µM	TOCRIS; UK
Murine EGF (1000x)	20 µl	50 ng/ml	50 µg/ml	Thermo Fisher Scientific; USA
Murine Noggin (1000x)	20 µl	100 ng/ml	100 µg/ml	Peprotech; USA
human R-Spondin (1000x)	20 µl - 40 µl	500 ng/ml - 1 µg/ml	500 µg/ml	Peprotech; USA
Y-27632 (1000x)	20 µl	10.5 µM	10.5 mM	Sigma Aldrich; USA
Wnt-3a	20 µl			

Table 4: Composition of organoid growth medium with indication of used volume, stock and final concentration of components and their manufacturers.

2.1.4.2 Other solutions

adDMEM/F12 + 10 % FCS

adDMEM/F12	500 ml
FCS	55 ml

DMEM + FCS (10 %, 5 %, 2 %)

DMEM	500 ml
FCS	55 ml, 25 ml, 10 ml

Virus plaque overlay medium (1.5 % CMC)

Carboxymethylcellulose sodium salt (CMC)	7.5 g
DMEM	500 ml
FCS	25 ml
Penicillin/Streptomycin (P/S)	5 ml

Crystal violet staining solution

Crystal Violet (408.6 g/mol)	0.13 % (1.3 g)
EtOH (100 %)	5 % (50 ml)
Formaldehyde (37 %)	11.1 % (300 ml)
H_2O	filled up to 1 l

Fixation agent

Base material: H_2O

PFA	2 %
Glutaraldehyde	0.1 %

Sucrose solution

20 % Sucrose in PBS

2.1.5 Consumables

Consumables	Manufacturer	Location
Cell strainer (EASYstrainer) 75 µm	Greiner Bio-One International GmbH	Kremsmünster, Austria
Combitips (ritips®) 12.5 ml	Ritter GmbH	Schwabmünchen, Germany
Conical tubes 15 ml, 50 ml	FALCON™, Corning	Corning, USA
Cryotubes (Cryogenic Vial) 1 ml	Corning	Corning, USA

gentleMACS™ C-Tube	Miltenyi Biotec B.V. & Co. KG	Bergisch Gladbach, Germany
Gelloader Pipette Tips 200 µl	Sarstedt AG & Co. KG	Nümbrecht, Germany
Pasteur pipettes 230 mm	WU Mainz	Mainz, Germany
Petri dish 60 x 15 mm	FALCON ™, Corning	Corning, USA
Pipette tips (TipOne) 100 µl, 200 µl	USA Scientific, Inc.	Ocala, USA
Pipette tips 1000 µl	Nerbe plus GmbH & Co. KG	Winsen, Germany
Pipettes 5 ml, 10 ml, 25 ml, 50 ml	Costar®, Corning	Corning, USA
Reaction tubes (Safe-Lock Tubes) 0.5 ml, 1.5 ml, 2 ml	Eppendorf AG	Hamburg, Germany
Tissue culture flask (CELLSTAR®) 175 cm^2, 550 ml	Greiner Bio-One International GmbH	Kremsmünster, Austria
Tissue culture plate 24 well	TPP Techno Plastic Products AG	Trasadingen, Switzerland
Tissue culture plate 48 well	Costar®, Corning	Corning, USA
Tissue culture plate 96 well	FALCON ™, Corning	Corning, USA

Table 5: Consumables used in experiments with specification of the manufacturer and its location.

2.1.6 Laboratory Equipment

Equipment	Manufacturer	Location
Autoclave (VARIOKLAV 75 T)	HP Medizintechnik GmbH	Oberschleißheim, Germany
Autoclave (VX-150)	Systec GmbH	Linden, Germany
Centrifuge (for Reaction Tubes)	Eppendorf AG	Hamburg, Germany
Centrifuge (Megafuge 2.0 R)	Heraeus®, Thermo Fisher Scientific, Inc.	Waltham, USA
ELISA reader (Synergy HT)	BioTek Instruments, Inc.	Winooski, USA
Fluorescence Microscope	Olympus	Tokio, Japan
GentleMACS dissociator	Miltenyi Biotec B.V. & Co. KG	Bergisch Gladbach, Germany
Haemocytometer	Hecht Assistant GmbH & Co. KG	Sondheim vor der Rhön, Germany
Heating Block (Eppendorf Thermo-mixer)	Eppendorf	Hamburg, Germany
Incubator (for non-infected cells)	Heraeus®, Thermo Fisher Scientific, Inc.	Hanau, Germany
Incubator (for infected cells and organoids)	Memmert GmbH + Co. KG	Büchenbach, Germany
Laminar Flow Work Bench (HERASafe)	Heraeus®, Thermo Fisher Scientific, Inc.	Waltham, USA

Light microscope	Olympus	Tokio, Japan
Multichannel pipette	Eppendorf AG	Hamburg, Germany
Multiple dispenser (Handy Step S)	Brand GmbH + Co. KG	Wertheim, Germany
Pipette aid (Pipette boy 2)	Integra Biosciences GmbH	Biebertal, Germany
Refrigerator (-18 °C)	Liebherr AG	Bulle, Switzerland
Refrigerator (-80 °C)	Forma Scientific	
Refrigerator (-150 °C)	SANYO	Osaka, Japan
Sonifier	Branson Ultrasonics	Danbury, USA
Thermomixer comfort	Eppendorf AG	Hamburg, Germany
Vortex Mixer VM-300	neoLab Migge GmbH	Heidelberg, Germany
Water bath	Köttermann GmbH	Uetze, Germany

Table 6: Laboratory Equipment used in experiments with specification of the manufacturer and its location.

2.2 Methods

2.2.1 Safety conditions

All experiments were conducted in the laboratory of Prof. Dr. med. Ulrich M. Lauer in the Hertie Institute, Otfried-Müller-Str. 27, 72076 Tübingen, Germany, 5th floor. This laboratory is a S2 safety laboratory which demands working with cells and genetically modified viruses under laminar flow work benches (Heraeus; Hanau, Germany) under sterile conditions. All surfaces that could potentially be contam-

inated were regularly disinfected with 70 % isopropanol or Descosept. Additionally, workbench surfaces were irradiated with ultraviolet light for at least 10 minutes.

2.2.2 Organoid culture

2.2.2.1 Cell culture conditions

Monolayer cells and organoids were cultured separately in incubators in a 37 °C-tempered humidified atmosphere with 5 % CO_2.

2.2.2.2 Tumor material

Tumor material from CRC-patients was obtained from the Department of General, Visceral and Transplant Surgery, University of Tübingen, Tübingen, Germany and the Institute of Pathology, University of Tübingen, Tübingen, Germany. The tumor material was kept in MACS® Tissue Storage Solution (Miltenyi Biotec) and stored in the fridge until further usage. Tumor material from 4 different patients was used which had characteristics as follows:

	Organoid 22	**Organoid 25**	**Organoid 29**	**Organoid 33**
Tumor entity	Adeno-carcinoma	Adeno-carcinoma	Adeno-carcinoma	Adeno-carcinoma
Localization	Rectosigmoid junction, 15 cm ab ano	Coecum	Right colonic flexure	Left colonic flexure
TNM-status	pT3, pN1b (2/15), cM0	pT3, pN2b (9/23), cM0	pT3, pN2a (6/30), cM0	pT4a, pN2a (4/19), cMx
Grading	G3, R0, L1, V1, Pn1	G3, R0, L0, V0, Pn0	G2, R0, L0, V0, Pn0	G3, R0, L0, V0, Pn0
PMS2-status	positive	negative	negative	negative
MLH1-status	not tested	negative	negative	negative

MSH2-status	not tested	positive	positive	positive
MSH6-status	positive	positive	positive	positive
CDX2-status	positive	50% positive	positive	positive
Micro-satellite-status	MSI-L /Most likely stable	MSI-H /instable	MSI-H/ instable	MSI-H /instable
BRAF-status	not tested	p. V600E	p. V600E	Wildtype
Patho-genesis	Sporadic CRC with MSI-L	Sporadic CRC with MSI-H	Sporadic CRC with MSI-H	HNPCC/ Lynch-Syn-drome

Table 7: Characteristics of tested organoids.
All tested organoids originated from adenocarcinomas. Localization was determined through preoperative endoscopy and surgery. Abbreviations: PMS2 = Postmeiotic Segregation Increased 2, MLH1 = mutL homolog 1, MSH2/6 = mutS homolog 2/6, CDX2 = caudal type homeobox 2, BRAF = proto-oncogene B-Raf.

2.2.2.3 Establishment of organoid cultures from patient material

The tumor tissue was transferred to a 6 cm diameter petri dish and cut into small pieces, cutting off the necrotic and connective tissue. The tissue fragments were then transferred into a gentleMACS™ C-tube together with 4.7 ml of advanced DMEM/F12 supplemented with 10 mM Hepes, L-glutamine and Penicillin/Streptomycin, 200 µl enzyme H, 100 µl enzyme R and 25 µl enzyme A. The C-tube was then put into the dissociator. For dissociation, programs „h_tumor_01“, „h_tumor_02” and „h_tumor_03“ were used. Between these dissociation steps, the C-tube was incubated for 30 minutes at 37 ° in a water bath under vigorous shaking. After the last dissociation step the cell suspension was transferred into a 15 ml tube which was centrifuged at 1500 rpm for 6 minutes. The supernatant was taken off, the remaining cell pellet was resuspended in 1 ml TrypLE Express and the suspension was transferred into a 2 ml reaction tube which was incubated for 15 minutes in a heating block at 37° C and 1000 rpm. To inactivate the TrypLE, 500 µl adDMEM/F12 with 10% FCS were added. Then, a 70 µm cell strainer was

put on a 50 ml tube and moistened with adDMEM/F12 and the cell suspension was sifted through the cell strainer. The 2 ml reaction tube was rinsed with 2 ml of adDMEM/F12. Then the cell strainer was rinsed again with 20 ml adDMEM/F12 to detach the remaining cells stuck on the cell strainer. The 50 ml tube was then centrifuged at 1500 rpm for 7 minutes. The supernatant was discarded and the cell pellet was resuspended in a suitable volume (100-300 µl) of adDMEM/F12, depending on the size of the pellet. A part of the cell suspension was mixed with Matrigel in a ratio of 1:1 and then distributed in a 48-well plate with 20 µl of the cell-Matrigel suspension per well. The 48-well plate was turned upside down and put in the incubator for 30 minutes. Then, when the Matrigel had solidified, 250 µl organoid medium were added to each well. The rest of the cell suspension was cryoconserved.

2.2.2.4 Medium change

Medium change had to be performed every three to four days, depending on culture density. The old medium was discarded and 250 µl organoid medium were added to each well. After that, the culture plate was stored in the incubator again.

2.2.2.5 Passaging of organoid cultures

When the organoids reached a certain density, they had to be passaged and plated in a new culture plate. The old medium was collected in a 15 ml tube. After that, the organoids were washed with PBS using 1 ml for 6 wells. As a next step, 1 ml TrypLE was spread on 6 wells and using the pipette tip, the Matrigel was scraped off the culture plate, shortly resuspended in TrypLE and then transferred into a 2 ml reaction tube. This tube was incubated in a heating block at 37 °C and 1400 rpm for 7-10 minutes, depending on the size and density of the organoids. Then, 250 µl adDMEM/F12 + 10 % FCS were added to inactivate the TrypLE. The organoids were then transferred to the 15 ml tube which was filled up with 10 ml of adDMEM/F12 and centrifuged for 10 minutes at 1500 rpm. The supernatant was taken off and the cell pellet was resuspended in a suitable volume (50-100 µl) of adDMEM/F12, depending on the size of the pellet. The desired

amount of cell suspension was mixed with Matrigel in a ratio of 1:1 and then spread onto a 48-well culture plate with 20 µl per well. The rest of the cell suspension was cryoconserved (see below). The 48-well culture plate was then put upside-down in the incubator for 30 minutes. After that, 250 µl organoid medium were added to each well. The culture plate was then put in the incubator again.

2.2.2.6 Cryoconservation

Organoids were harvested and centrifuged for passaging as described above. The cell pellet was resuspended in an appropriate volume of adDMEM/F12 and freezing medium was added in a ratio of 9:1. The cell suspension was transferred into a cryotube which was then put into a Mr. Frosty freezing container which ensures a slow freezing of the cell suspension. After one day in the -80 °C freezer, the cryotube was transferred to a -150 °C freezer.

2.2.2.7 Thawing of organoid cultures

Organoids were thawed by putting the cryotubes in a warm water bath. After that, they were transferred to a 15 ml tube containing 10 ml adDMEM/F12 and centrifuged at 1500 rpm for 10 minutes. The supernatant was discarded and the remaining cell pellet was suspended in a suitable amount of organoid medium and Matrigel, depending on the size of the pellet.

2.2.2.8 Cell Counting

Cells were counted with an improved Neubauer haemocytometer.

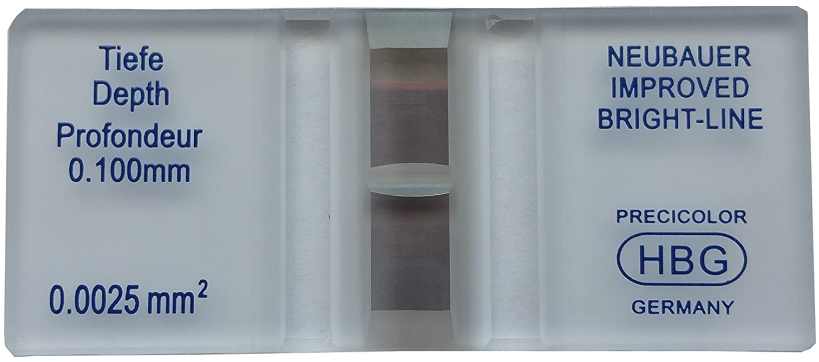

Figure 15: Neubauer Haemocytometer.

The cell pellet was suspended in a suitable amount of organoid medium. It was important to thoroughly resuspend the pellet to avoid cell clusters. 10 µl of this suspension were mixed with 90 µl of Trypan Blue in a separate reaction tube. With the help of Trypan Blue, viable and dead cells can be differentiated, as vital cells do not take up the dye and appear white due to their intact cell membrane in contrast to the dead cells which appear blue due to the stain. Again, this suspension was thoroughly mixed. The Neubauer haemocytometer was prepared by slightly moistening the surface of the counting chamber and then pressing a cover glass onto the top. The cover slip was positioned correctly when Newton rings could be detected. Then, 10 µl of the cell suspension mixture were pipetted close to the edge of the cover glass of the Neubauer haemocytometer. Vital cells were then counted under a CK40 light microscope (Olympus) with the 10x objective.

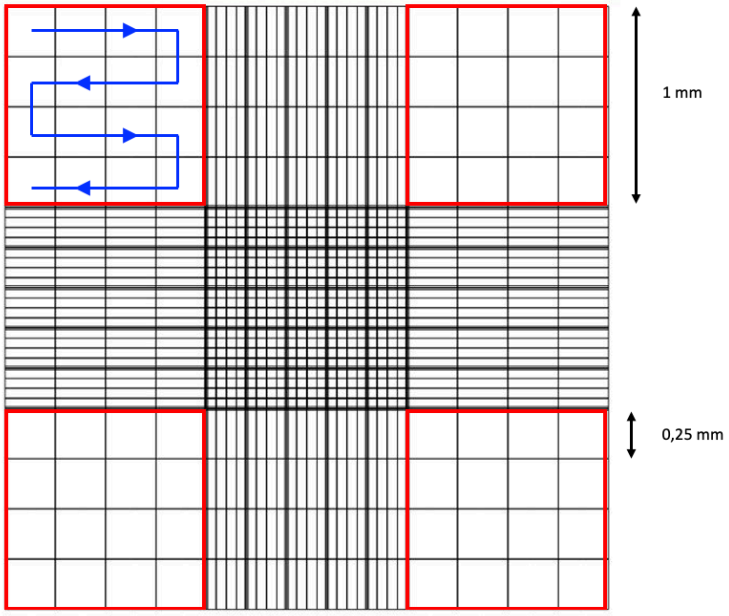

Figure 16: Scheme of the Neubauer haemocytometer counting chamber with 4 corner squares (red) and directions in which order cells in the smaller squares (blue) were counted.

The Neubauer haemocytometer is divided into 4 corner squares which are subdivided into 16 smaller squares, and 5 middle squares. Cells were counted in the four corner squares, starting from left above and counting to the right. Cells which were on the boundary line were only counted if it was the top or right boundary line, making sure not to count the same cells twice. Each corner square has a surface of 1 mm x 1 mm. The height of the counting chamber is 0.1 mm which

makes the volume of each corner square 1 mm x 1 mm x 0.1 mm = 0.1 mm^3. To calculate the cells per milliliter, the following formula was used:

$$Concentration\ \left(\frac{cells}{ml}\right) = \frac{number\ of\ cells\ \times 10.000 \times dilution}{number\ of\ counted\ squares}$$

Equation 1: Calculation of the concentration in cells per milliliter using the Neubauer haemocytometer.

2.2.2.9 Organoids for infection

To ensure a better spreading of the virus, organoids were seeded in a 10 % Matrigel and medium mixture for infection. Organoids were harvested and centrifuged as described. Then, cells were counted and the required amount of cell suspension for the required number of wells was calculated. The 10 % Matrigel solution was prepared by calculating the total amount of solution for half a well more than needed, making sure there is enough of the suspension for all required wells. Wnt3a was added at the end in a 1:1000 concentration.

$$V_{total} = (x_{number\ of\ wells} + 0{,}5) \times\ 250\mu l$$
$$V_M = V_{total} \times 10^{-1}$$
$$V_W\ =\ V_{total} \times 10^{-3}$$
$$V_{OM} = V_{total} - (V_M + V_W + V_C)$$

Equation 2: Calculation for volumes of organoid medium (OM), Matrigel (M), Wnt3a (W) and cell suspension (C).

The Matrigel cell suspension was seeded in a 48-well plate, with 2.5 x 10^4 cells in 250 µl of 10 % Matrigel in organoid medium per well. Organoids were incubated for one more day prior to infection.

2.2.2.10 Fixation of organoids

To prove that the cultured organoids were in fact tumor cells, staining was performed. First, organoids had to be fixated to be further examined. Four droplets of Matrigel and organoid solution were seeded per well in a 6-well plate and incubated until they reached a high density after 3-4 days. Organoid medium was carefully removed without damaging the Matrigel domes. Wells were rinsed with 3 ml of PBS. PBS was discarded as well and 3 ml of fixation agent were pipetted in each well. Culture plates were incubated for 30 minutes at room temperature.

After that, fixation solution was removed and each well was washed three times with 3 ml of PBS for 10 minutes. Then, PBS was removed and the now fixated Matrigel spheres were carefully scraped off the wells and transferred into a 50 ml conical tube containing previously prepared sucrose solution. The 50 ml tubes were then put into a 4 °C refrigerator. After two days, the Matrigel spheres had sunk to the ground. The sucrose solution was carefully removed and the Matrigel spheres were transferred into a previously prepared aluminum hood filled with Tissue compound. These aluminum caps were snap frozen in liquid nitrogen and then put into the -80 °C freezer. Cryosectioning and staining of the fixated organoid blocks was kindly performed by Prof. Bence Sipos at the Institut für Pathologie und Neuropathologie, Tübingen.

2.2.3 Cell culture

2.2.3.1 Vero cells

Vero cells are derived from the normal kidney of an adult African green monkey and are adherent elongated, fibroblast-like cells which grow in monolayers. Vero cells used in this experiment are derived from the Vero lineage VERO-B4 and were obtained from the DSMZ (Deutsche Sammlung von Mikroorganismen und Zellkulturen, Bereich Menschliche und Tierische Zellkulturen, Braunschweig; Germany).

2.2.3.2 CV-1 cells

CV-1 cells were isolated from the kidney of an adult African green monkey and exhibit a fibroblast morphology. CV-1 cells were obtained from ATCC®.

2.2.3.3 Cell culture conditions

Cells were cultured in 175 cm^2 tissue culture flasks in 25 ml of DMEM + 10 % FCS and stored at 37 °C in an incubator in a humidified atmosphere with 5 % CO_2. Cell density was checked every day under a CK40 contrast light microscope.

2.2.3.4 Passaging

For passaging, medium was discarded and cells were washed with 10 ml of PBS. Then 3 ml of Trypsin/EDTA (Biochrom, Berlin; Germany) were pipetted into the flask to detach cells. After an incubation for 3-4 minutes, when cells had detached, they were suspended in 10 ml of DMEM + 10 % FCS, transferred into a 15 ml tube and centrifuged for 3 minutes at 1200 rpm. The supernatant was carefully taken off and the remaining cell pellet was suspended in 10 ml of DMEM + 10 % FCS. 1 ml of this suspension was then transferred back in the flask containing 25 ml fresh DMEM + 10 % FCS. The flask remained in the incubator for 2-3 days until the next passage.

2.2.4 Virological methods

2.2.4.1 Infection of organoids

One day after seeding, organoids in 10% Matrigel solution were infected with the viruses at different multiplicities of infection (MOIs). Virus solution for each virus was prepared for 2.5 wells and calculated for each individual virus titer as well as different concentrations of 5-FU solution, as shown in the table below. 50 µl of virus solution in organoid medium per well were pipetted with a GELloader pipette tip. For better spreading the GELloader pipette was placed at several spots in the well to ensure an even distribution of the virus suspension.

Treatment	Titer (PFU/ml)	Volume Treatment	Volume Medium	Volume 5-FC
MOCK			125 µl	
5-FC (1 mM)			110 µl	15 µl
MeV-GFP (MOI 10)	2 x 10^7	31.25 µl	93.75 µl	
MeV-SCD (MOI 10)	2.4 x 10^7	26 µl	99 µl	
MeV-SCD (MOI 10) + **5-FC**	2.4 x 10^7	26 µl	84 µl	15 µl

T-VEC (MOI 1)	8.4 x 10^7	7.4 µl (1:10)	117.6 µl	
GLV-0b347 (MOI 10)	3.7 x 10^9	16.9 µl (1:100)	108.1 µl	
GLV-1h94 (MOI 10)	1.1 x 10^8	5.7 µl	119.3 µl	
GLV-1h94 (MOI 10) + **5-FC**	1.1 x 10^8	5.7 µl	104.3 µl	15 µl
GLV-4h463 (MOI 10)	1.8 x 10^8	3.47 µl	121.53 µl	
GLV-1h254 (MOI 10)	2.9 x 10^8	2.16 µl	122,84 µl	
GLV-1h68 (MOI 10)	1.49 x 10^8	4.2 µl	120.8 µl	
5-FU (1 mM)		16.25 µl (1:10)	108.75 µl	
5-FU (0.1 mM)		16.25 µl (1:100)	108.75 µl	
5-FU (0.01 mM)		16.25 µl (1:1000)	108.75 µl	

Table 8: List of virotherapeutic agents and treatments used with indication of treatment volume and medium volume in microliters.

2.2.4.2 Phase contrast and fluorescence microscopy

Spreading of the infection was tracked by phase contrast and fluorescence microscopy. To record the morphological effects of oncolysis, pictures were taken at 24, 48, 72 and 96 hours post infection (hpi) at different magnifications (5x, 10x and 20x). Wells infected with MeV-GFP, GLV-0b347, GLV-1h94, GLV-4h463, GLV-1h254 and GLV-1h68, which express fluorescent marker proteins, were also photographed with an IX 50 fluorescence microscope and an F-view camera system.

2.2.4.3 CellTiter-Blue® Cell Viability Assay

To assess cell viability, CellTiter-Blue® Cell Viability Assay was performed as an endpoint measurement after the intended incubation time of 96 hpi. This assay is based on the ability of living cells to metabolize resazurin (7-Hydroxy-3H-phenoxazin-3-one-10-oxide), a dark blue redox dye to the pink, fluorescent end product resofurin (7-Hydroxy-3H-phenoxazin-3-one). Thus, viable cells emit a fluorescent signal proportional to the number of living cells in the well. In contrast, dead cells do not reduce the indicator dye as they have lost their metabolic capacity and subsequently do not produce a fluorescent signal. Fluorescence of a non-treated well was used as a reference and relative viability of the organoids after different treatments could be determined.

In each well, 60 µl Cell Titer reagent were pipetted using GELloader pipette tips as well. The culture plate was then placed in the incubator until the color started to turn from blue to red. Fluorescence was measured in an ELISA reader. Viability of untreated organoids was set 100 %.

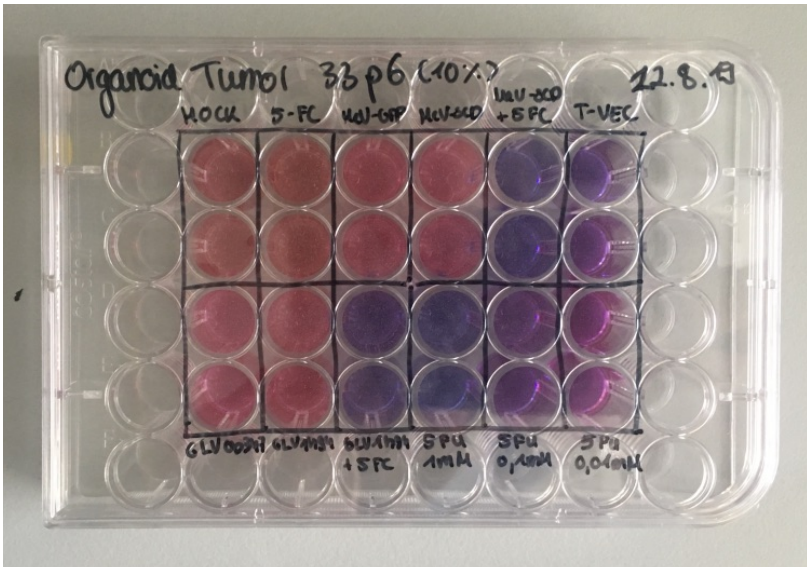

Figure 17: Exemplary culture plate with pink wells (fully metabolized, thus viable cells) and blue wells (non-metabolized redox dye resazurin, mostly dead cells).

2.2.4.4 Infection of organoids for virus quantification

Organoids were cultured and seeded for infection as described in a 10 % Matrigel medium solution. Cell Matrigel suspension was pipetted into 16 wells with 250 µl

each. The next day organoids were infected with the respective virus. The infected organoid-Matrigel suspension was harvested by pipetting at five different time points (3, 24, 48, 72, 96 hpi) with three wells for each time point. Wells were then washed with 200 µl of adDMEM/F12, making sure to get all the content of the well. Samples were immediately frozen in reaction tubes at –80 °C. One well was not infected (MOCK), instead 50 µl of organoid medium were added.

Virotherapeutic agent	Titer (PFU/ml)	Volume Medium	Volume of virotherapeutic agent
MeV-GFP	2.0 x 10^7	581.3 µl	193.8 µl
GLV-0b347	3.7 x 10^9	532.8 µl	242.2 µl (1:100)
T-VEC	8.4 x 10^7	728.9 µl	46.1 µl (1:10)

Table 9: Calculated volume for each virotherapeutic agent and respective organoid medium for 15.5 wells with 50 µl of virotherapeutic agent and medium solution per well.

Virus titration is a method to determine an unknown concentration of infectious viral particles in a sample. In this case, the quantity of infectious particles in the respective organoid at different time points was determined by titrating the supernatant on so-called indicator cells, which differ dependent on the virus.

2.2.4.4.1 Titration of MeV-GFP

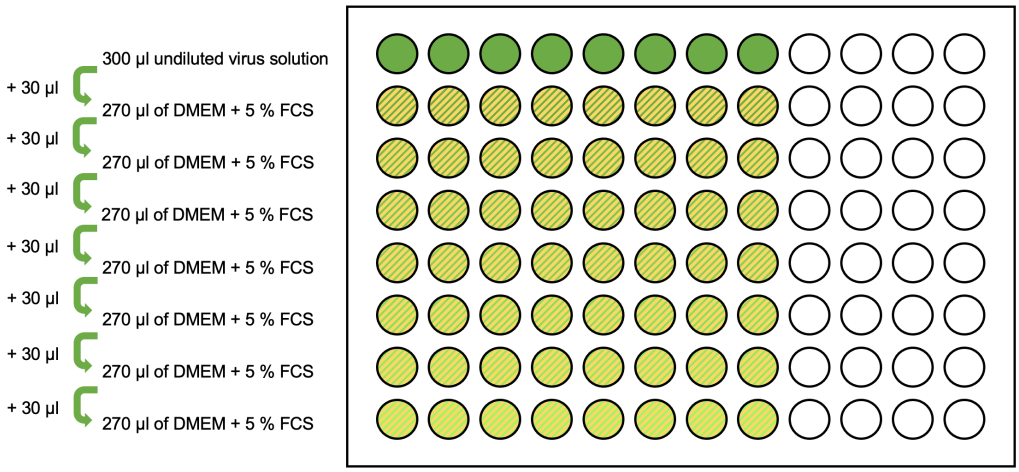

Figure 18: Exemplary dilution series in a 96-well culture plate for titration of MeV-GFP. 300 µl of undiluted virus solution were pipetted into the first row. Then 30 µl of this undiluted virus solution were added to 270 µl DMEM + 5 % FCS in the next row. As a next step, adding 30 µl of this new dilution were added to the next row of 270 µl DMEM + 5 % FCS. This procedure was repeated until a dilution of 10^{-7} was created.

The day before titration, Vero cells were seeded in 96-well plates with 1 x 10^4 cells per well in 200 µl DMEM + 5 % FCS. To determine the viral concentration of MeV-GFP in the respective organoid, samples were thawed in a water bath, shortly vortexed and then centrifuged for 2 min at 3000 rpm. The supernatant was used to prepare a dilution series. A 96-well plate was prepared with one column (eight wells) for each sample. The first well was left empty for the undiluted virus solution generated from the organoid material; the following seven wells of each column were prepared with 270 µl of DMEM + 5 % FCS each. Then, 300 µl of the virus containing supernatant were pipetted in the first well. 30 µl of the supernatant from the first well were transferred into the next well. Then the solution was resuspended and the pipette tip was discarded. This was repeated up to a dilution of 10^{-7}.

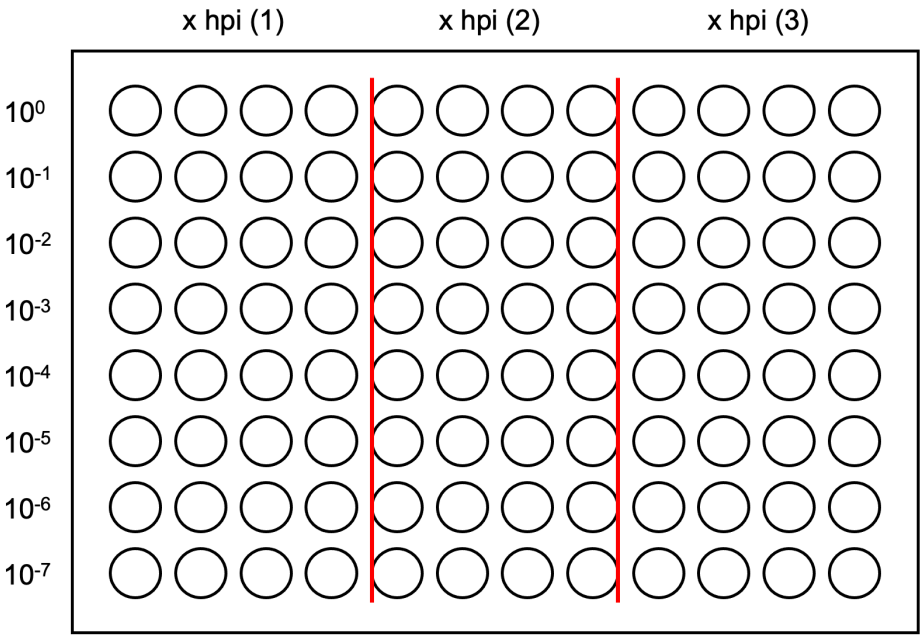

Figure 19: Exemplary 96-well plate dilution series of three samples for one time point.

Using a multichannel pipette, 50 µl of each well of the dilution series were transferred to eight wells of the previously plated Vero cells. This was repeated three more times with one sample, resulting in 4 replicates per sample. Plates were incubated for four days at 37 °C and then analyzed using a fluorescence microscope (Olympus). For each sample, the number of fluorescent wells per dilution

were counted. A well was considered “positive” if a fluorescent signal could be detected, irrespective of its fluorescent strength. The results were evaluated using the following formula:

$$x\left(\frac{pfu}{ml}\right) = a \times 10^{y-0.5+1.5}$$

Equation 3: Calculation of the number of infectious particles per milliliter.
With: a = 0.7 which is the conversion factor of the original $TCID_{50}$-method to the less abstract unit plaque forming units (pfu) and y= sum of the fractions of positive wells per dilution factor.

2.2.4.4.2 Titration of VACV GLV-0b347

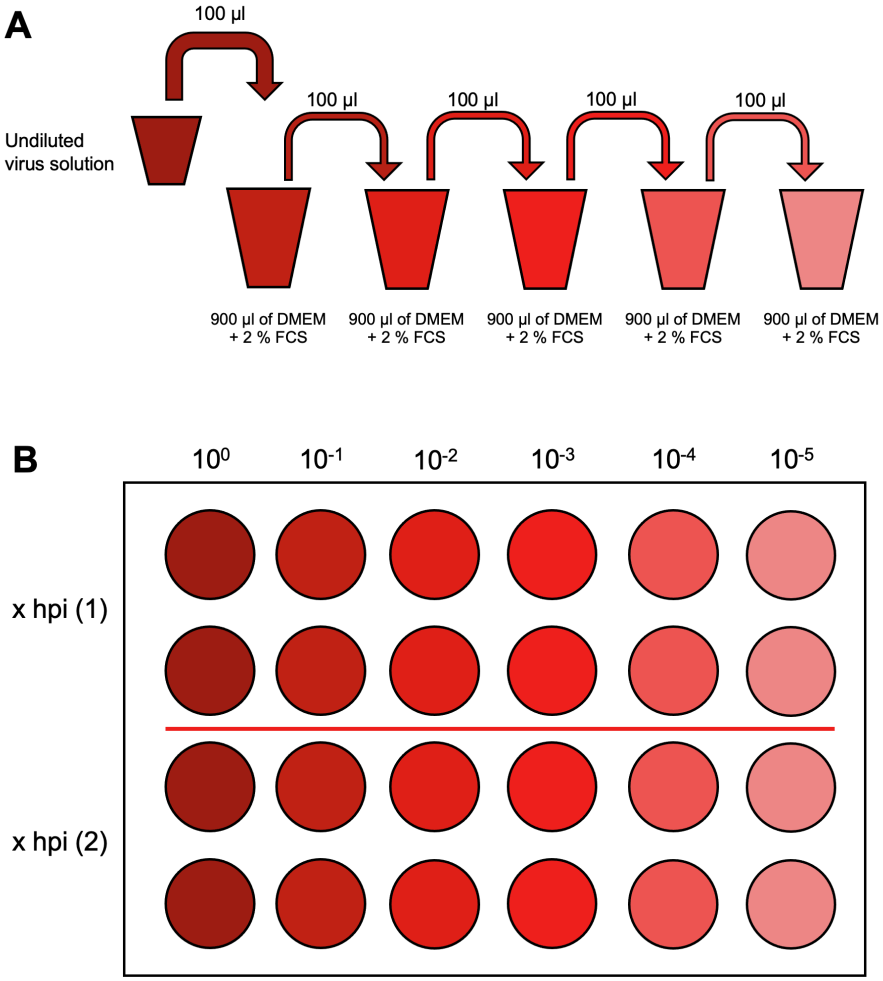

Figure 20: Step by step procedure for titration of GLV-0b347.
(A) Titration series for GLV-0b347.100 µl of the undiluted virus solution were added to 900 µl of DMEM + 5 % FCS. This procedure was repeated up to a dilution of 10^{-5}. **(B)** Exemplary culture plate for the titration of GLV-0b347 and T-VEC growth curves.

For titration of GLV-0b347 CV-1 cells were used. Cells were plated in 24-well-plates with 1 x 10^5 cells per well in DMEM + 10 % FCS. The next day, dilution series were prepared for each sample. Alternatively, 5 x 10^4 cells were seeded and titration was performed two days later, when cells were confluent. Four samples at a time were thawed in the water bath, vortexed and sonified for 30 seconds. Then, a dilution series up to 10^{-5} was created. For this purpose, 100 µl of the undiluted virus solution were transferred into a reaction tube containing 900 µl of DMEM + 2 % FCS. This dilution step was repeated four times. Then medium was removed from two wells of the CV-1 cells and 250 µl of virus dilution were added in duplicate. This was repeated for each dilution. On one 24-well plate two samples could be titrated. The plate was incubated for one hour. Then one ml of overlay medium containing 1.5 % carboxymethylcellulose, 5 % FCS and P/S was added to avoid viral spreading. After 2 days of incubation at 37 °C, 1 ml of crystal violet staining solution was added to each well. Staining was performed for at least three hours. Then, the overlay medium and staining solution were removed and discarded carefully, as crystal violet is a hazardous solution. Wells were washed several times with water until all of the staining solution was removed. After that, culture plates were irradiated under UV-light for at least 10 minutes, making sure to eradicate all of the left infectious particles. After drying, culture plates were laid on a luminous table to count the number of plaque forming units (PFU) with the naked eye. Only wells with 1-100 PFU were taken into account. Virus titer was then calculated by multiplying the average plaque count of the two samples by 4, as the medium volume in which the cells were infected was 250 µl and the titer is indicated per ml in the end. Then the result was multiplied by the inverse dilution rate. This calculation can be summarized by the following formula:

$$Virus\ titre\ \left(\frac{pfu}{ml}\right) = average\ plaque\ count\ (per\ dilution) x\ 4\ x\ dilution^{-1}$$

Equation 4: Calculation of the virus titer in pfu per ml.

2.2.4.4.3 Titration of T-VEC

Titration of T-VEC was performed on Vero cells. Vero cells were seeded in 24 well plates, with 5 x 10^4 cells and 500 µl per well. Further steps were as described in 2.2.4.4.2.

3 Results

In total, organoids from four different CRC patients could be established and cultured. Every organoid was infected with a panel of two Measles vaccine viruses (MeV-GFP and MeV-SCD), five different Vaccinia vaccine viruses (GLV-0b347, GLV-1h94, GLV-1h68, GLV-4h463 and GLV-1h254) and one Herpes simplex virus (Talimogene Laherparepvec; T-VEC). Pictures were taken of each CRC organoid and each treatment, respectively, at defined time points after infection (at 24 hpi, 48 hpi, 72 hpi and 96 hpi) with a phase contrast and fluorescence microscope.

The respective cell viability of each CRC organoid and treatment was measured at 96 hours post infection in a cell viability assay. Additionally, the effect of the well-known and established chemotherapeutic 5-fluorouracil (5-FU) was tested in different concentrations on these organoids as well.

Furthermore, growth curves of different virotherapeutics were generated for each CRC organoid, characterizing viral replication at different time points (at 24 hpi, 48 hpi, 72 hpi and 96 hpi).

Finally, CRC organoids were examined histologically, making sure that the tested organoids were harboring CRC tumor cells.

3.1 Organoid 22

3.1.1 Cell Viability Assay

The first cell viability assay of organoid 22 was conducted with a panel of five different viruses (MeV-GFP, GLV-0b347, MeV-SCD, GLV-1h94 and T-VEC), all at a multiplicity of infection (MOI) of 10, except T-VEC with a MOI of 1. Additionally, organoids were treated with MeV-SCD or GLV-1h94 in combination with 5-FC. As a reference for cell viability of organoids at 96 post infection (hpi) without any virotherapeutic or cell reductive treatment, organoids were treated only with medium (MOCK). To exclude any possible cell lytic effects of 5-FC on its own, 1 mM 5-FC was applied to organoids as well.

As expected, treatment with 1 mM 5-FC did not reduce viability, it was even slightly higher than in mock treated controls (113 %) (Fig. 21). Organoids which were infected with MeV-GFP at MOI 10 showed a mean viability reduction of almost 20 % (left cell viability of 82 %) in reference to MOCK. A similar outcome was seen in organoids treated with MeV-SCD at MOI 10 with a remaining cell viability of 83 %. In contrast, treatment with GLV-0b347 at MOI 10 reduced viability by 42 %. Infection with T-VEC at MOI 1 reduced viability by 47 %. In contrast, after combination treatment with MeV-SCD at MOI 10 and 1 mM 5-FC, viability was reduced to 12 %.

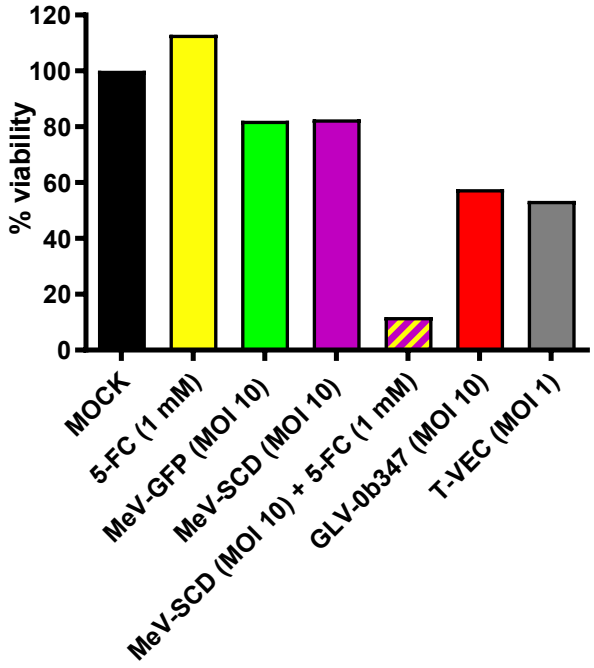

Figure 21: Cell viability assay of organoid 22 p11.
Cell viability of organoid 22 in passage no. 11 (p11) was measured at 96 hours post infection (hpi) in relation to treatment with only medium (MOCK; per definition 100 % cell viability). Results are given as percent cell viability in relation to MOCK. Organoids were treated with 5-FC (1 mM) as well as MeV-GFP (MOI 10), MeV-SCD (MOI 10), GLV-0b347 (MOI 10), MeV-SCD (MOI 10) + 5-FC (1 mM), and T-VEC (MOI 1). Mean values of one experiment performed in duplicates are shown.

In summary, organoid 22 treated with this selection of OVs showed the most efficient reduction in cell viability with combination treatment of MeV-SCD (MOI 10) and 1 mM 5-FC.

As treatment with Measles virus with suicide gene enhancement (MeV-SCD) worked well in the first experiment, another trial with a Vaccinia virus enhanced with a suicide gene (GLV-1h94) with an MOI of 10 was conducted. GLV-1h94 on its own showed a similar viability reduction as GLV-0b347 (29 %) (Fig. 22) in the experiment before (remaining cell viability of 71 %) (Fig. 21). The combination of GLV-1h94 (MOI 10) and 5-FC (1 mM) was even more efficient than the combination of MeV-SCD and 1 mM 5-FC in the first experiment with a remaining cell viability of 4.05%. As a control, organoids were treated with 5-FU (1 mM). Organoid 22 was highly susceptible to 5-FU with a remaining viability of only 0.8 %. Again, combination treatment of GLV-1h94 (MOI 10) and 1 mM 5-FC was superior to monotherapy with GLV-1h94 and almost as efficient as 5-FU on its own.

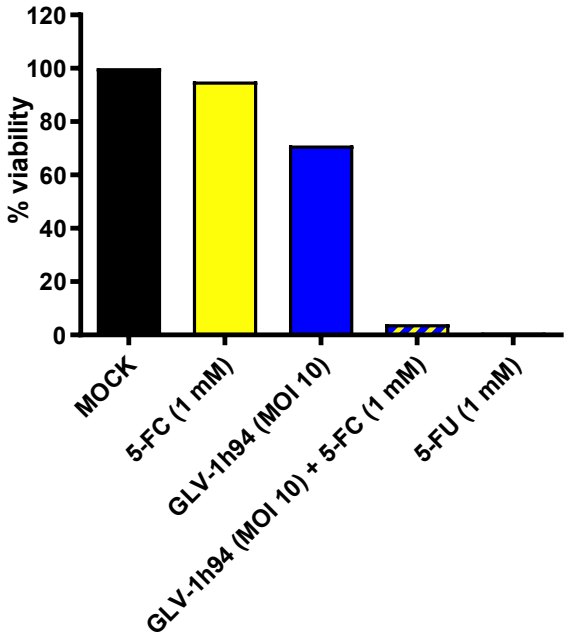

Figure 22: Cell viability assay of organoid 22 p19.
Cell viability of organoid 22 in passage no. 19 (p19) was measured at 96 hours post infection (hpi) in relation to treatment with only medium (MOCK; per definition 100 % cell viability). Results are given as percent cell viability in relation to MOCK. Organoids were treated with 5-FC (1 mM) as well as GLV-1h94 (MOI 10), GLV-1h94 (MOI 10) + 5-FC (1 mM) and 5-FU (1 mM). Mean values of one experiment performed in duplicates are shown.

In a next step a selection of different vaccinia virus strains was tested on organoid 22. Besides the already tested vaccinia viruses GLV-0b347 and GLV-1h94, organoid 22 was infected with three other vaccinia viruses (GLV-1h68, GLV-1h254 and GLV-4h463) as well, all at a MOI of 10.

As seen in passage 11 (Fig. 21), GLV-0b347 reduced viability by 42 %. GLV-1h94 reduced viability to 64 %. This is congruent with the results in passage 19 with a remaining viability of over 71 % (Fig. 22). Again, combination of GLV-1h94 and 5-FC was superior to monotherapy with a remaining cell viability of 7 %. The other three Vaccinia viruses showed similar results: GLV-4h463 was most effective in this panel with a viability reduction by 53 %, GLV-1h254 reduced viability by 48 % and GLV-1h68 by 42 %.

Furthermore, organoid 22 p20 was also treated with different concentrations of 5-FU (1 mM, 0.1 mM, and 0.01 mM) resulting in a dose-dependent reduction of viability. 5-FU treatment with a concentration of 1 mM reduced viability down to 1.2 % (Fig. 23), which was congruent to treatment of organoids in passage 19. At a concentration of 0.1 mM viability was reduced to 10.6 %, whereas organoids

treated with a concentration of 0.01 mM of 5-FU showed a remaining cell viability of 41 %.

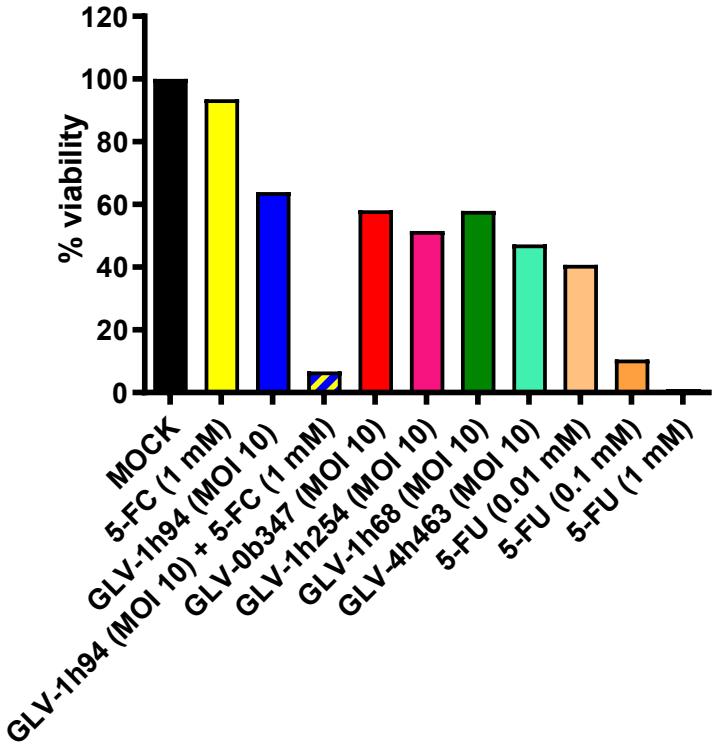

Figure 23: Cell viability assay of organoid 22 p20.
Cell viability of organoid 22 in passage no. 20 (p20) was measured at 96 hours post infection (hpi) in relation to treatment with only medium (MOCK; per definition 100 % cell viability). Results are given as percent cell viability in relation to MOCK. Organoids were treated with 5-FC (1 mM) as well as GLV-0b347 (MOI 10), GLV-1h94 (MOI 10), GLV-1h94 (MOI 10) + 5-FC (1 mM), GLV-1h68, GLV1h254 and GLV-4h463 (all MOI 10). Additionally, three different concentrations of 5-FU (0.01 mM, 0.1 mM and 1 mM were tested. Mean values of one experiment performed in duplicates are shown.

To sum it up: In general, combination therapy of virus with suicide gene enhancement and 1 mM 5-FC was most effective regarding reduction of cell viability in CRC organoid 22. Concerning monotherapy with virus, T-VEC (MOI 1) led to the highest reduction in cell viability compared to other monotherapies.

3.1.2 Phase contrast and fluorescence microscopic monitoring of cell growth and marker protein expression

Organoids were monitored by phase contrast and fluorescence microscopy during this 96-hour period. Phase contrast microscope pictures were used to identify changes in morphology of respective organoids. Cell lysis could be identified by the formation of small, round spheres at the edge of the organoids and disintegration. In this time span, organoids treated with OVs as well as chemotherapeutics or combination therapy showed distinct morphological changes which were (for the most part) congruent with decays in cell viability measured in previously shown cell viability assays. Infection of respective organoids could be monitored by expression of different marker proteins, which were detectable by fluorescence microscopy.

3.1.2.1 MOCK, 1 mM 5-FC, 0.01 mM 5-FU, 0.1 mM 5-FU and 1 mM 5-FU

Phase contrast pictures showed morphological changes of organoids during this 96-hour period being congruent to decays in cell viability. Organoids only treated with medium or 1 mM 5-FC showed no to minimal cell lysis and grew distinctly in the first 48 hours (Fig. 24). This is congruent to results in the cell viability assay, as organoids treated with 1mM 5-FC showed no significant reduction in cell viability compared to MOCK (Fig. 21, 22, 23). Organoids treated with 0.01 mM 5-FU also showed only minimal signs of cell lysis. In contrast, organoids treated with a higher concentration of 5-FU (0.1 mM) showed signs of disintegration starting at 72 hours post treatment (hpt). This effect was even more drastic in organoids treated with the highest concentration of 5-FU (1 mM), which already disintegrated at 48 hpt.

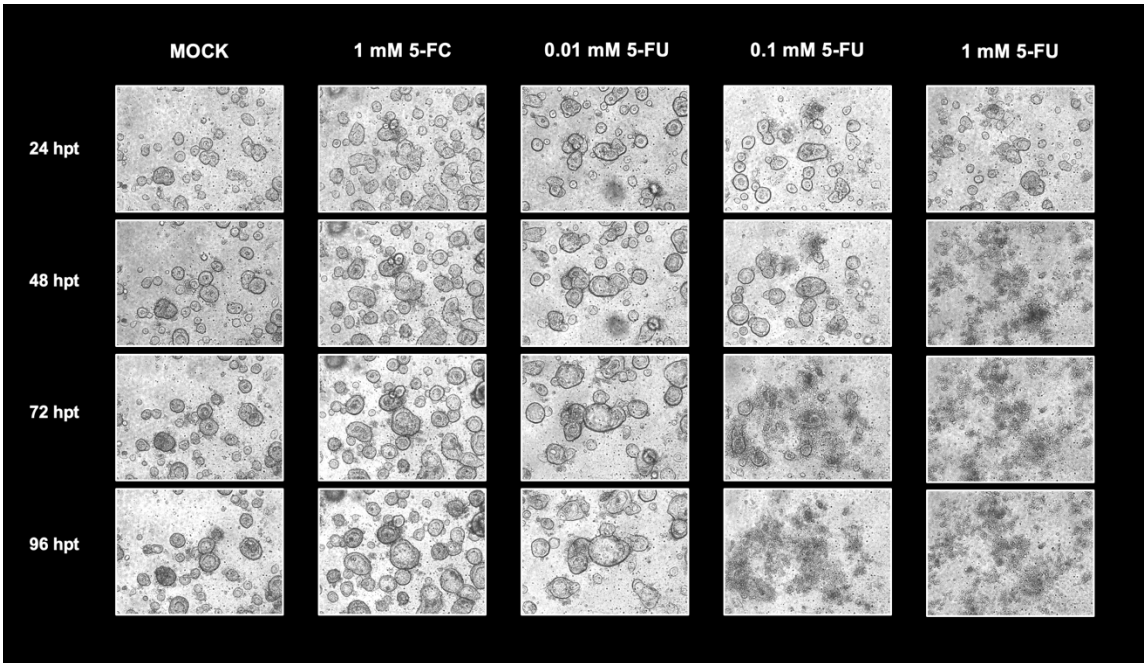

Figure 24: Phase contrast and fluorescence microscope pictures (10-fold magnification) of organoid 22 p20 treated with medium (MOCK), 1 mm 5-FC, 0.01 mM 5-FU, 0.1 mM 5-FU and 1 mM 5-FU at 24, 48, 72 and 96 hpt.

In summary, morphological changes detected by phase contrast microscopy were congruent to cell viability reduction measured in the Cell Titer Blue Assay.

3.1.2.2 MeV-GFP, MeV-SCD and MeV-SCD + 1 mM 5-FC

Organoids infected with MeV-GFP (MOI 10) presented little to no growth during this 96-hour time span. At 96 hpi these organoids showed signs of cell lysis. A fluorescent signal and thus sign of infection was detected at 48 hpi, increasing in intensity at 72 hpi (Fig. 25).

Organoids treated with MeV-SCD (MOI 10) and MeV-SCD + 1 mM 5-FC showed a syncytial growth pattern with separate organoid spheres merging with others. Organoids treated with MeV-SCD (MOI 10) showed almost no signs of cell lysis at 96 hpi (Fig. 25), which was congruent with high cell viability measured in the previously shown cell viability assay (Fig. 21). In contrast, organoids treated with MeV-SCD (MOI 10) in combination with 1 mM 5-FC already showed pronounced signs of disintegration at 48 hpi, resulting in a massive extent of cell lysis at 96 hpi. This was congruent with the significant reduction in cell viability previously measured (Fig. 21).

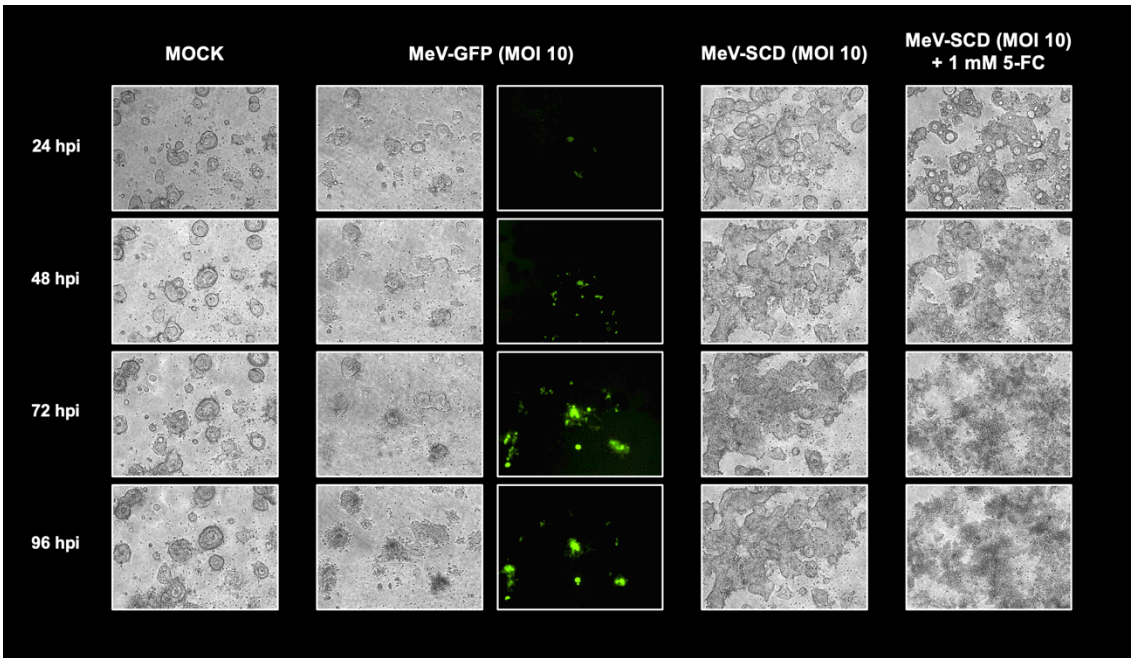

Figure 25: Phase contrast and fluorescence microscope pictures of organoid 22 p11 treated with medium (MOCK), MeV-GFP (MOI 10), MeV-SCD (MOI 10) and MeV-SCD (MOI 10) + 1 mM 5-FC at 24, 48, 72 and 96 hpi.

3.1.2.3 VACV GLV-1h94, GLV-1h94 + 1 mM 5-FC, GLV-0b347, GLV-1h254, GLV-1h68 and GLV-4h463

Organoids infected with GLV-1h94 (MOI 10) showed a homogenous fluorescent signal already at 24 hpi which did not change throughout the 96 hours after infection (Fig. 26).

Notably, organoids which received combination treatment of GLV-1h94 and 5-FC showed signs of cell lysis already at 48 hpi (Fig. 26). Interestingly, fluorescence seemed to be increasing as cell lysis increased during the 96-hour period in organoids treated with GLV-1h94 (MOI 10) + 1 mM 5-FC.

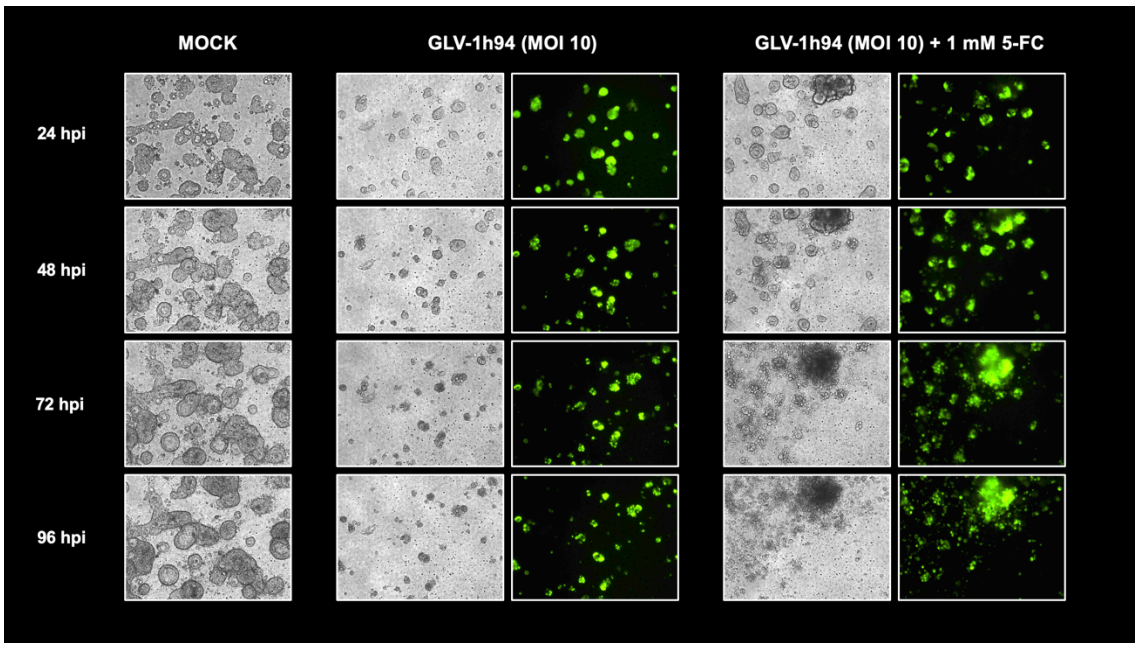

Figure 26: Phase contrast and fluorescence pictures of organoid 22 p19 treated with medium (MOCK), GLV-1h94 (MOI 10) and GLV-1h94 + 1 mM 5-FC at 24, 48, 72 and 96 hpi.

Organoid 22 was infected with GLV-0b347 as well. A red fluorescent signal could already be detected at 24 hpi which increased over the first 72 hours and finally decreased with organoids disintegrating in the last 24 hours of the 96-hour period (Fig. 27).

At 24 hpi, infection of individual organoids with GLV-1h254 could be detected. Viral infection spread along organoids, as visualized in fluorescent imaging at 48 and 72 hpi. Fluorescence signal stayed relatively homogenous for the rest of the 96 hours (Fig. 27).

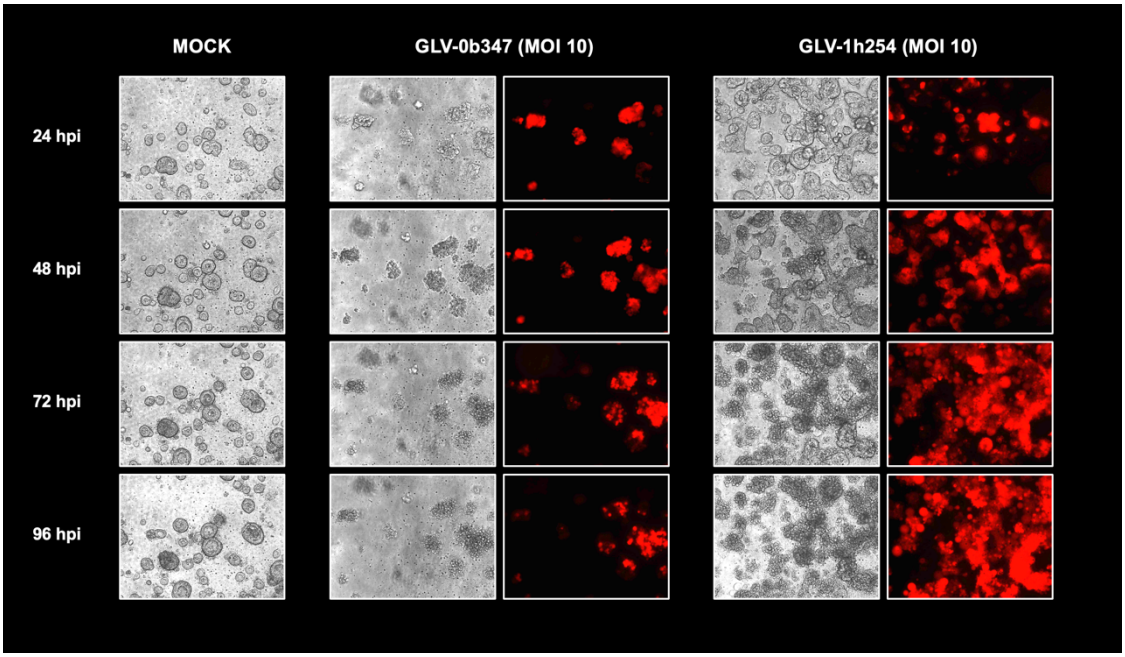

Figure 27: Phase contrast and fluorescence microscope pictures of organoid 22 p20 treated with medium, MOCK, GLV-0b347 (MOI 10) and GLV-1h254 (MOI 10) at 24, 48, 72 and 96 hpi.

A similar pattern of fluorescent signaling and beginning of cell lysis was seen in organoids infected with GLV-1h68 (MOI 10) and GLV-4h463 (MOI 10). At 24 hpi, organoids were successfully infected with respective OV as a fluorescent signal could be detected. Organoids showed signs of cell lysis starting at 48 hpi. Notably, fluorescent signal strongly increased at 72 and 96 hpi in organoids infected with GLV-4h463 (MOI 10) (Fig. 28).

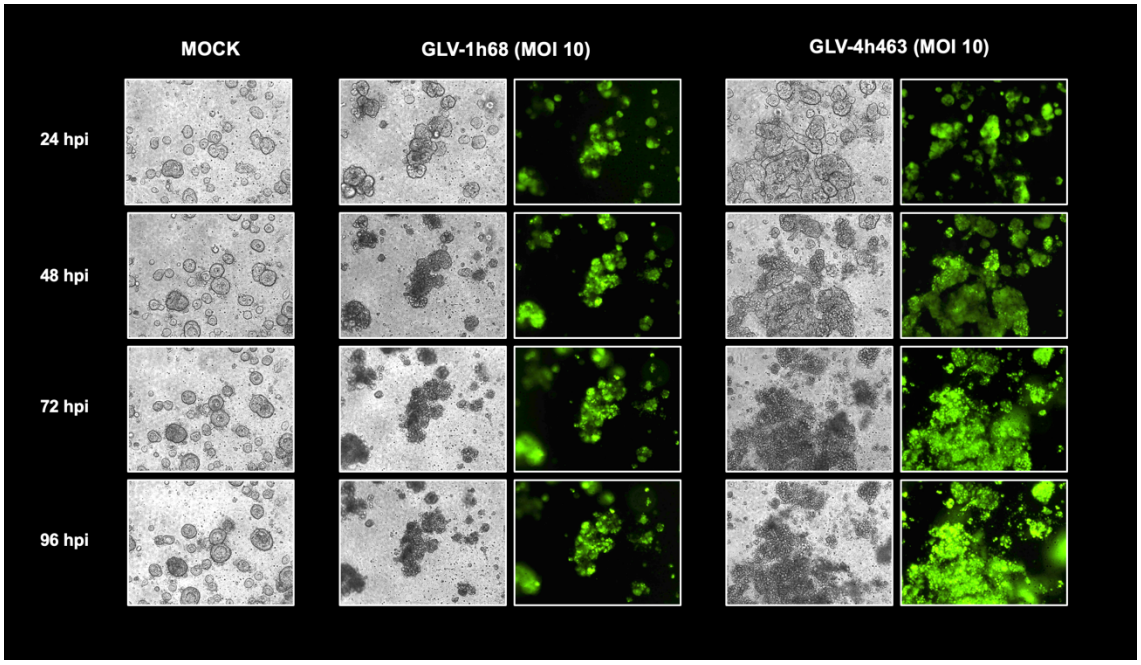

Figure 28: Phase contrast and fluorescence microscope pictures of organoid 22 p20 treated with medium (MOCK), GLV-1h68 (MOI 10) and GLV-4h463 (MOI 10) at 24, 48, 72 and 96 hpi.

To sum it up, infection of organoid 22 with all vaccinia viruses was already visible at 24 hpi. In total, vaccinia viruses showed a strong fluorescent signal, with fluorescence increasing during the 96-hour period and decreasing as cell lysis progressed. Notably, cell lysis and thus decrease of fluorescent signal started earlier in organoids treated with combination therapy of GLV-1h94 (MOI 10) + 1 mM 5-FC.

3.1.2.4 T-VEC

After infection of organoid 22 p11 with T-VEC (MOI 1), first signs of cell lysis could be detected at 48 hpi. At 72 hpi, signs of disintegration of organoids were clearly visible, especially compared to MOCK (Fig. 29).

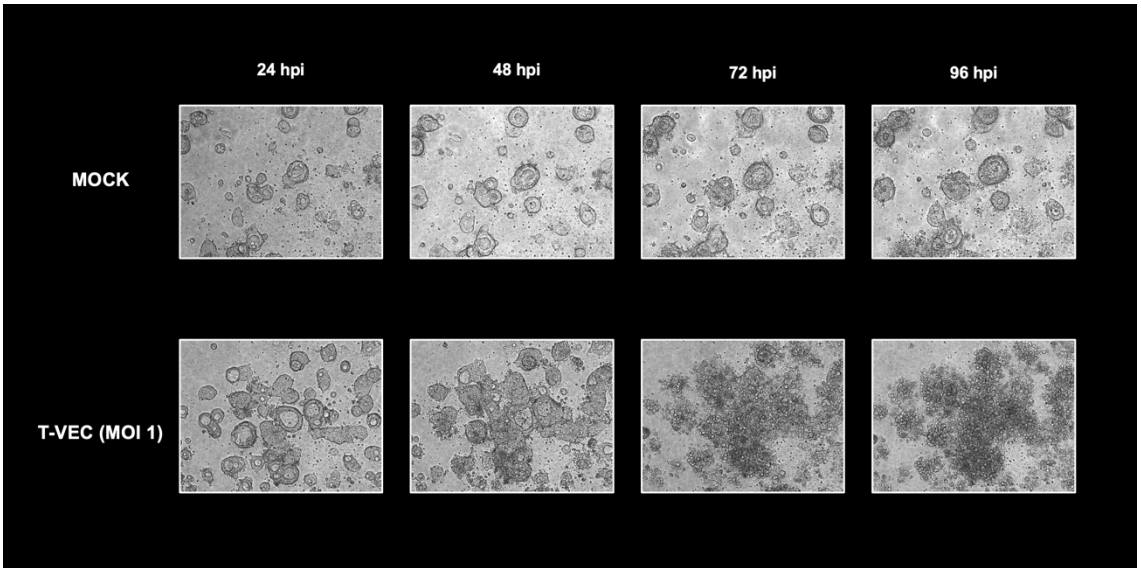

Figure 29: Phase contrast pictures of organoid 22 p11 treated with medium (MOCK) and T-VEC (MOI 1) at 24, 48, 72 and 96 hpi.

3.1.3 Virus Growth Curves

Viral growth curves show the number of infectious particles at different time points. Growth curves were generated for all organoids with three different viruses (MeV-GFP, GLV-0b347 and T-VEC).

3.1.3.1 MeV-GFP

Interestingly, viral titers of MeV-GFP showed a decline in the first 48 hpi, starting at over 1.8×10^5 PFU/ml at 3 hpi to 1.8×10^4 PFU/ml at 24 hpi and 2.1×10^3 PFU/ml at 48 hpi. From 48 hpi to 96 hpi viral titers remained on a plateau (Fig. 30).

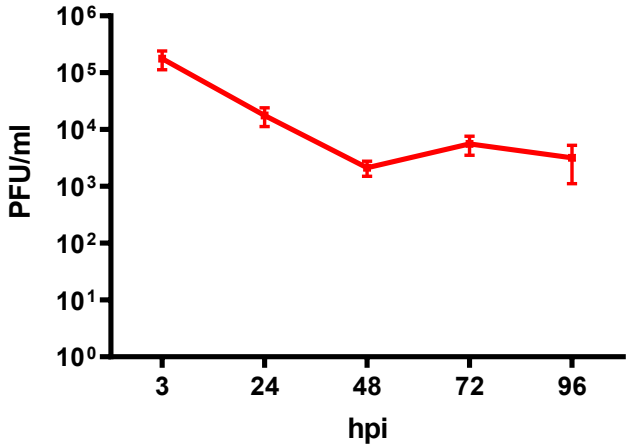

Figure 30: Virus growth curve of MeV-GFP in organoid 22.
Organoid 22 was infected with MeV-GFP at a multiplicity of infection of 10. Virus harvest took place at 3, 24, 48, 72 and 96 hpi. Samples were analysed via titration on Vero cells, the number of plaque forming units (PFU) was calculated per milliliter for each time point. Squares in this graphic represent the mean values of three independently analysed samples, error bars represent SD.

All in all, viral titers of MeV-GFP declined in the course of the first 48 hpi before hitting a plateau phase at 5.6×10^3 PFU/ml for the rest of the 96 hours.

3.1.3.2 GLV-0b347

The number of infectious particles of GLV-0b347 at 3 hpi was already relatively high with a viral load of 1.5×10^6 PFU/ml which did not change drastically during the whole observation period (Fig. 31).

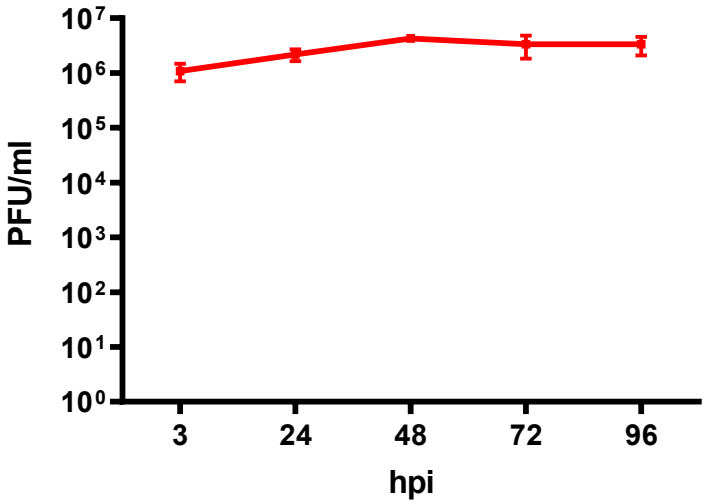

Figure 31: Virus growth curve of GLV-0b347 in organoid 22.
Organoid 22 was treated with GLV-0b347 at a multiplicity of infection of 10. Virus harvest took place at 3, 24, 48, 72 and 96 hpi. Samples were analysed via titration on CV-1 cells, the number of plaque forming units (PFU) was calculated per milliliter for each time point. Squares in this graphic represent the mean values of three independently analysed samples, error bars represent SD.

To sum it up: Viral titers of GLV-0b347 in organoid 22 stayed at a concentration of 1.5×10^6 PFU/ml during the duration of the assay. This indicates that there was no replication of GLV-0b347, as the number of plaque forming units at 3 hpi represents the inoculum.

3.1.3.3 T-VEC

At 3 hpi, organoids infected with T-VEC showed (in comparison to the other viruses) a relatively low number of infectious particles, corresponding to the lower multiplicity of infection. The number of infectious particles then increased from 2.5×10^4 PFU/ml at 3 hpi to 2.7×10^5 PFU/ml at 24 hpi to over $3x10^6$ PFU/ml at 48 hpi. Then viral growth reached a plateau phase at 4.7×10^6 PFU/ml from 72 hpi until 96 hpi (Fig. 32).

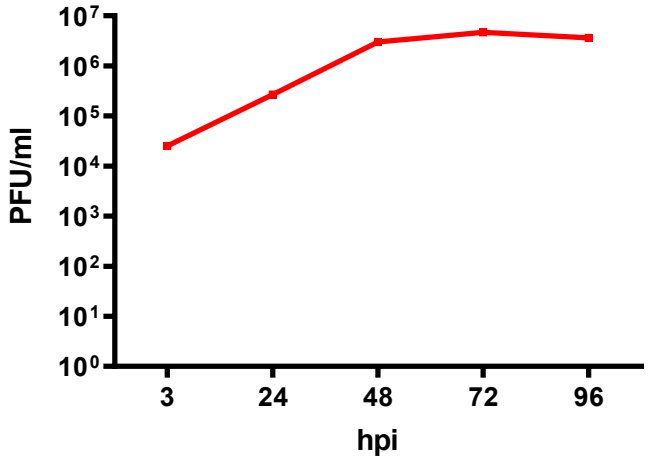

Figure 32: Virus growth curve of T-VEC in organoid 22.
Organoid 22 was infected with T-VEC at a multiplicity of infection of 1. Virus harvest took place at 3, 24, 48, 72 and 96 hpi. Samples were analysed via titration on Vero cells, the number of plaque forming units (PFU) was calculated per milliliter for each time point. Squares in this graphic represent the mean values of three independently analysed samples, error bars represent SD.

In summary, concentration of infectious particles of T-VEC started low at 2.7×10^4 PFU/ml and increased up to 48 hpi when a plateau phase was reached until 96 hpi.

3.2 Organoid 25

3.2.1 Cell Viability Assay

Organoid 25 in passage 16 was tested with the whole selection of viruses. Treatment with 5-FC alone showed a small reduction in viability of less than 6 %. Infection with MeV-GFP resulted in a reduction in viability of 54 %. Monotherapy with MeV-SCD (MOI 10) reduced cell viability by 49 %. In contrast, combination of MeV-SCD with 5-FC completely killed the organoid (remaining cell viability of 0.6 %). T-VEC was tested at a MOI of 1 and showed the highest efficacy in cell viability reduction of all viruses without suicide gene enhancement resulting in a remaining cell viability of less than 20 % (Fig. 33).

In this organoid, vaccinia viruses showed a much higher heterogeneity in cell viability reduction than previously seen in organoid 22 (Fig. 33). Infection with GLV-0b347 reduced cell viability by 55 %. Treatment with GLV-1h94 was more effective, reducing cell viability by more than 68 %. Combination treatment of GLV-1h94 with 5-FC reduced cell viability to 1.5 %, similar to combination treatment of MeV-SCD with 5-FC. GLV-4h463 and GLV-1h254 were the most effective vaccinia viruses, both reducing cell viability by more than 70 % in this passage (Fig. 33). As a positive control, 5-FU in different concentrations was tested as well. Interestingly, in contrast to organoid 22, even the lowest concentration of 0.01 mM 5-FU reduced viability to 1.7 %. Treatment with 0.1 mM FU reduced viability to 0.6 %, treatment with 1 mM 5-FU to 0.5%.

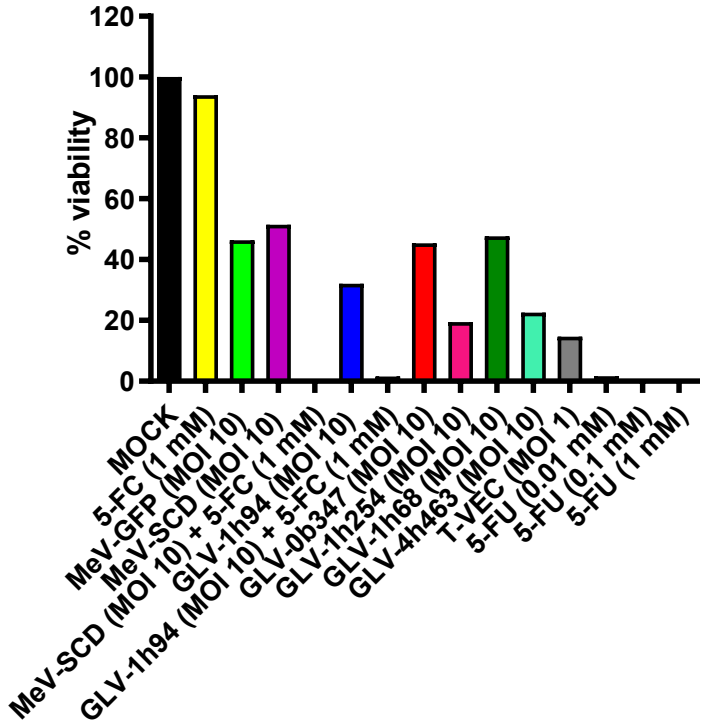

Figure 33: Cell Viability Assay of organoid 25 p16.
Cell viability of organoid 25 in passage no. 16 (p16) was measured at 96 hours post infection (hpi) in relation to treatment with only medium (MOCK; per definition 100 % cell viability). Results are given as percent cell viability in relation to MOCK. Organoids were treated with 5-FC (1 mM) as well as MeV-GFP (MOI 10), MeV-SCD (MOI 10), MeV-SCD (MOI 10) + 5-FC (1 mM), GLV-0b347 (MOI 10), GLV-1h94 (MOI 10), GLV-1h94 (MOI 10) + 5-FC (1 mM), GLV-1h68 (MOI 10), GLV-1h254 (MOI 10), GLV-4h463 (MOI 10) and T-VEC (MOI 1). Additionally, Organoid 25 p16 was treated with three different concentrations of 5-FU (0.01 mM, 0.1 mM and 1 mM). Mean values of one experiment performed in duplicates are shown.

To sum it up: Combination treatment with MeV-SCD and 5-FC or GLV-1h94 and 5-FC proved to be most effective in this selection of tested virotherapeutics. Organoid 25 was highly sensitive to 5-FU. Notably, T-VEC at a lower MOI of 1 turned out to be the most effective virus without suicide gene enhancement.

3.2.2 Phase contrast and fluorescence microscopic monitoring of cell growth and marker protein expression

3.2.2.1 MOCK, 1 mM 5-FC, 0.01 mM 5-FU, 0.1 mM 5-FU and 1 mM 5-FU

After treatment with medium or 1mM 5-FC organoid 25 showed almost no signs of cell lysis. In fact, organoids seemed to grow in this 96-hour period. Interestingly, phase contrast pictures of organoid 25 treated with three different concentrations of 5-FU all showed extensive signs of cell lysis already at 24 hpt (Fig. 34). This is congruent with the massive cell reduction of organoid 25 in the cell viability assay, even at low concentrations of 5-FU (Fig. 33).

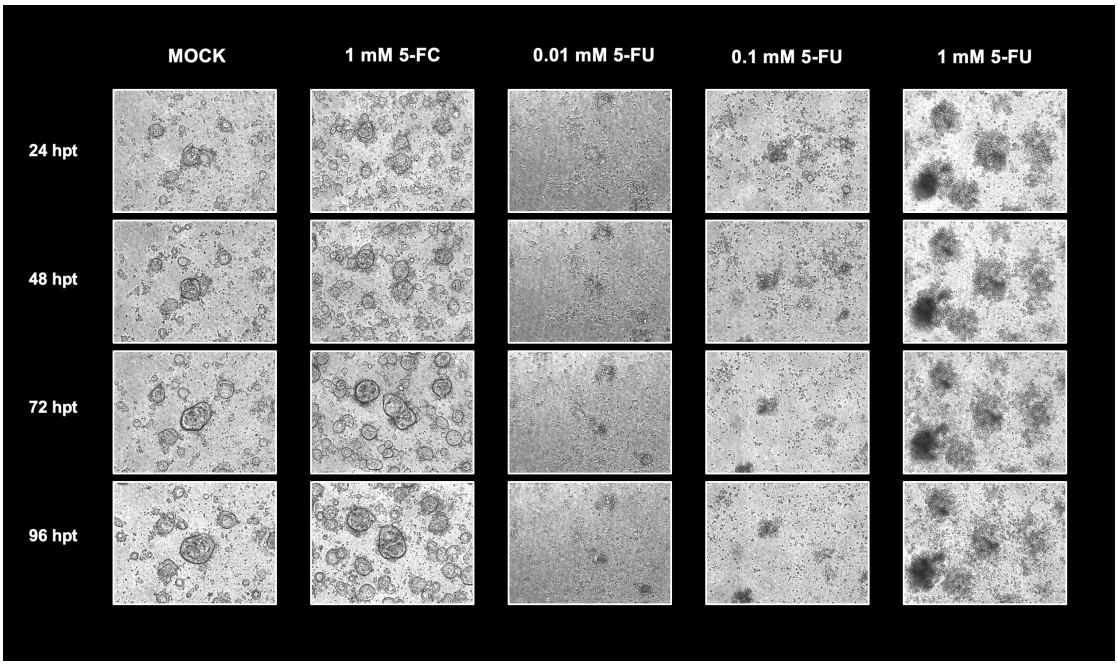

Figure 34: Phase contrast and fluorescence microscope pictures (10-fold magnification) of organoid 25 p16 treated with medium (MOCK), 1 mm 5-FC, 0.01 mM 5-FU, 0.1 mM 5-FU and 1 mM 5-FU at 24, 48, 72 and 96 hpt.

3.2.2.2 MeV-GFP, MeV-SCD and MeV-SCD + 1 mM 5-FC

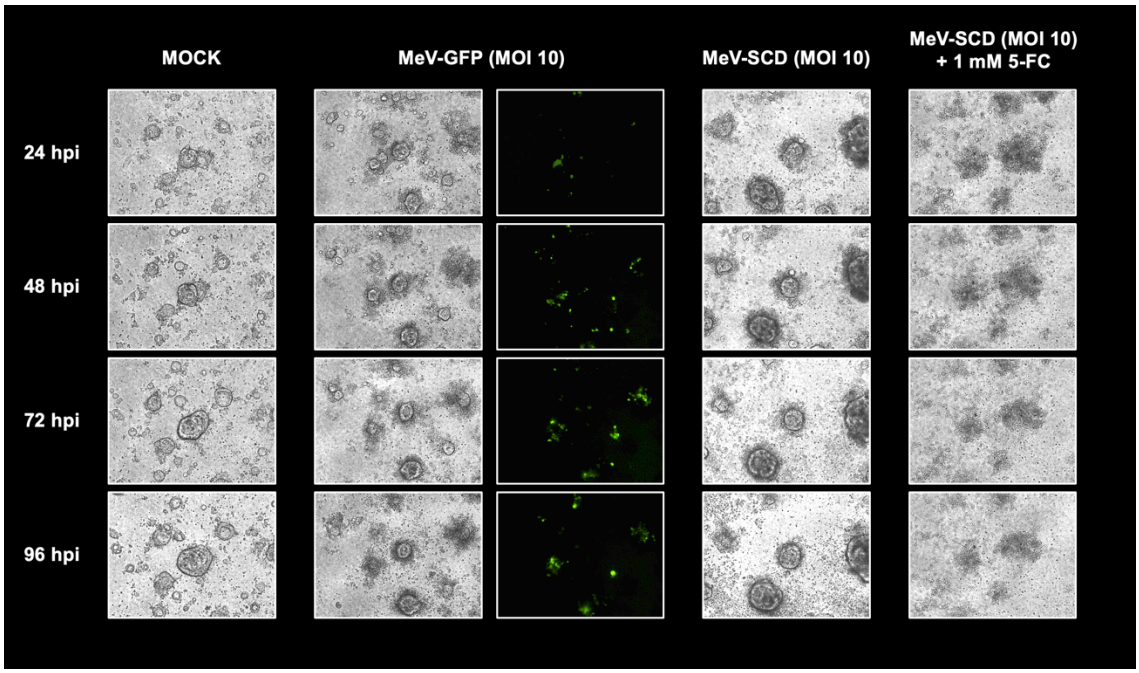

Figure 35: Phase contrast and fluorescence microscope pictures of organoid 25 p16 treated with medium (MOCK), MeV-GFP (MOI 10), MeV-SCD (MOI 10) and MeV-SCD (MOI 10) + 1 mM 5-FC at 24, 48, 72 and 96 hpi.

Organoid 25 treated with MeV-GFP (MOI 10) showed signs of cell lysis as early as 24 hpi in phase contrast pictures, but they weren't as extensive as in organoids treated with 5-FU (Fig. 35). Signs of cell lysis in organoid 25 as seen in phase contrast pictures increased during the 96-hour period. A fluorescent signal was detected at 24 hpi which only slightly increased in the next 48 hours. Similar to that, organoid 25 treated with MeV-SCD also showed discrete signs of cell lysis but was still relatively intact after 96 hours. In contrast, combination therapy of MeV-SCD (MOI 10) and 1 mM 5-FC in organoid 25 resulted in massive signs of cell lysis already after 24 hours. At 96 hpi it was completely disintegrated (Fig. 35).

3.2.2.3 VACV GLV-1h94, GLV-1h94 + 1 mM 5-FC, GLV-0b347, GLV-1h254, GLV-1h68 and GLV-4h463

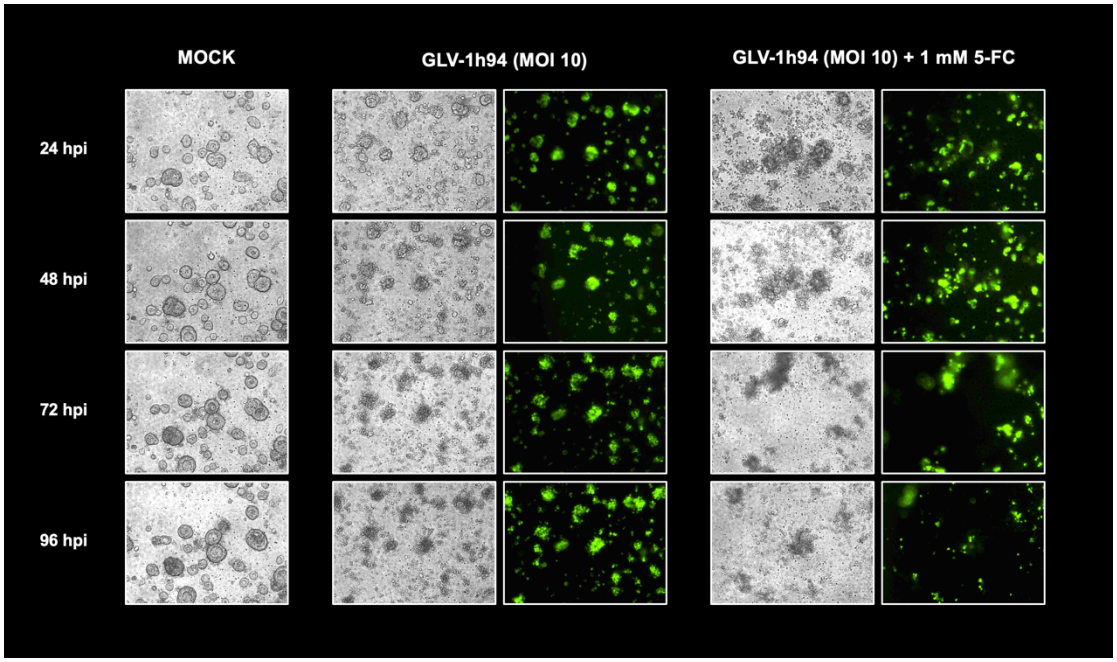

Figure 36: Phase contrast and fluorescence pictures of organoid 25 p16 treated with medium (MOCK), GLV-1h94 (MOI 10) and GLV-1h94 + 1 mM 5-FC at 24, 48, 72 and 96 hpi.

In organoid 25 infected with GLV-1h94, a fluorescent signal could already be detected at 24 hpi. Interestingly, extensive morphological changes were not detectable until 48 hpi (Fig. 36). In contrast, similar to organoids treated with combination therapy of MeV-SCD (MOI 10) and 1 mM 5-FC, organoids treated with combination therapy of GLV-1h94 (MOI 10) and 1 mM 5-FC showed massive signs of cell lysis already at 24 hpi and were completely disintegrated at 96 hpi. A fluorescent signal in organoids treated with combination therapy could be detected as well at 24 hpi (Fig. 36).

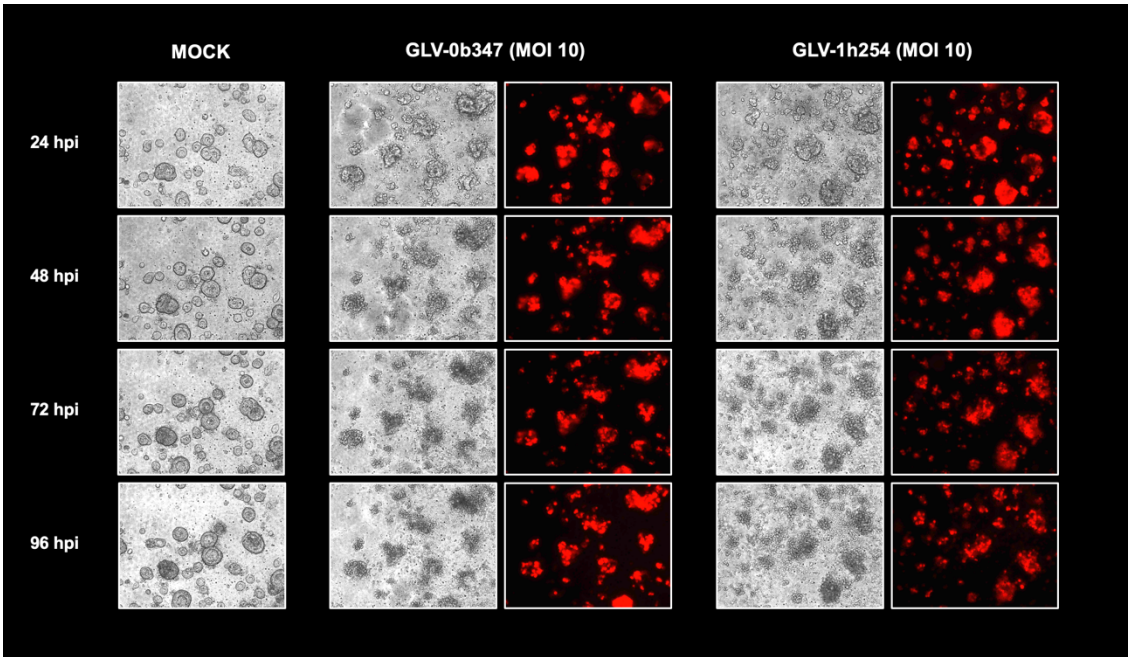

Figure 37: Phase contrast and fluorescence microscope pictures of organoid 25 p16 treated with medium (MOCK), GLV-0b347 (MOI 10) and GLV-1h254 (MOI 10) at 24, 48, 72 and 96 hpi.

In organoid 25 infected with GLV-0b347, a strong fluorescent signal could already be detected at 24 hpi. Interestingly, distinct morphological changes could only be spotted at 48 hpi. Areas with fluorescent signal were congruent with areas of extensive cell lysis. This was also the case in organoids treated with GLV-1h254: a fluorescent signal could already be detected at 24 hpi, but distinct morphological changes in phase contrast pictures were not observable until 48 hpi. Both organoids treated with GLV-0b347 or GLV-1h254 respectively were completely disintegrated after 96 hours (Fig. 37).

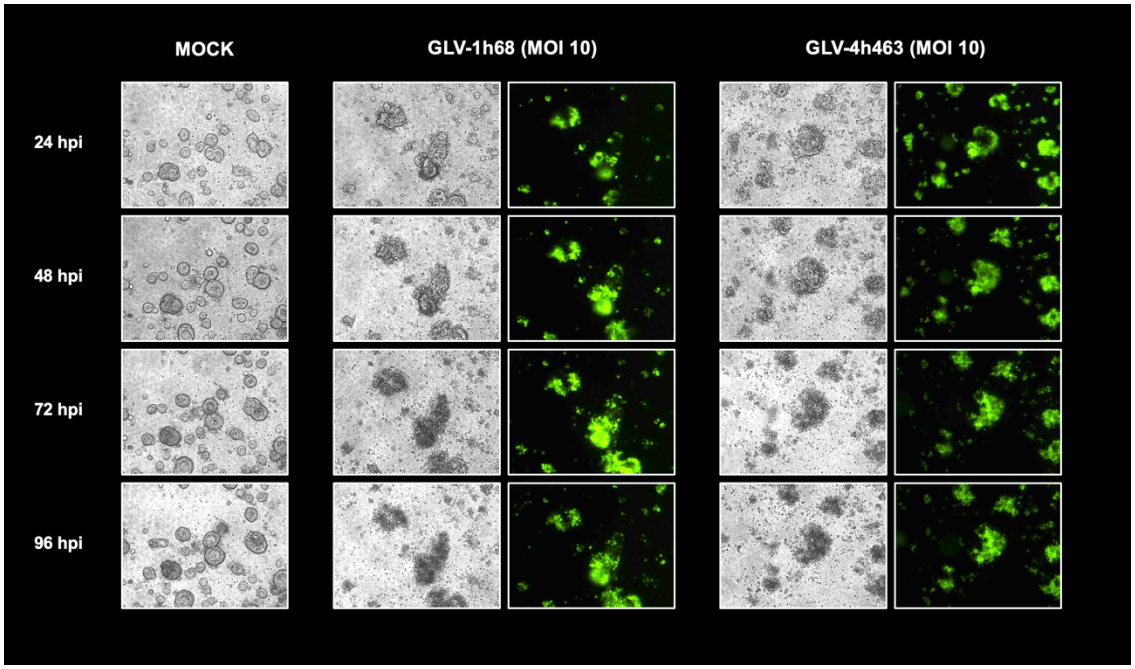

Figure 38: Phase contrast and fluorescence microscope pictures of organoid 25 p16 treated with medium (MOCK), GLV-1h68 (MOI 10) and GLV-4h463 (MOI 10) at 24, 48, 72 and 96 hpi.

Like organoids treated with vaccinia viruses before, in organoid 25 infected with GLV-1h68 a fluorescent signal could be detected at 24 hpi. Again, distinct morphological changes were not detectable until 48 hpi. At 72 hpi, organoids were completely disintegrated (Fig. 38). In organoids treated with GLV-4h463, a fluorescent signal was also detectable at 24 hpi and distinct morphological changes could be observed at 48 hpi. Like organoids infected with GLV-1h68, organoids treated with GLV-4h463 were completely disintegrated at 72 hpi (Fig. 38).

3.2.2.4 T-VEC

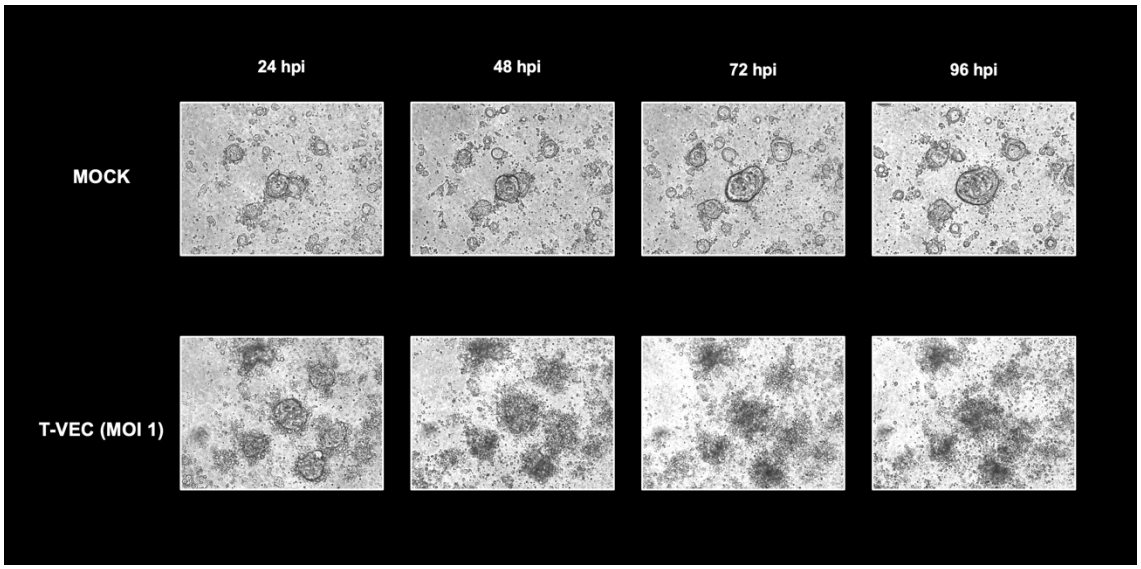

Figure 39: Phase contrast pictures of organoid 25 p16 treated with medium (MOCK) and T-VEC (MOI 1) at 24, 48, 72 and 96 hpi.

In organoid 25 infected with T-VEC (MOI 1), morphological changes could already be detected at 24 hpi. These signs of cell lysis spread throughout the next 72 hours. At 96 hpi, organoid 25 was completely disintegrated (Fig. 39).

3.2.3 Virus Growth Curves

3.2.3.1 MeV-GFP

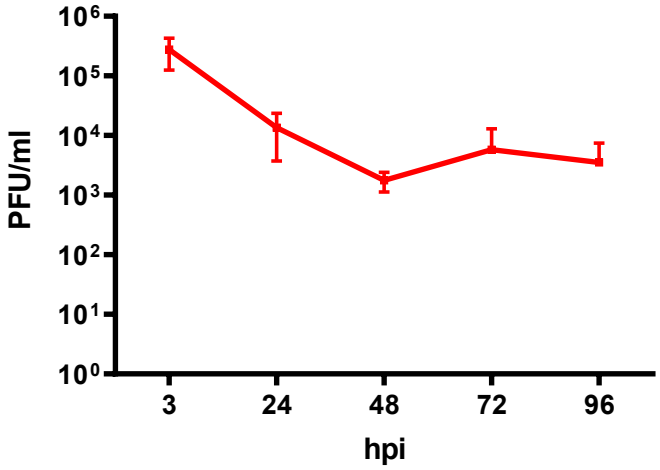

Figure 40: Virus growth curve of MeV-GFP (MOI 10) in organoid 25.
Organoid 25 was infected with MeV-GFP at a multiplicity of infection of 10. Virus harvest took place at 3, 24, 48, 72 and 96 hpi. Samples were analysed via titration on Vero cells, the number of plaque forming units (PFU) was calculated per milliliter for each time point. Squares in this graphic represent the mean values of three independently analysed samples, error bars represent SD.

Viral titers of MeV-GFP in organoid 25 showed, similar to organoid 22, a decline between 3 hpi and 48 hpi from 2.8×10^5 PFU/ml to 2.1×10^3 PFU/ml. In contrast to organoid 22, there was a rise in viral titer to 5.6×10^4 at 72 hpi. After that, the titer decreased again to 3.2×10^3 PFU/ml at 96 hpi (Fig. 40).

To sum it up, titers of MeV-GFP in organoid 25 decreased in the time span of 96 hours, starting at 2.8×10^5 PFU/ml at 3 hpi and ending at 3.2×10^3 PFU/ml at 96 hpi.

3.2.3.2 GLV-0b347

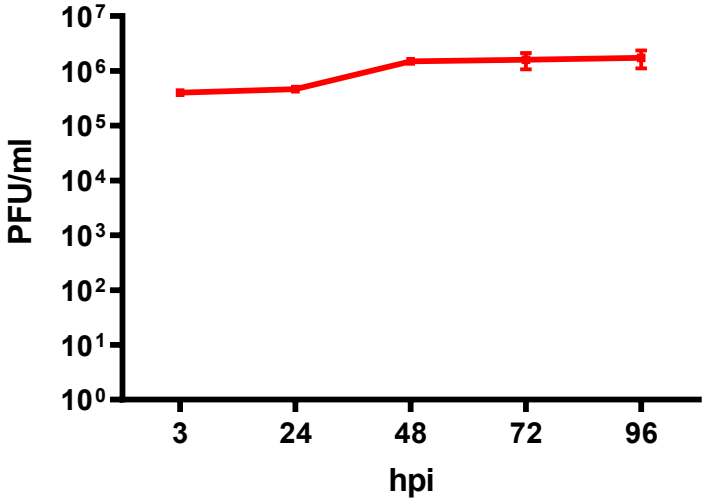

Figure 41: Virus growth curve of GLV-0b347 in organoid 25.
Organoid 25 was infected with GLV-0b347 at a multiplicity of infection of 10. Virus harvest took place at 3, 24, 48, 72 and 96 hpi. Samples were analysed via titration on CV-1 cells, the number of plaque forming units (PFU) was calculated per milliliter for each time point. Squares in this graphic represent the mean values of three independently analysed samples, error bars represent SD.

In organoid 25, viral titers of GLV-0b347 showed no significant change between 3 hpi and 24 hpi, starting at 4.1×10^5 PFU/ml. The number of infectious particles increased slightly between 24 hpi and 48 hpi from 4.7×10^5 to 1.5×10^6 before hitting a plateau phase from 48 hpi to 96 hpi (Fig. 41).

3.2.3.3 T-VEC

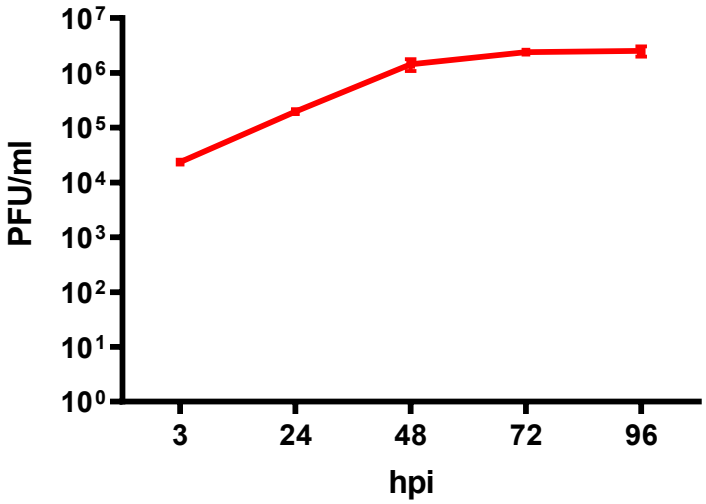

Figure 42: Virus growth curve of T-VEC in organoid 25.
Organoid 25 was infected with T-VEC at a multiplicity of infection of 1. Virus harvest took place at 3, 24, 48, 72 and 96 hpi. Samples were analysed via titration on Vero cells, the number of plaque forming units (PFU) was calculated per milliliter for each time point. Squares in this graphic represent the mean values of three independently analysed samples, error bars represent SD.

Virus growth curve for T-VEC showed a similar pattern in organoid 25 as in organoid 22: Starting from 2.3×10^4 PFU/ml at 3 hpi, the titer rose to 2×10^5 at 24 hpi and 1.4×10^6 at 48 hpi. At 48 hpi a plateau was reached and no further increase in viral titers could be observed at 72 and 96 hpi (Fig. 42).

3.3 Organoid 29

3.3.1 Cell Viability Assay

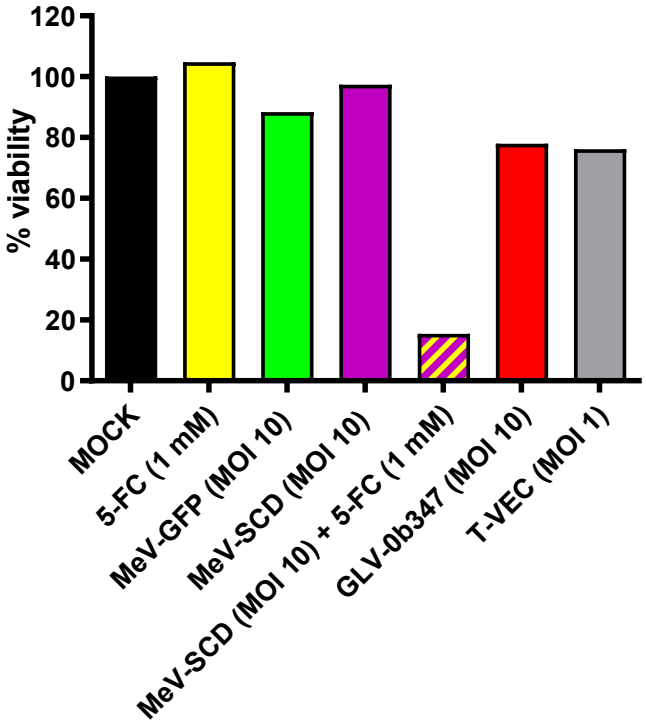

Figure 43: Cell Viability Assay of organoid 29 p9.
Cell viability of organoid 29 in passage no. 9 (p9) was measured at 96 hours post infection (hpi) in relation to treatment with only medium (MOCK; per definition 100 % cell viability). Results are given as percent cell viability in relation to MOCK. Organoids were treated with 5-FC (1 mM) as well as MeV-GFP (MOI 10), MeV-SCD (MOI 10), MeV-SCD (MOI 10) + 5-FC (1 mM), GLV-0b347 (MOI 10) and T-VEC (MOI 1). Mean values of one experiment performed in duplicates are shown.

In a first experiment organoid 29 p9 was infected with 4 different viruses, namely MeV-GFP, MeV-SCD with or without 5-FC, GLV-0b347 and T-VEC. In addition, the organoid was treated with 5-FC only. As expected, treatment with 5-FC (1 mM) did not reduce cell viability. Organoids infected with MeV-GFP at a MOI of 10 showed a minimal reduction in viability of 11.4 %. Treatment with MeV-SCD showed similar results: monotherapy with MeV-SCD at a MOI of 10 showed almost no reduction in cell viability (remaining cell viability of 97 %). In contrast, combination treatment of MeV-SCD with 5-FC was strikingly more effective with a cell viability reduction of 85 %. Treatment with GLV-0b347 showed similar results as treatment with MeV-GFP with a remaining cell viability of 78 %. Surprisingly, monotherapy with T-VEC only reduced viability by 24 % (Fig. 43).

To sum it up: This organoid showed a much higher resistance to the whole selection of tested OVs compared to the other organoids. All tested monotherapies had similar results. An exception was combination treatment of MeV-SCD with 5-FC, which showed a pronounced reduction of cell viability.

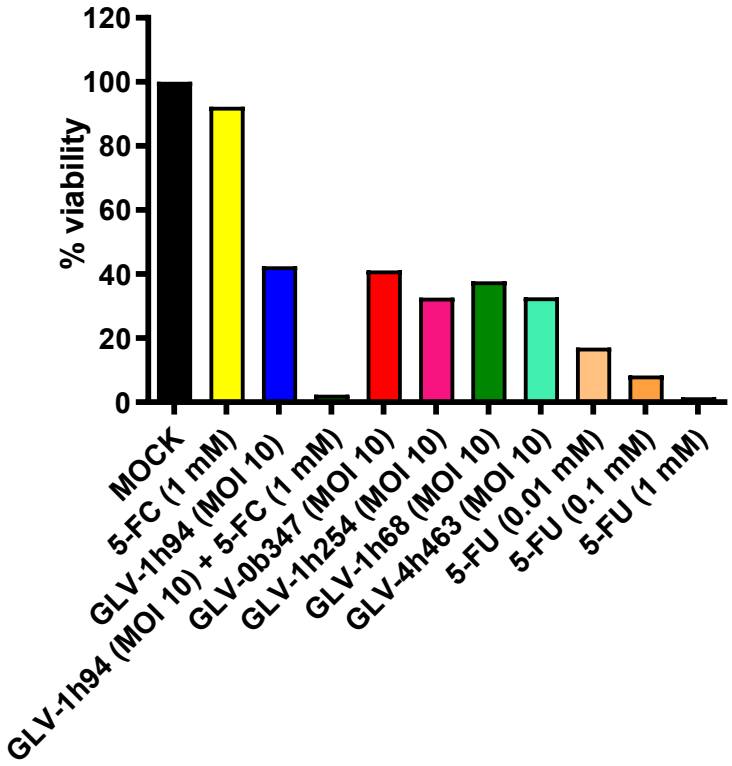

Figure 44: Cell Viability Assay of organoid 29 p23.
Cell viability of organoid 29 in passage no. 23 (p23) was measured at 96 hours post infection (hpi) in relation to treatment with only medium (MOCK; per definition 100 % cell viability). Results are given as percent cell viability in relation to MOCK. Organoids were treated with 5-FC (1 mM) as well as GLV-0b347 (MOI 10), GLV-1h94 (MOI 10), GLV-1h94 (MOI 10) + 5-FC (1 mM), GLV-1h68, GLV1h254 and GLV-4h463 (all at MOI 10). Additionally, three different concentrations of 5-FU (0.01 mM, 0.1 mM and 1 mM) were tested on organoid 29 p23 as well. Mean values of one experiment performed in duplicates are shown.

Next, organoid 29 was treated with a selection of different vaccinia viruses as well as different concentrations of 5-FU (1 mM, 0.1 mM and 0.01 mM). As expected, treatment with 5-FC showed no reduction in cell viability with a remaining cell viability of 92 %. In contrast to the first experiment, infection with GLV-0b347 at MOI 10 now reduced cell viability by 59 % (Fig. 44) compared to 22 % in the first experiment (Fig. 43). Infection with GLV-1h94 reduced viability by 58 %. Combination treatment with GLV-1h94 (MOI 10) and 1 mM 5-FC showed a massive reduction in cell viability with a remaining cell viability of only 2.4%. This value is comparable to the effect of 1 mM 5-FU in this organoid. The other tested

vaccinia viruses (GLV-4h463, GLV-1h254 and GLV-1h68) showed similar effects with a cell viability reduction of over 60 % as well. 5-FU showed a dose dependent effect on viability. Interestingly, organoid 29 was not as susceptible to 5-FU as organoid 25 with a remaining cell viability of 17 % at 0.01 mM 5-FU, 8 % at 0.1 mM 5-FU and 2 % at 1 mM 5-FU (Fig. 44).

To sum it up: All tested vaccinia viruses showed similar efficacies regarding cell viability reduction. Combination treatment of GLV-1h94 with 5-FC (1 mM) showed the highest reduction in cell viability, similar to treatment with 1 mM 5-FU.

3.3.2 Phase contrast and fluorescence microscopic monitoring of cell growth and marker protein expression

3.3.2.1 MOCK, 1 mM 5-FC, 0.01 mM 5-FU, 0.1 mM 5-FU and 1 mM 5-FU

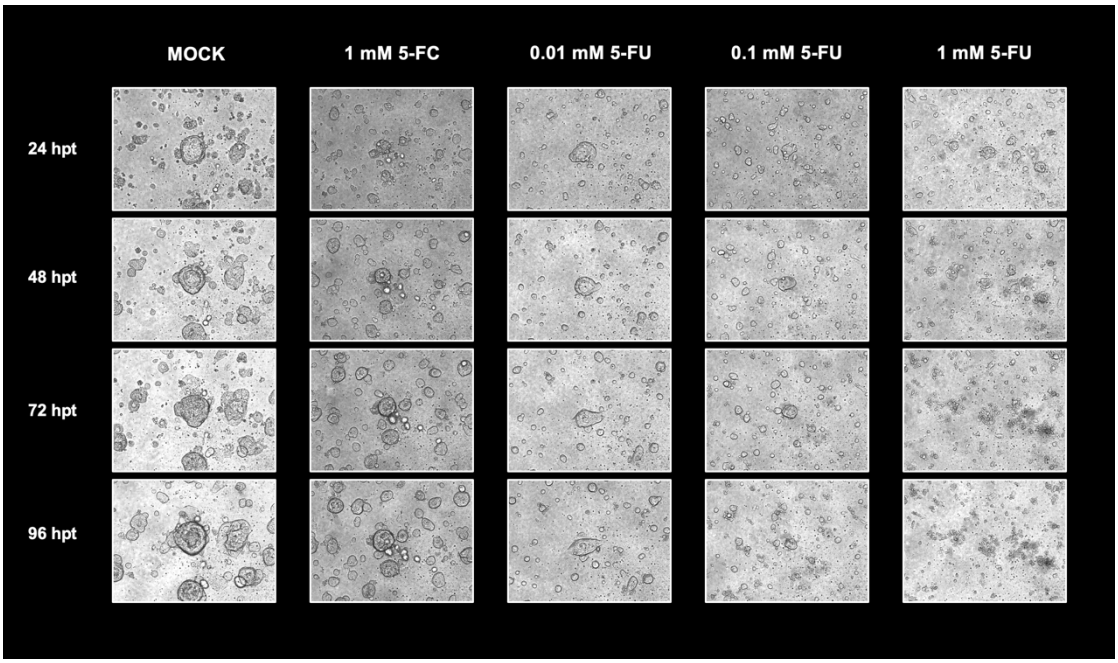

Figure 45: Phase contrast and fluorescence microscope pictures (10-fold magnification) of organoid 29 p23 treated with medium (MOCK), 1 mm 5-FC, 0.01 mM 5-FU, 0.1 mM 5-FU and 1 mM 5-FU at 24, 48, 72 and 96 hpt.

Similar to previously tested organoids, organoid 29 treated with either medium only (MOCK) or 1 mM 5-FC grew during the observation period of 96 hours and showed no signs of cell lysis. In contrast, organoids treated with 1 mM 5-FU showed extensive morphological changes and were fully disintegrated at 72 hpi. Organoids treated with 0.1 mM 5-FU also fully disintegrated, but not until 96 hpi. Interestingly, organoids treated with 0.01 mM 5-FU, the lowest concentration, showed no distinct signs of cell lysis (Fig. 45).

3.3.2.2 MeV-GFP, MeV-SCD and MeV-SCD + 1 mM 5-FC

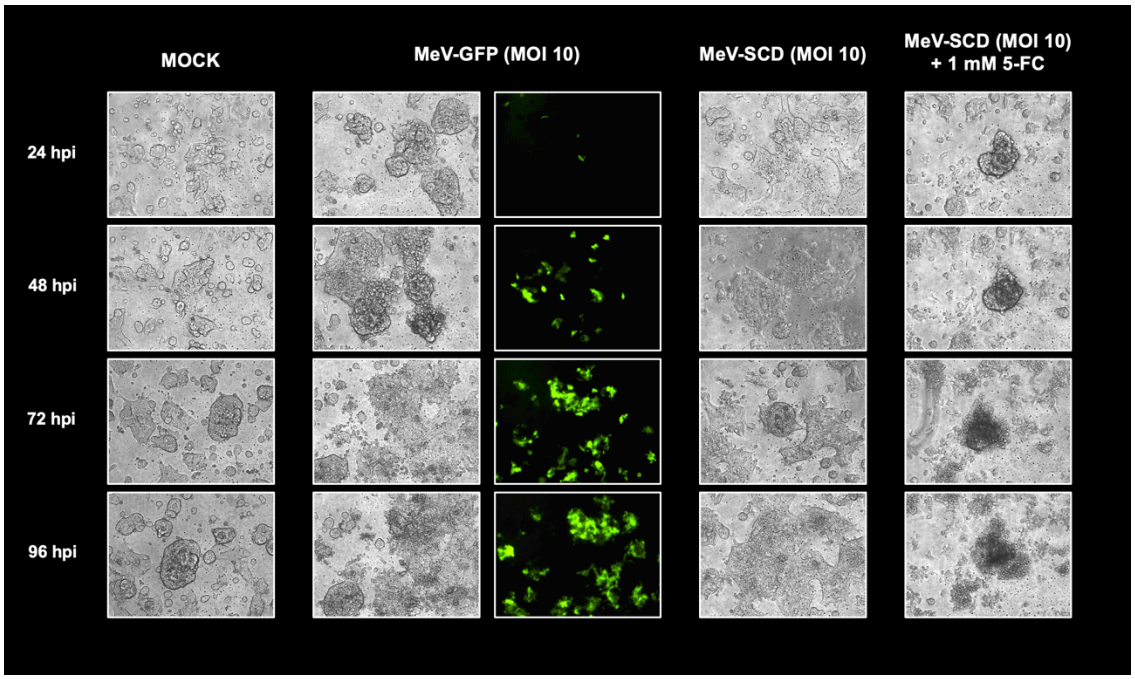

Figure 46: Phase contrast and fluorescence microscope pictures of organoid 29 p9 treated with medium (MOCK), MeV-GFP (MOI 10), MeV-SCD (MOI 10) and MeV-SCD (MOI 10) + 1 mM 5-FC at 24, 48, 72 and 96 hpi.

As observed in previously tested organoids, organoid 29 treated with MeV-GFP (MOI 10) showed a significant fluorescent signal at 48 hpi. Slight morphological changes could be observed at 72 hpi, but organoid 29 was still relatively intact at 96 hpi. This was also the case after infection with MeV-SCD (MOI 10), where only minor morphological changes could be detected at 96 hpi. In contrast to that, phase contrast pictures of organoid 29 treated with combination therapy of MeV-SCD (MOI 10) + 1 mM 5-FC showed massive signs of cell lysis at 72 hpi. Organoid 29 treated with combination therapy was completely disintegrated at 96 hpi (Fig. 46).

3.3.2.3 VACV GLV-1h94, GLV-1h94 + 1 mM 5-FC, GLV-0b347, GLV-1h254, GLV-1h68 and GLV-4h463

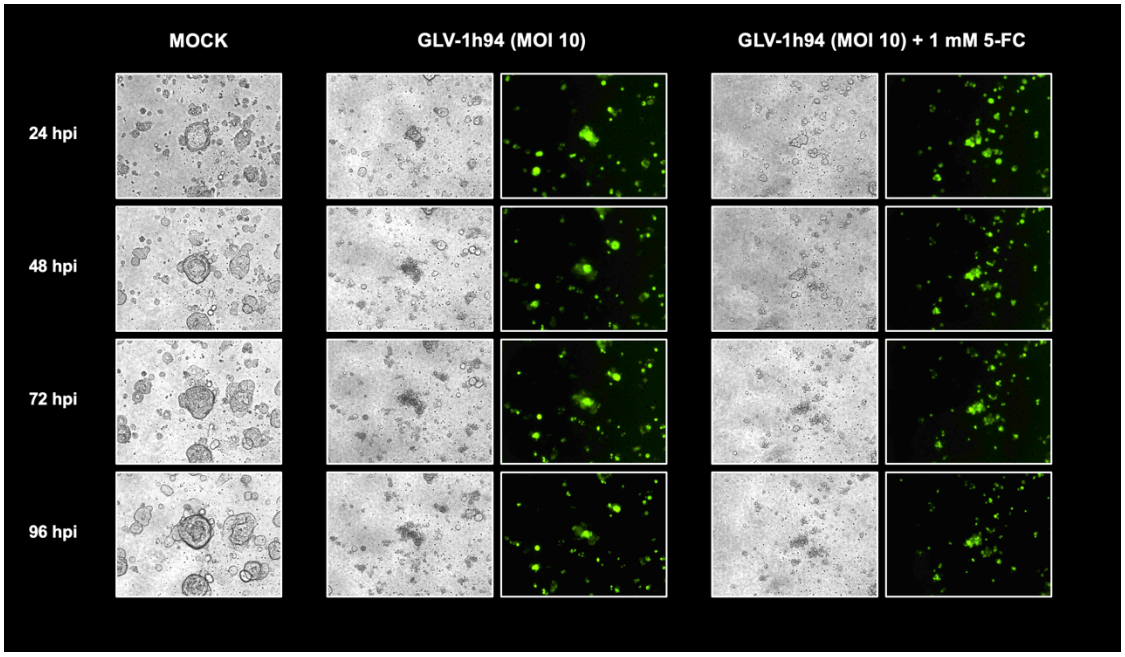

Figure 47: Phase contrast and fluorescence pictures of organoid 29 p23 treated with medium (MOCK), GLV-1h94 (MOI 10) and GLV-1h94 + 1 mM 5-FC at 24, 48, 72 and 96 hpi.

Similar to previously tested organoids infected with vaccinia viruses, a fluorescent signal was detectable at 24 hpi in organoids infected with GLV-1h94 as well as organoids treated with combination therapy of GLV-1h94 (MOI 10) and 1 mM 5-FC. Morphological changes during monotherapy with GLV-1h94 (MOI 10) were observed at 48 hpi and in organoids treated with combination therapy only at 72 hpi (Fig. 47). Notably, density of organoids in both pictures was rather low, so changes in morphology could not be judged reliably.

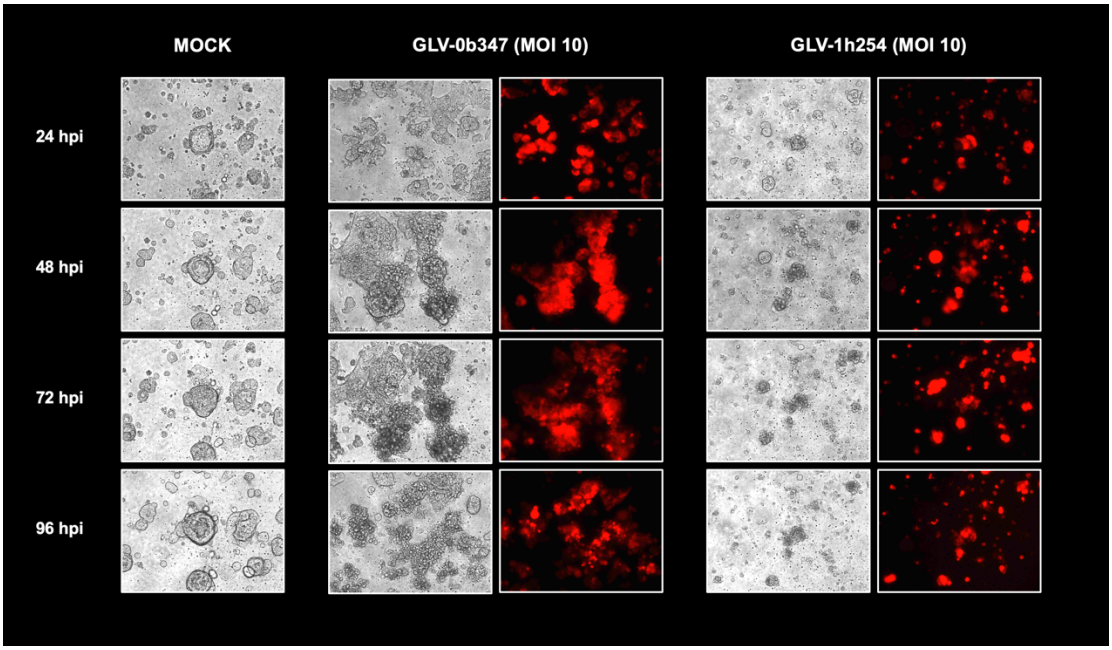

Figure 48: Phase contrast and fluorescence pictures of organoid 29 p9 treated with medium (MOCK) and GLV-0b347 (MOI 10) and organoid 29 p23 infected with GLV-1h254 at 24, 48, 72 and 96 hpi.

In organoids infected with GLV-0b347 (MOI 10) or with GLV-1h254 (MOI 10), a fluorescent signal could be detected as early as 24 hpi whereas morphological changes were detectable not until 48 hpi. Organoid 29 treated with GLV-0b347 (MOI 10) showed massive signs of cell lysis at 96 hpi (Fig. 48).

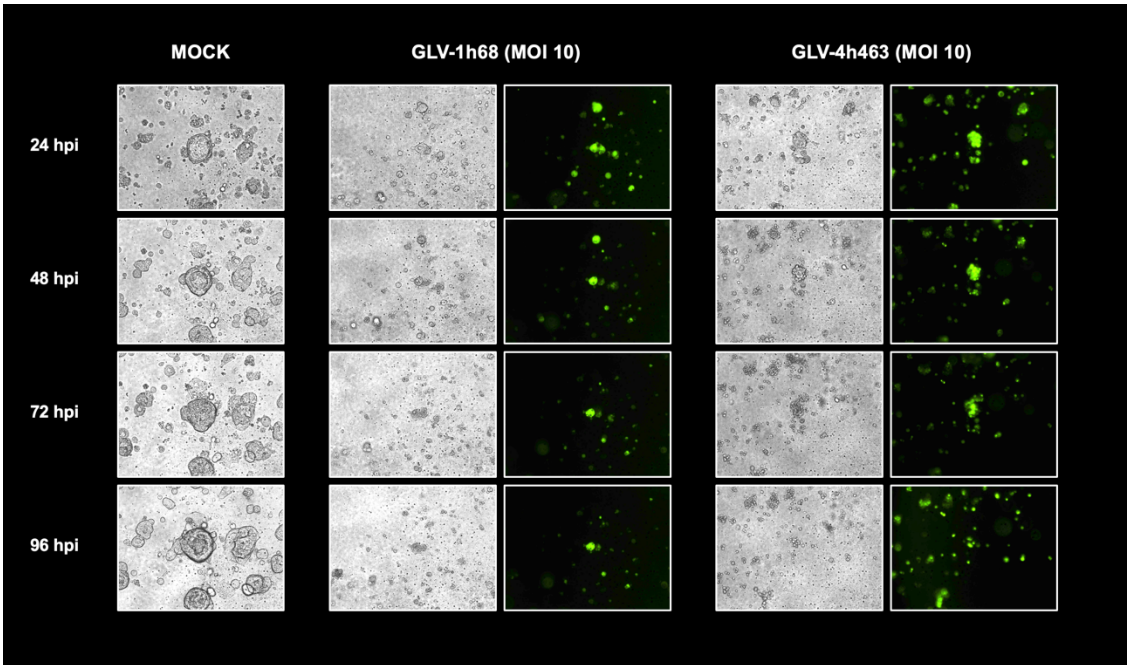

Figure 49: Phase contrast and fluorescence pictures of organoid 29 p23 treated with medium (MOCK), GLV-1h68 (MOI 10) and GLV-4h463 (MOI 10) at 24, 48, 72 and 96 hpi.

After infection with GLV-1h68 or GLV-4h463 at MOI 10, respectively, a fluorescent signal could be detected at 24 hpi. Signs of cell lysis in phase contrast pictures could be observed at 48 hpi in both organoids resulting in a complete disintegration of organoid 29 at 72 hpi. Again, organoids were relatively small, so morphological changes could only be assessed to a limited extent (Fig. 49).

3.3.2.4 T-VEC

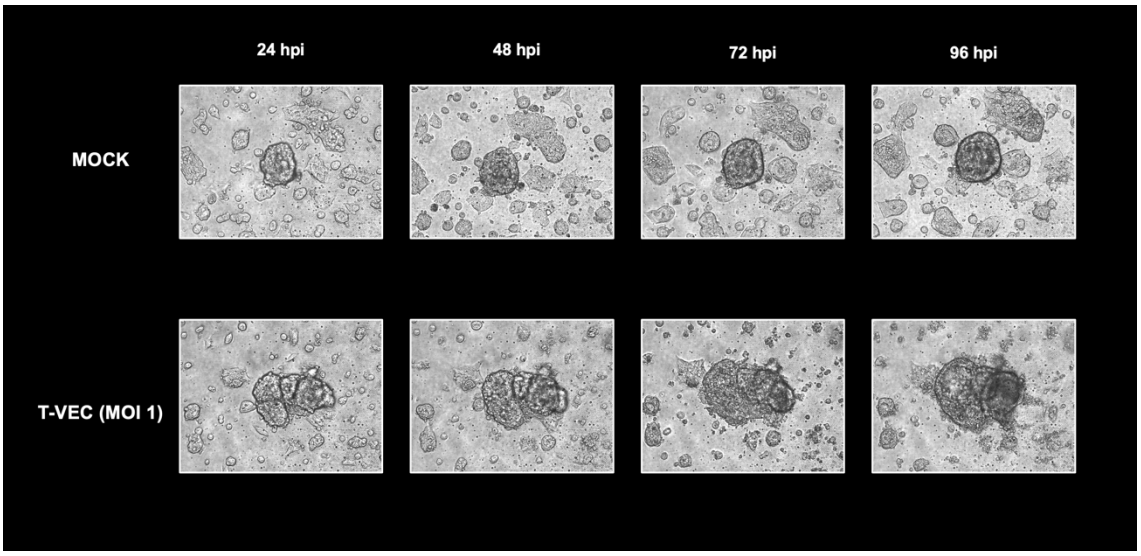

Figure 50: Phase contrast pictures of organoid 29 p9 treated with medium (MOCK) and T-VEC at 24, 48, 72 and 96 hpi.

Organoid 29 in passage 9 infected with T-VEC (MOI 1) showed an interesting growth pattern: organoids grew in this 96-hour period but at the same time showed signs of cell lysis with apoptotic bodies forming at the edge of respective organoid. Notably, in these pictures a rather sizeable organoid with a syncytial growth pattern was observed, which was surrounded by smaller cell conglomerations (Fig. 50).

3.3.3 Virus growth curves

3.3.3.1 MeV-GFP

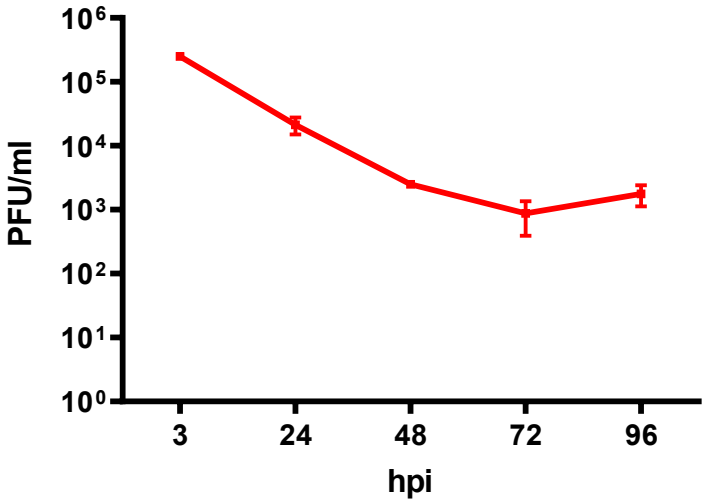

Figure 51: Virus growth curve of MeV-GFP (MOI 10) in organoid 29.
Organoid 29 was infected with MeV-GFP at a multiplicity of infection of 10. Virus harvest took place at 3, 24, 48, 72 and 96 hpi. Samples were analysed via titration on Vero cells, the number of plaque forming units (PFU) was calculated per milliliter for each time point. Squares in this graphic represent the mean values of three independently analysed samples, error bars represent SD.

Congruent to the virus growth curves before, viral titers in organoid 29 showed a decline from 2.5×10^5 PFU/ml at 3 hpi to 2.1×10^4 PFU/ml at 24 hpi and 2.5×10^3 PFU/ml at 48 hpi before hitting the minimum of 8.8×10^2 PFU/ml at 72 hpi. Interestingly, replication then increased to 1.8×10^3 PFU/ml at 96 hpi (Fig. 51). This decline in infectious particles in the first 48 hpi before hitting a plateau phase between 48 hpi and 96 hpi is similar to results in organoid 22 (Fig. 30).

3.3.3.2 GLV-0b347

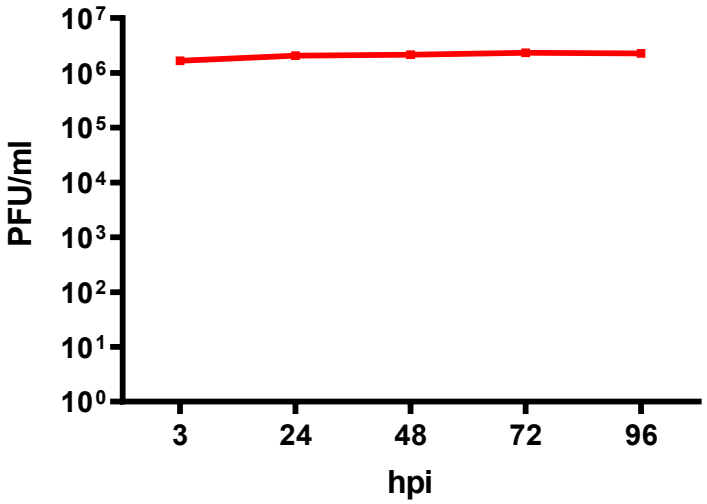

Figure 52: Virus growth curve of GLV-0b347 in organoid 29.
Organoid 29 was infected with GLV-0b347 at a multiplicity of infection of 10. Virus harvest took place at 3, 24, 48 , 72 and 96 hpi. Samples were analysed via titration on CV-1 cells, the number of plaque forming units (PFU) was calculated per milliliter for each time point. Squares in this graphic represent the mean values of three independently analysed samples, error bars represent SD.

Viral titers of GLV-0b347 in organoid 29 showed a plateau phase at 1.7×10^6 PFU/ml between 3 hpi and 96 hpi (Fig. 52). This growth curve is also very similar to the growth curves of GLV-0b347 of organoid 22 (Fig. 31) and 25 (Fig. 41), which also showed no or only very small increases in titers.

3.3.3.3 T-VEC

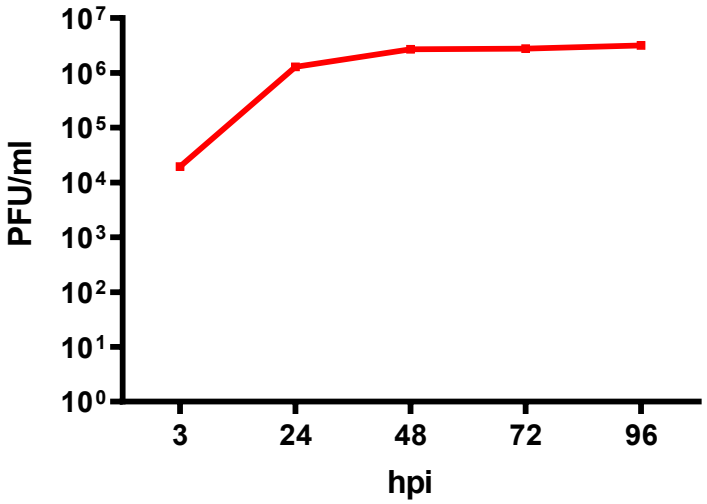

Figure 53: Virus growth curve of T-VEC in organoid 29.
Organoid 29 was infected with T-VEC at a multiplicity of infection of 1. Virus harvest took place at 3, 24, 48, 72 and 96 hpi. Samples were analysed via titration on Vero cells, the number of plaque forming units (PFU) was calculated per milliliter for each time point. Squares in this graphic represent the mean values of three independently analysed samples, error bars represent SD.

The number of infectious particles in organoids treated with T-VEC increased from 2×10^4 PFU/ml at 3 hpi to 1.3×10^6 PFU/ml at 24 hpi. After that, virus replication only increased slightly between 24 hpi and 48 hpi before hitting a plateau between 48 hpi and 96 hpi at 3.1×10^6. Compared to the other organoids treated with T-VEC, replication in organoid 29 showed a similar total increase of infectious particles from 2×10^4 to 1.3×10^6 PFU/ml, but in contrast to the others, in a period of 24 hours compared to 48 hours (Fig. 53).

3.3.3.4 MeV-SCD and MeV-SCD + 1 mM 5-FC

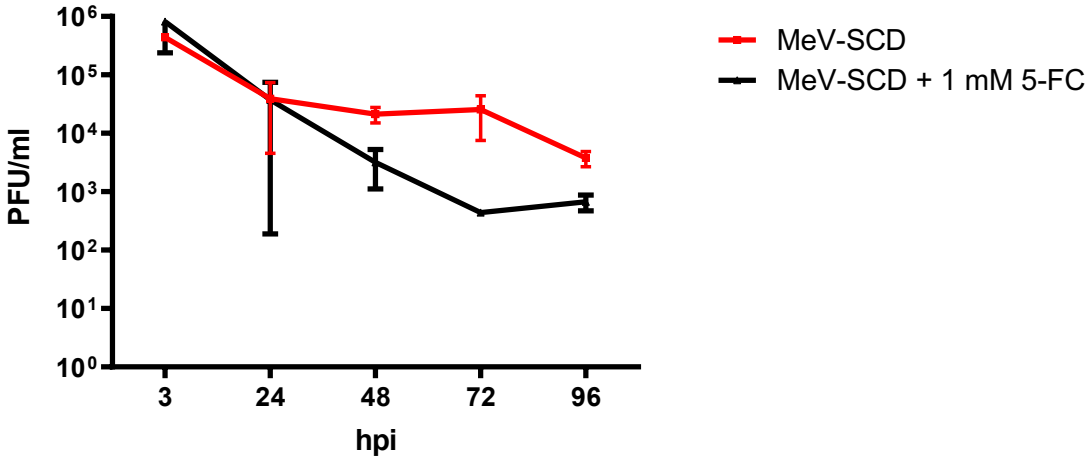

Figure 54: Virus growth curve of MeV-SCD and MeV-SCD + 1 mM 5-FC in organoid 29.
Organoid 29 was treated with MeV-SCD and MeV-SCD + 1 mM 5-FC at a multiplicity of infection of 10. Virus harvest took place at 3, 24, 48, 72 and 96 hpi. Samples were analysed via titration on Vero cells, the number of plaque forming units (PFU) was calculated per milliliter for each time point. Squares/triangles in this graphic represent the mean values of three independently analysed samples, error bars represent SD.

Organoid 29 p26 was treated with MeV-SCD (MOI 10) and MeV-SCD (MOI 10) + 1 mM 5-FC, respectively. Viral titers in organoids treated with MeV-SCD alone declined from 4.4×10^5 PFU/ml at 3 hpi to 3.9×10^4 PFU/ml at 24 hpi and 2.1×10^4 PFU/ml at 48 hpi. From 2.6×10^4 PFU/ml at 72 hpi the number of infectious particles declined again to 3.8×10^3 PFU/ml at 96 hpi (Fig. 54). Similar to MeV-GFP, viral replication declined in the course of the 96 hpi, but in contrast to MeV-GFP, viral replication hit the plateau phase earlier.

Organoids treated with the combination treatment of MeV-SCD (MOI 10) + 1 mM 5-FC showed a similar number of infectious particles at 3 hpi (8.1×10^4 PFU/ml). Viral titers then declined to 3.7×10^4 PFU/ml at 24 hpi, 3.2×10^3 PFU/ml, 4.4×10^2 PFU/ml and 6.73×10^2 PFU/ml. Compared to monotherapy, decline of viral titers in the first 24 hpi was almost identical. Then, however, viral replication in organoids treated with the combination therapy further declined in contrast to viral replication in organoids treated with monotherapy, which showed a plateau phase from 48 hpi to 72 hpi (Fig. 54).

3.3.3.5 GLV-1h94 and GLV-1h94 + 1 mM 5-FC

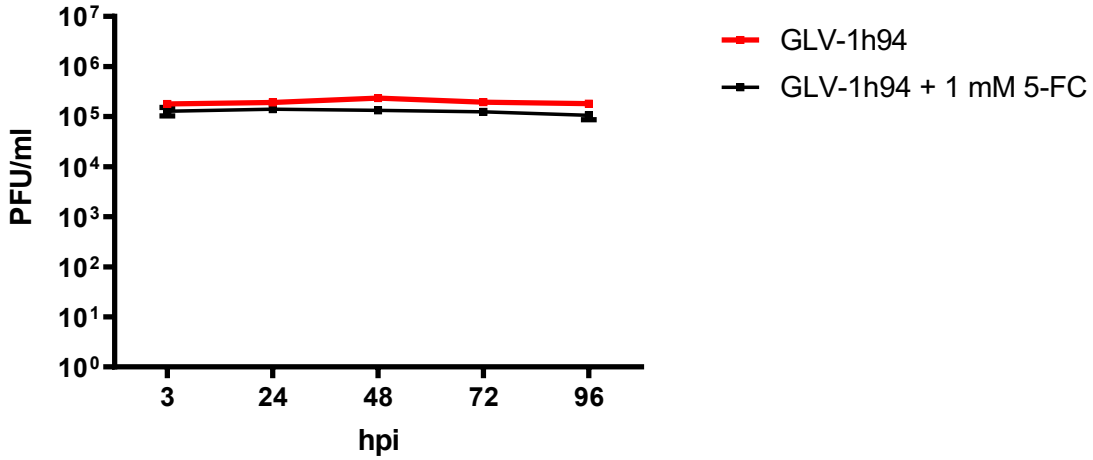

Figure 55: Virus growth curve of GLV-1h94 (MOI 10) and GLV-1h94 (MOI 10) + 1 mM 5-FC in organoid 29. Organoid 29 was treated with GLV-1h94 (MOI 10) and GLV-1h94 (MOI 10) + 1 mM 5-FC, respectively. Virus harvest took place at 3, 24, 48, 72 and 96 hpi. Samples were analyzed via titration on CV-1 cells, the number of plaque forming units (PFU) was calculated per milliliter for each time point. Squares in this graphic represent the mean values of three independently analysed samples, error bars represent SD.

Viral replication of GLV-1h94 and GLV-1h94 + 1mM 5-FC in organoid 29 showed similar growth curves. At 3 hpi, the number of infectious particles in organoids infected with GLV-1h94 was $1{,}8\times10^5$ PFU/ml, compared to $1{,}3\times10^5$ PFU/ml in organoids treated with GLV-1h94 (MOI 10) + 1 mM 5-FC (Fig. 55). Titers remained in a plateau phase during the whole observation period showing no striking difference with or without 5-FC.

3.3.3.6 GLV-1h68

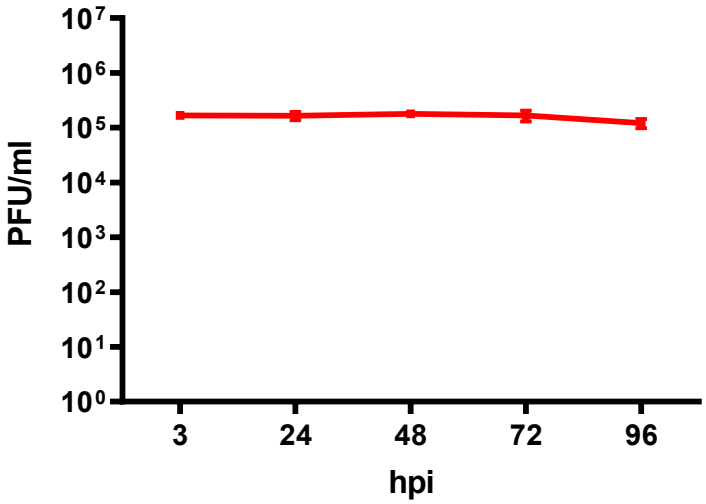

Figure 56: Virus growth curve of GLV-1h68 in organoid 29.
Organoid 29 was infected with GLV-1h68 at a multiplicity of infection of 10. Virus harvest took place at 3, 24, 48, 72 and 96 hpi. Samples were analyzed via titration on CV-1-cells, the number of plaque forming units (PFU) was calculated per milliliter for each time point. Squares in this graphic represent the mean values of three independently analyzed samples, error bars represent SD.

The number of infectious particles of GLV-1h68 started at 1.7×10^5 PFU/ml at 3 hpi and did not change during the observation period of 96 hpi (Fig. 56). This is congruent to results of viral replication of other vaccinia viruses, where the numbers of viral particles also remained constant throughout the whole time span monitored (Fig. 52).

3.4 Organoid 33

3.4.1 Cell Viability Assay

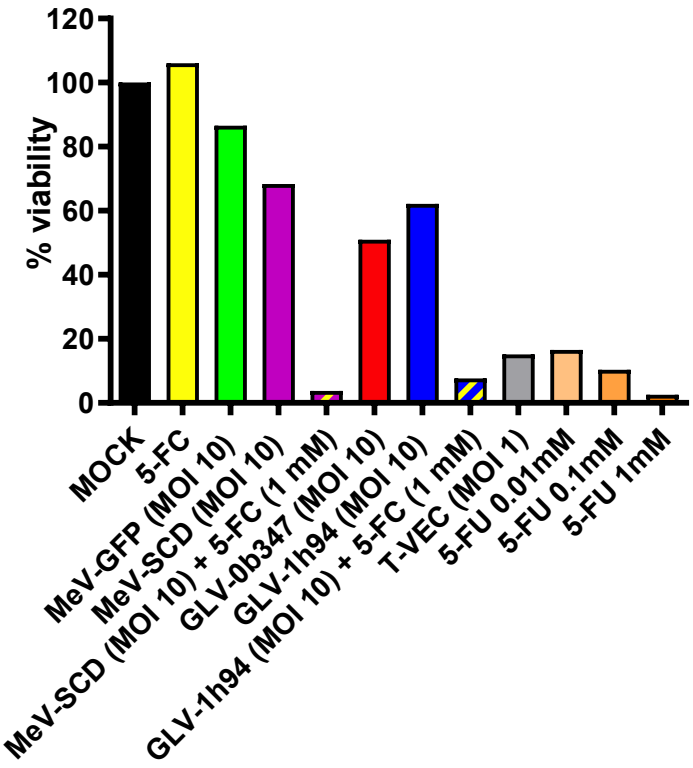

Figure 57: Cell Viability Assay of organoid 33 p6.
Cell viability of organoid 33 in passage no. 6 (p6) was measured at 96 hours post infection (hpi) in relation to treatment with only medium (MOCK; per definition 100 % cell viability). Results are given as percent cell viability in relation to MOCK. Organoids were treated with 5-FC (1 mM) as well as MeV-GFP (MOI 10), MeV-SCD (MOI 10), MeV-SCD (MOI 10) + 5-FC (1 mM), GLV-0b347 (MOI 10), GLV-1h94 (MOI 10), GLV-1h94 (MOI 10) + 5-FC (1 mM) and T-VEC (MOI 1). Additionally, organoid 25 p6 was treated with three different concentrations of 5-FU (0.01 mM, 0.1 mM and 1 mM). Mean values of one experiment performed in duplicates are shown.

In a first experiment, organoid 33 was infected with two different measles vaccine viruses (MeV-GFP and MeV-SCD), two different vaccinia viruses (GLV-0b347 and GLV-1h94) and the Herpes simplex Virus T-VEC. In general, measles viruses were less effective than the other viruses reducing cell viability by 20 % (MeV-GFP) and 38 % (MeV-SCD), respectively. Combination treatment of MeV-SCD (MOI 10) with 1 mM 5-FC was highly efficient with a remaining cell viability of only 3 %. Notably, T-VEC at a MOI of 1 showed similar results as the combination treatment of MeV-SCD with 5-FC with a remaining cell viability of 5 %. Compared to the other organoids, T-VEC was most effective in organoid 33. Both vaccinia viruses reduced cell viability to a similar extent: GLV-0b347 by 52 %,

GLV-1h94 by 48 %. Combination treatment of GLV-1h94 (MOI 10) with 5-FC (1 mM) was again highly efficient reducing cell viability by more than 95 %. Again, different concentrations of 5-FU were tested as well, showing a massive reduction in cell viability of almost 100 % in organoids treated with 1 mM 5-FU with a remaining cell viability of 1 %. Lower concentrations of 5-FU (0.1 mM and 0.01 mM) also led to a massive reduction in cell viability by 94 % (0.1 mM 5-FU) and 92 % (0.01 mM 5-FU), respectively (Fig. 57).

To sum it up: Monotherapy with T-VEC at a MOI of 1 as well as combination treatment of either MeV-SCD or GLV-1h94 with 5-FC were very effective in organoid 33, all reducing viability to below 10 %. In addition, organoid 33 was highly sensitive to 5-FU.

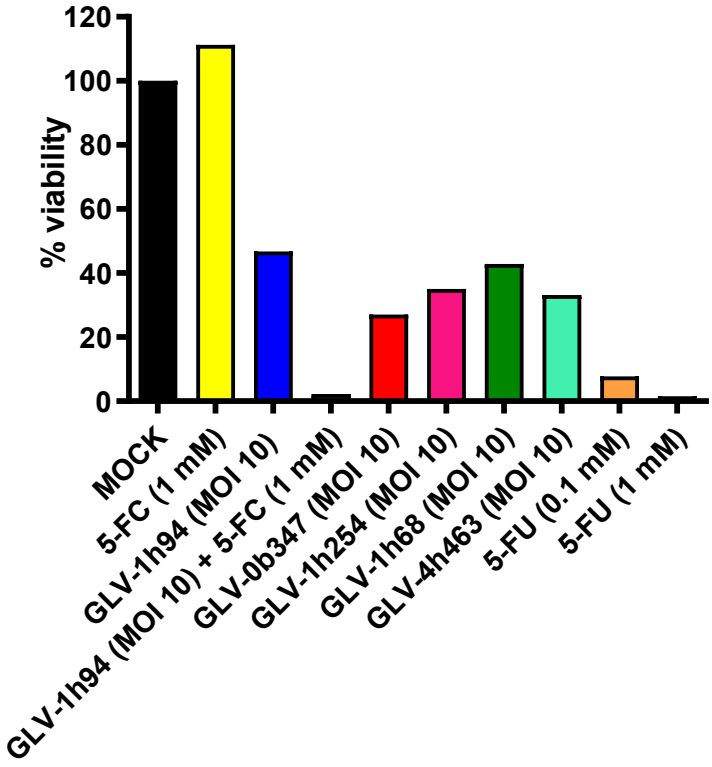

Figure 58: Cell Viability Assay of organoid 33 p9.
Cell viability of organoid 33 in passage no. 9 (p9) was measured at 96 hours post infection (hpi) in relation to treatment with only medium (MOCK; per definition 100 % cell viability). Results are given as percent cell viability in relation to MOCK. Organoids were treated with 5-FC (1 mM) as well as GLV-0b347 (MOI 10), GLV-1h94 (MOI 10), GLV-1h94 (MOI 10) + 5-FC (1 mM), GLV-1h68, GLV1h254 and GLV-4h463. Additionally, two different concentrations of 5-FU (0.1 mM and 1 mM) were tested. Mean values of one experiment performed in duplicates are shown.

Next, organoid 33 was tested with a selection of 5 different vaccinia viruses. Compared to the first experiment, GLV-0b347 showed a higher efficacy in cell viability reduction of more than 70 % (Fig. 58) compared to 50 % (Fig. 57) before (remaining cell viability of 27 %). GLV-1h94 showed a similar reduction in cell viability as before with a remaining cell viability of 46.8 % (Fig. 58). Combination treatment of GLV-1h94 with 1 mM 5-FC was again highly effective in organoid 33, with a remaining cell viability of only 2 %. Interestingly, the other tested vaccinia viruses showed similar results: GLV-4h463 and GLV-1h254 reduced cell viability by more than 60 %, GLV-1h68 by 57 %. 5-FU again reduced viability by more than 90 % with a remaining cell viability of 7.8 % in organoids treated with 0.1 mM 5-FU and 1.5 % in organoids treated with 1 mM 5-FU, demonstrating the high sensitivity of organoid 33 to 5-FU (Fig. 58).

To sum it up: All vaccinia viruses reduced viability of organoid 33 similarly. Combination treatment of GLV-1h94 and 5-FC was very effective with a cell viability reduction to almost 0 %. Furthermore, organoid 33 proved to be very sensitive to 5-FU.

3.4.2 Phase contrast and fluorescence microscopic monitoring of cell growth and marker protein expression

3.4.2.1 MOCK, 1 mM 5-FC, 0.01 mM 5-FU, 0.1 mM 5-FU and 1 mM 5-FU

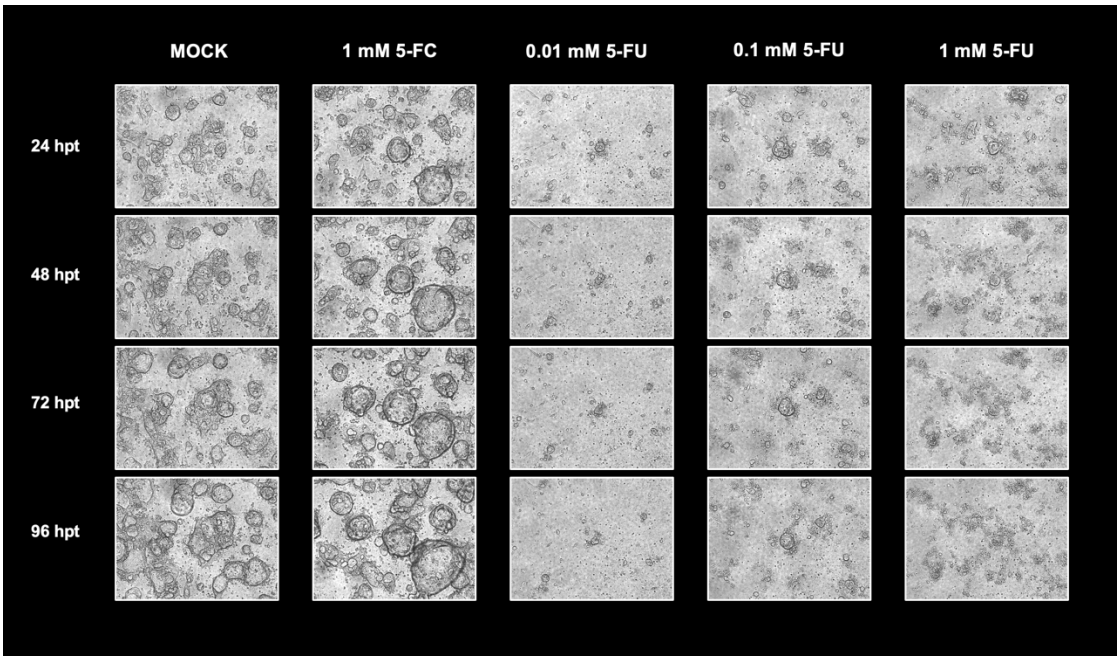

Figure 59: Phase contrast and fluorescence microscope pictures (10-fold magnification) of organoid 33 p6 treated with medium (MOCK), 1 mm 5-FC, 0.01 mM 5-FU, 0.1 mM 5-FU and 1 mM 5-FU at 24, 48, 72 and 96 hpt.

Organoid 33 in passage 6 treated with medium only (MOCK) or with 1 mM 5-FC showed a constant growth in phase contrast pictures. In contrast, organoids treated with different concentrations of 5-FU showed almost no or very little growth. Organoids treated with the highest concentration of 5-FU (1 mM) showed extensive signs of cell lysis already at 24 hpt (Fig. 59).

To sum it up: Organoid 33 was highly sensitive to 5-FU, even at the lowest concentration of 0.01 mM, as organoid growth was drastically limited already at 24 hpt.

3.4.2.2 MeV-GFP, MeV-SCD and MeV-SCD + 1 mM 5-FC

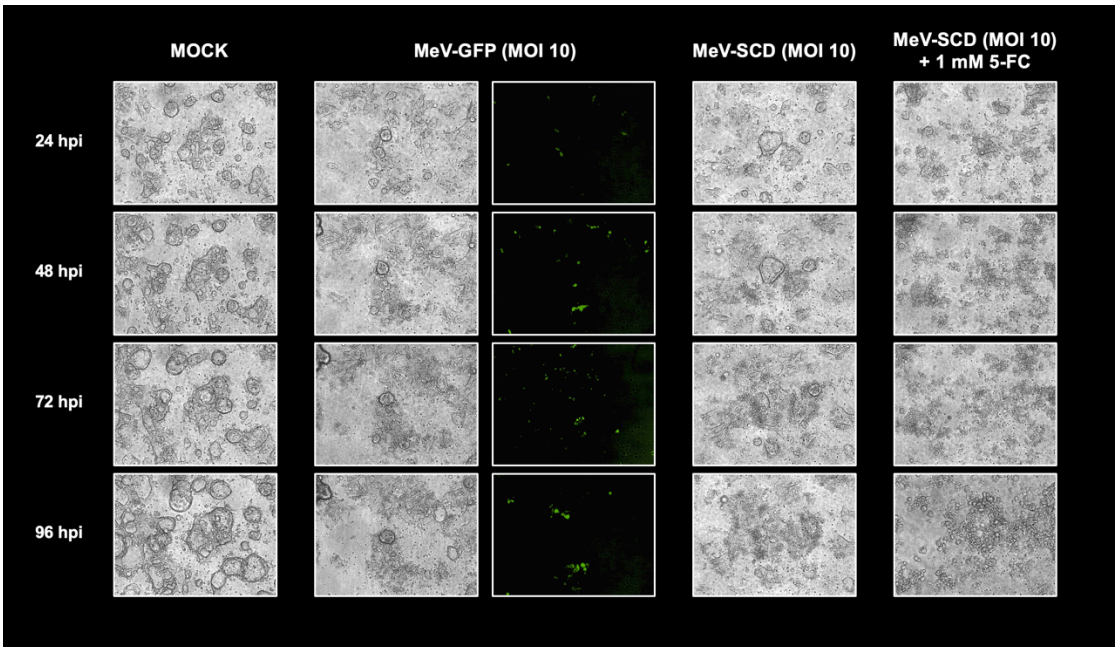

Figure 60: Phase contrast and fluorescence microscope pictures of organoid 33 p6 treated with medium (MOCK), MeV-GFP (MOI 10), MeV-SCD (MOI 10) and MeV-SCD (MOI 10) + 1 mM 5-FC at 24, 48, 72 and 96 hpi.

Organoid 33 infected with MeV-GFP showed a rather weak fluorescent signal throughout the whole observation period. Interestingly, morphological changes, like signs of cell lysis, could be detected, nonetheless. Organoid 33 infected with MeV-SCD (MOI 10) showed signs of cell lysis at 48 hpi with massive cell destruction at 96 hpi. This was even more striking in organoids treated with combination therapy of MeV-SCD (MOI 10) and 1 mM 5-FC as signs of extensive cell lysis were already detectable at 24 hpi and organoids were completely disintegrated at 96 hpi (Fig. 60).

3.3.4.2 VACV GLV-1h94, GLV-1h94 + 1 mM 5-FC, GLV-0b347, GLV-1h254, GLV-1h68 and GLV-4h463

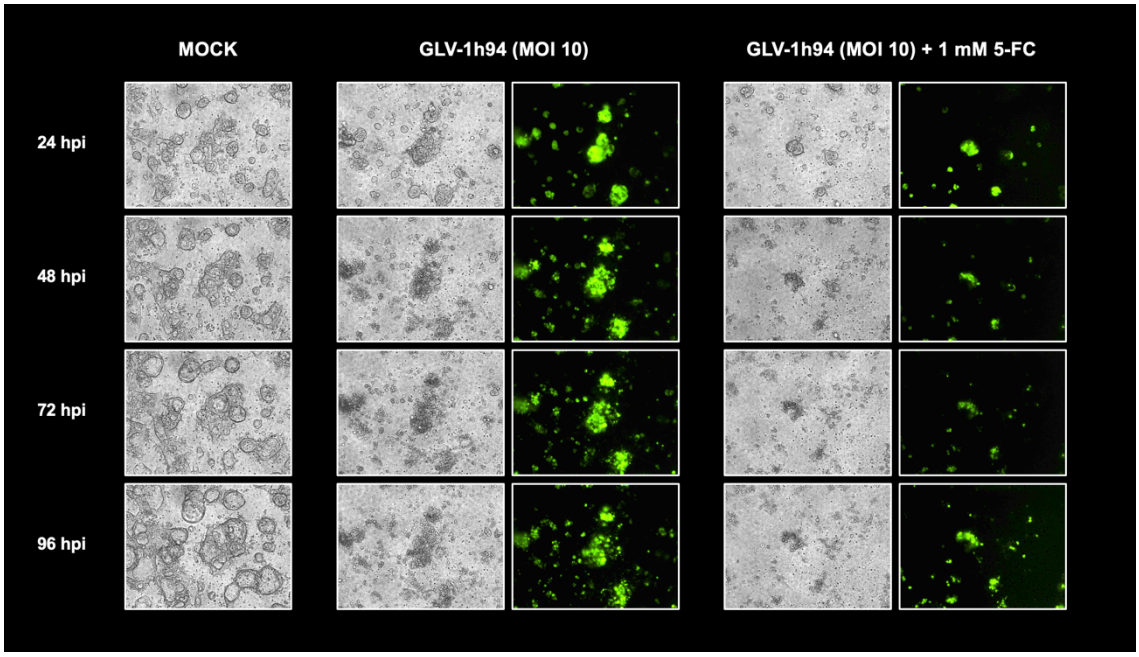

Figure 61: Phase contrast and fluorescence pictures of organoid 33 p6 treated with medium (MOCK), GLV-1h94 (MOI 10) and GLV-1h94 + 1 mM 5-FC at 24, 48, 72 and 96 hpi.

Organoid 33 in passage 6 infected with GLV-1h94 (MOI 10) showed a distinct fluorescent signal already at 24 hpi, like all previously tested organoids infected with vaccinia viruses. Although slight morphological changes could already be observed in phase contrast pictures at 24 hpi, distinct signs of cell lysis were clearly visible at 48 hpi. A similar pattern was observable after treatment with combination therapy of GLV-1h94 (MOI 10) + 1 mM 5-FC, as a fluorescent signal was visible at 24 hpi, but signs of cell lysis in phase contrast pictures were not observable until 48 hpi. This was different to organoids 22, 25 and 29 treated with combination therapy, where morphological changes were already observable at 24 hpi. At 96 hpi, organoids treated with monotherapy of GLV-1h94 as well as organoids treated with combination therapy of GLV-1h94 + 1 mM 5-FC were completely lysed (Fig. 61).

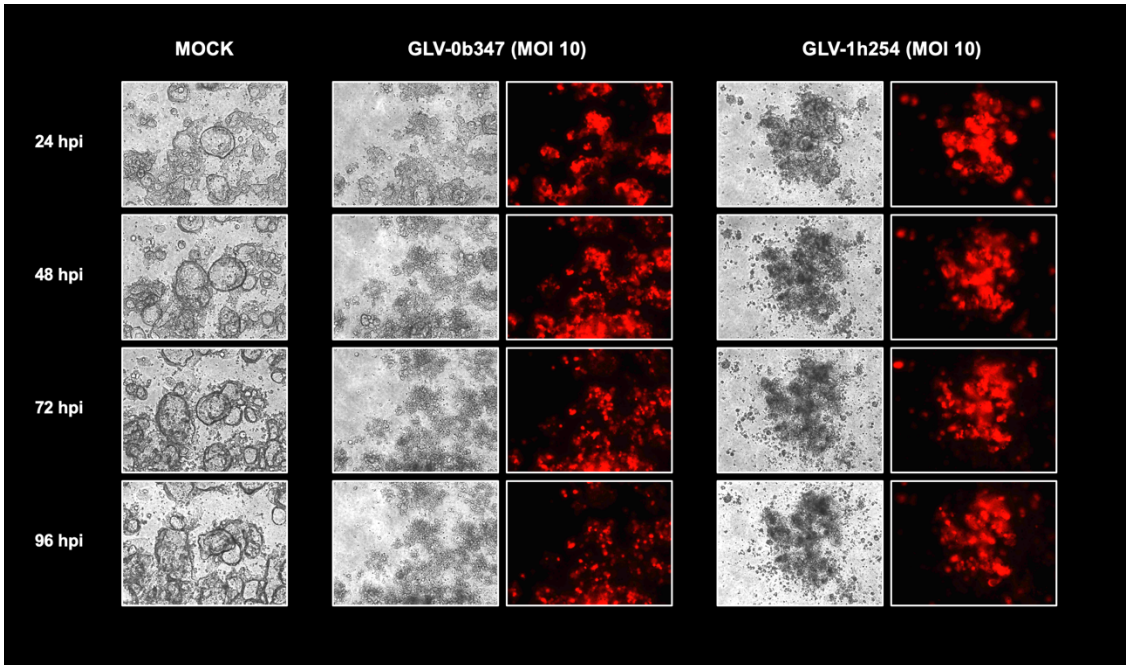

Figure 62: Phase contrast and fluorescence microscope pictures of organoid 33 p9 treated with medium (MOCK), GLV-0b347 (MOI 10) and GLV-1h254 (MOI 10) at 24, 48, 72 and 96 hpi.

As in all previously tested organoids infected with vaccinia virus, a fluorescent signal was already detectable at 24 hpi in organoid 33 treated with GLV-0b347 (MOI 10). Signs of cell lysis in phase contrast pictures could be observed at 48 hpi. At 96 hpi, most of the organoids were disintegrated. After infection with GLV-1h254 (MOI 10) a fluorescent signal as well as extensive signs of cell lysis were detectable at 24 hpi with a complete disintegration of organoids already at 48 hpi (Fig. 62).

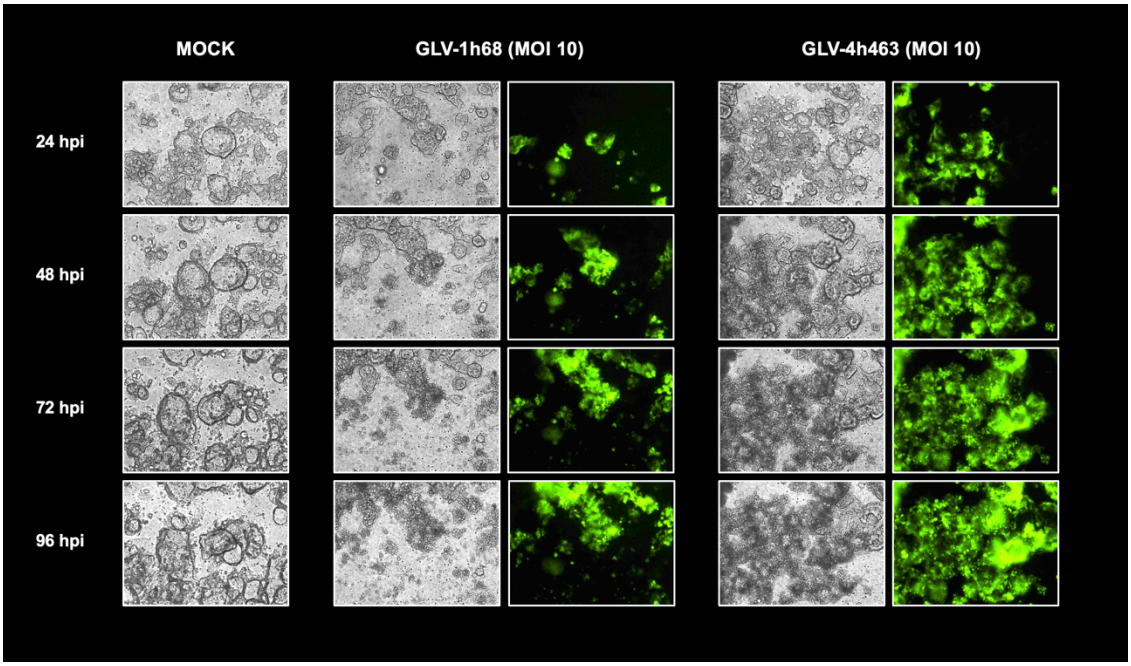

Figure 63: Phase contrast and fluorescence pictures of organoid 33 p9 treated with medium (MOCK), GLV-1h68 (MOI 10) and GLV-4h463 at 24, 48, 72 and 96 hpi.

Organoid 33 infected with GLV-1h68 (MOI 10) showed a fluorescent signal at 24 hpi, which increased over the 96 hours indicating a spread of viral infection. First morphological signs of cell lysis were observable at 48 hpi and increased over time with a complete disintegration of organoids at 96 hpi. In organoids treated with GLV-4h463 (MOI 10) spreading of infection was also well observable, as the fluorescent signal expanded over the 96 hours. This was congruent with morphological changes observable in phase contrast pictures, as signs of cell lysis began to appear at 48 hpi and expanded until 96 hpi (Fig. 63).

3.4.2.3 T-VEC

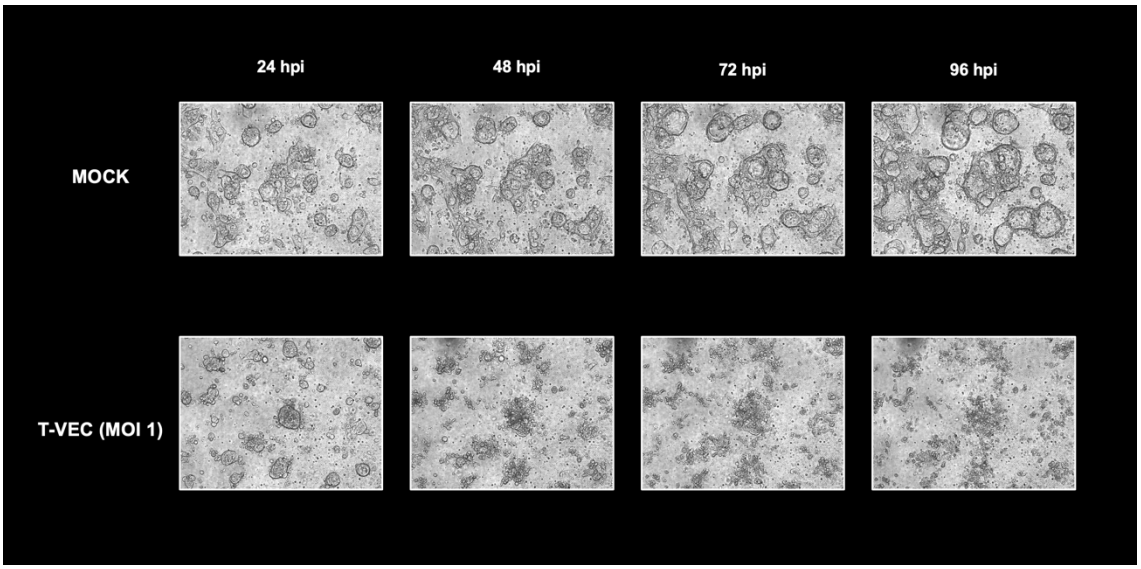

Figure 64: Phase contrast pictures of organoid 33 p6 treated with medium (MOCK) and T-VEC at 24, 48, 72 and 96 hpi.

Finally, organoid 33 in passage 6 was infected with T-VEC (MOI 1) as well. First signs of cell lysis were visible at 48 hpi. At 96 hpi organoids were completely disintegrated (Fig. 64).

3.4.3 Virus Growth Curves

3.4.3.1 MeV-GFP

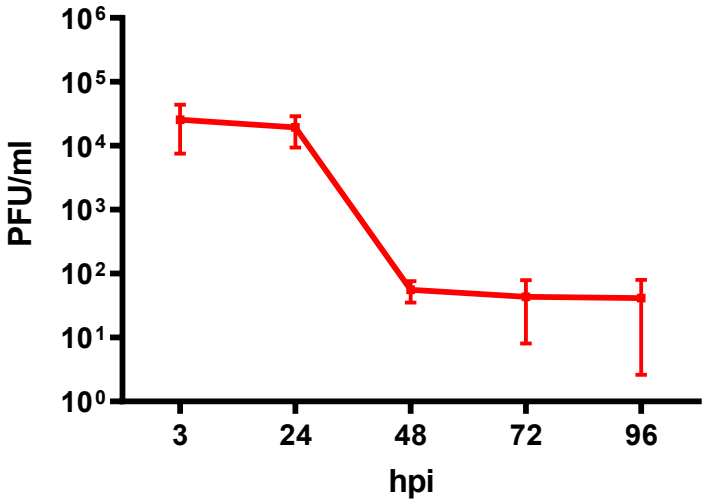

Figure 65: Virus growth curve of MeV-GFP in organoid 33.
Organoid 33 was infected with MeV-GFP at a multiplicity of infection of 10. Virus harvest took place at 3, 24, 48, 72 and 96 hpi. Samples were analysed via titration on Vero cells, the number of plaque forming units (PFU) was calculated per milliliter for each time point. Squares in this graphic represent the mean values of three independently analysed samples, error bars represent SD.

Viral titers of MeV-GFP declined in the time span of 96 hpi. At 3 hpi the number of infectious particles was almost at 2.5×10^4 PFU/ml. Then titers further declined to 2×10^4 PFU/ml at 24 hpi and 5.6×10^1 PFU/ml at 48 hpi. At 96 hpi, a minimal titer of 4.1×10^1 PFU/ml was reached (Fig. 65). This is coherent with the low sensitivity of organoid 33 to MeV-GFP.

3.4.3.2 GLV-0b347

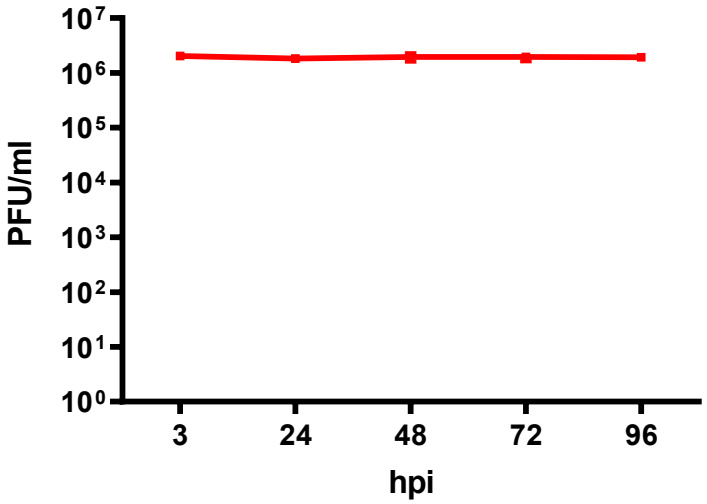

Figure 66: Virus growth curve of GLV-0b347 in organoid 33.
Organoid 33 was infected with GLV-0b347 at a multiplicity of infection of 10. Virus harvest took place at 3, 24, 48, 72 and 96 hpi. Samples were analysed via titration on CV-1 cells, the number of plaque forming units (PFU) was calculated per milliliter for each time point. Squares in this graphic represent the mean values of three independently analysed samples, error bars represent SD.

In organoid 33, the growth curve of GLV-0b347 was almost identical to the one in organoid 29 (Fig. 52). At 3 hpi, the number of infectious particles was 2×10^6 PFU/ml. The number of infectious particles stayed almost the same, resulting in a plateau phase from 3 hpi to 96 hpi (Fig. 66). This is congruent to growth curves of GLV-0b347 in other organoids.

3.4.3.3 T-VEC

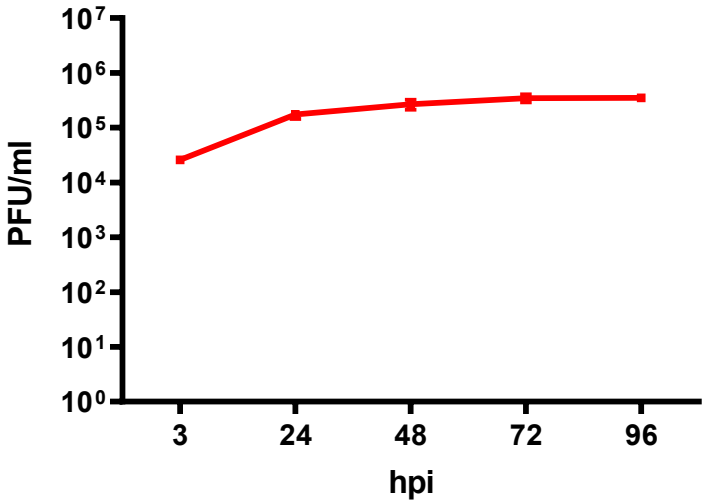

Figure 67: Virus growth curve of T-VEC in organoid 33.
Organoid 33 was treated with T-VEC at a multiplicity of infection of 1. Virus harvest took place at 3, 24, 48, 72 and 96 hpi. Samples were analysed via titration on Vero cells, the number of plaque forming units (PFU) was calculated per milliliter for each time point. Squares in this graphic represent the mean values of three independently analysed samples, error bars represent SD.

Replication of T-VEC in organoid 33 showed an overall increase of infectious particles in the course of 96 hpi. Between 3 hpi and 24 hpi, the number of infectious particles increased from 2.6×10^4 PFU/ml to 1.7×10^5 PFU/ml. After that, viral titers increased only slightly, resulting in a plateau phase at 3.5×10^5 PFU/ml between 24 hpi and 96 hpi (Fig. 67). Interestingly, replication of T-VEC in organoid 33 was the weakest compared to the other organoids but showed the highest efficacy in cell viability reduction.

4 Discussion

Colorectal Cancer (CRC) is still one of the most common cancers worldwide. As cancer research evolves and therapy modalities undergo a transformation to more individual / personalized approaches, we are in dire need for more representative *in vitro* models. Tumor organoids seem to be a promising model which embodies both pragmatic considerations as well as the aspiration for individuality in therapeutic methods.

4.1 CRC organoids are susceptible to infection with OVs

As mentioned earlier, tumor organoids employed in virotherapy research are still a relatively new approach and only a few papers have been published so far which investigate the possible administration of OVs to tumor organoids in cancer research. To this date, there are no published studies investigating the possibility of using organoids as a culture model to test OVs as a treatment option for CRC.

When looking for the usage of “only” monolayer cell cultures, there are numerous studies investigating the effectiveness of oncolytic virotherapy in the context of CRC treatment, testing different viral agents (e.g. measles[130,133], vaccinia[134–136], herpes simplex[137–142] virus but also adenovirus[143], Newcastle disease virus[144], Coxsackievirus[145]).

As discussed earlier, a critical component of systemic chemotherapy protocols in clinical CRC treatment is the chemotherapeutic 5-FU. This is also significant within the scope of virotherapy: cells infected with oncolytic viruses enhanced with suicide genes express the enzyme supercytosine deaminase which converts the pro-drug 5-FC into the effective chemotherapeutic compound 5-FU. There are several studies that investigate the predictability and mechanisms of effectiveness of 5-FU in CRC organoids[146,147], but the effectiveness of suicide gene therapy using oncolytic viruses in organoids has not been studied so far.

We used two different measles viruses, five different vaccinia viruses and one herpes simplex virus (Talimogene Laherparepvec; T-VEC) to infect organoids established from patient-derived CRC specimen via reductions of the tumor cell masses. All tested OVs were able to infect these patient derived tumor organoids

(PDTOs), as seen by phase contrast and fluorescence microscopy. In general, a fluorescent signal was detectable at 24 hpi. In organoids infected with T-VEC or MeV-SCD, which both do not encode for a fluorescent protein, signs of cell lysis could be detected during the observation period. In contrast, organoids which only received medium did not show any signs of cell lysis but rather grew during the observation period.

This indicates that CRC PDTOs are susceptible to OVs and represent a possible model to further investigate oncolytic virotherapy for CRC treatment in a prether-apeutic setting.

4.2 Creating a personalized “virogram”

The main goal of this thesis was to create a personalized “virogram” and thus determine the best treatment option for each individual patient. To achieve this goal, resectates of tumors were used to generate organoids which were then in-fected with a selection of different OVs. Below, the individual virogram for each patient is discussed extensively.

4.2.1 Organoid 22

The most effective treatment for CRC tumor organoid 22 was the combination therapy of **GLV-1h94 + 1 mM 5-FC**. Compared to other organoids, this organoid was most resistant to oncolytic virotherapy. Notably, organoid 22 was not very susceptible to treatment with either GLV-1h94 nor 5-FU on its own (Fig. 22, 23). Only the highest concentration of 5-FU (1 mM) showed a high reduction in tumor cell viability (Fig. 22, 23). These findings suggest that tumor cell viability reduction in organoids treated with combination therapy of GLV-1h94 (MOI 10) and 1 mM 5-FC which is locally converted into 5-FU by virus encoded SCD was mainly due to the cytotoxic effect of 5-FU.

In general, monotherapy with OVs was less effective in organoid 22 than in other organoids: treatment with both measles viruses reduced cell viability only by 17 %, treatment with vaccinia viruses only by 36-53 %.

4.2.2 Organoid 25

Organoid 25 was very susceptible to treatment with 5-FU, as even the lowest concentration of 5-FU (0.01 mM) showed massive reduction in cell viability.
The most effective treatment options for organoid 25 were **combination therapies with MeV-SCD (MOI 10) + 1 mM 5-FC and GLV-1h94 (MOI 10) + 1 mM 5-FC** reducing cell viability to 0.6 and 1.5 %, respectively, similar to monotherapy with 5-FU (Fig. 33).

4.2.3 Organoid 29

Compared to other organoids, organoid 29 showed a medium susceptibility to 5-FU. The most effective treatment was **combination therapy of GLV-1h94 and 5-FC** with a remaining cell viability of 2.4 %. In contrast, combination therapy of MeV-SCD and 5-FC was less effective, especially when compared to other organoids. Notably, organoid 29 was not susceptible to measles viruses, as monotherapy with MeV-GFP only led to a reduction in cell viability of 11 % and even less in monotherapy with MeV-SCD. The reduction of cell viability in organoids treated with combination therapy of MeV-SCD and 5-FC is probably mostly due to the cytotoxic effects of 5-FU. Treatment with T-VEC was the least effective compared to other organoids (Fig. 44).

4.2.4 Organoid 33

Organoid 33 was highly susceptible to treatment with 5-FU. At the highest concentration, a tumor cell viability reduction of 99 % was achieved. Again, **combination therapies of GLV1h94 (MOI 10) + 1 mM 5-FC** (remaining cell viability of 2 %) **and MeV-SCD + 1 mM 5-FC** (remaining tumor cell viability of 3 %) were most effective (Fig. 57, 58). Notably, treatment with T-VEC as a monotherapy was highly effective in organoid 33 with a remaining cell viability of 5 % (Fig. 57). Interestingly, there was a difference in efficacy between the two measles viruses, as treatment with MeV-SCD led to a reduction of viability of 39 % compared to 20 % in organoids treated with MeV-GFP. Monotherapy with vaccinia viruses was relatively congruent with a cell viability reduction between 65 and 53 %, except for GLV-0b347, which led to a cell viability reduction of 80 % (Fig. 58).

4.2.5 General observations

Looking at all individual virograms (n = 4) a general trend can be observed: combination therapy of a suicide gene enhanced OV together with 5-FC was the most successful treatment in all tested organoids. Most often, **GLV1h94 + 1 mM 5-FC was the most successful therapy.** Viability reductions in organoids treated with combination therapy resembled those of 5-FU. This suggests that the success of combination therapy is mostly due to cytotoxic effects mediated by the conversion of 5-FC to 5-FU.

4.3 Morphological changes did not necessarily correlate with cell viability reduction

To monitor growth as well as morphological changes of organoids during treatment, pictures were taken with a phase contrast microscope. Furthermore, viral spreading in organoids infected with OVs was captured by fluorescence microscopy.

In organoids which underwent extensive lysis, most often induced by combination therapy, morphological changes included destruction of cell formations (previously grown three-dimensional structures dispersed) as well as disintegration of cells (observable as generation of small spheres).

In general, alterations in the fluorescence signals (being indicative for virus spreading) and morphological changes were relatively congruent:

- In organoids infected with measles viruses, only a weak fluorescent signal could be detected. This was congruent with at most slight morphological changes in phase contrast pictures.
- In organoids infected with VACV on the other hand, a strong fluorescent signal was detectable, independently of the virus strain or organoid infected. Fluorescent areas showed a high grade of disintegration. Interestingly, viability reduction differed with remaining cell viabilities ranging from 32 % up to 58 %. As cells disintegrated upon viral infection, the reason for the rather low reduction in cell viability may be insufficient viral spreading from infected

to not yet infected cells. To disclose the reason for this spreading inhibition, further investigation upon host defense mechanisms, viral virulence factors and maybe also the impact of culture modalities have to be made.

4.4 Virus species showed specific replication behaviors

To further investigate replication behavior and to better understand individual virus preferences, organoids were infected with a selection of viruses, namely MeV-GFP, GLV-0b347 and T-VEC (one virus of each species) and harvested at different time points after infection. The numbers of infectious viral particles at different time points were determined to elucidate replication kinetics. The same MOI was used for the generation of the growth curves as for the cell viability assays.

Remarkably, each virus species showed a distinct replication behavior, independently of the organoid infected.

The number of PFUs in organoids infected with MeV-GFP declined during the observation period, predominantly in the first 48 hours after infection before the number of PFUs hit a plateau phase. This was the case in all organoids infected with MeV-GFP. Except for organoid 25, every other organoid was not susceptible to oncolysis by MeV-GFP either, with a rather low reduction in cell viability as seen in the cell viability assay.

This phenomenon could be explained by different considerations:

- One possibility is that infection was insufficient in the first place and resulted in a lack of replication, regardless of the MOI applied. This is supported by the fact, that MeV-GFP on its own was not able to generate a sufficient reduction in cell viability in all organoids, as seen in cell viability assays. To determine the exact reason for this, further experiments are necessary.
- Alternatively, but highly unlikely, the already large number of viral particles being present in the beginning of the observation period led to a situation at which no further tumor cells could be infected and consequently no increase in infectious particles could take place; however, this is contradicted by the

fact that the fluorescence images show only a small proportion of infected cells, indicated by the expression of the fluorescent protein GFP.

Another trend can be seen in all organoids infected with GLV-0b347: the number of infectious particles remained at a plateau during the whole observation period. In contrast to MeV-GFP, all organoids infected with vaccinia viruses showed a strong and relatively homogenous fluorescent signal already at 24 hpi. To further investigate replication behavior, a smaller multiplicity of infection (MOI) should be chosen, as tumor cells seemed to be very susceptible to infection. A study which investigated the replication behavior of another vaccinia virus (GLV-1h153) in the LS174 colon cancer cell line showed that GLV-1h153 was competent for replication in these cells as seen by an increase of PFUs. Interestingly, a low MOI of 5 has been used in these experiments.[136] Also, cytotoxicity was much higher than in organoids infected with vaccinia viruses, even at a MOI of 0.01. But this can only be compared to a limited extent and with caution, as different vaccinia viruses and different CRC cells lines, but not organoids had been used.

Compared to the other OVs, only T-VEC showed an increase in infectious particles in the course of the observation period. One possible explanation could be attributed to the fact that T-VEC was applied with a lower MOI than the aforementioned OVs. When a low number of viral particles is applied in the beginning, more cells stay uninfected initially and can then be infected at later time points during the observation period. Interestingly, T-VEC was the most efficient monotherapy throughout all tested organoids, so not only infectivity but also the oncolytic capacity of T-VEC could be attributed to that.

T-VEC (also known as OncoVEX$^{GM\text{-}CSF}$) was to date only tested in one phase I clinical trial for the therapy of colorectal cancer. Hu et al. applied OncoVEX$^{GM\text{-}CSF}$ only to two patients with colorectal carcinoma (among other patients exhibiting other solid tumors), which both showed neither a response to the treatment nor disease-site specific side effects.[148] Preclinical investigations are limited to a study by Shayalan et al. which investigated the oncolytic capacity of a herpes simplex virus type 1 (HSV-1) in colon cancer cell lines under different oxygenic

conditions. They discovered that CRC cells responded differently dependent on peculiar cell context factors.[139]

To further investigate replication behavior in organoids treated with combination therapy, growth curves of both GLV-1h94 and MeV-SCD as monotherapy as well as in combination with 5-FC were generated. Again, virus species determined the overall trend of replication.

In organoids infected with MeV-SCD, independently of mono- or combination therapy, the overall number of infectious particles declined during the observation period, even more so in organoids treated with combination therapy. Interestingly, monotherapy with MeV-SCD did not reduce cell viability significantly in contrast to combination therapy, where cell viability was reduced by more than 80 %. This indicates that the stronger decline in the number of infectious particles in organoids treated with combination therapy could be attributed to a more efficient killing of cells and thus less possibility for the virus to replicate.

Comparing this to combination therapy of GLV-1h94, a somewhat different picture emerges: both mono- as well as combination therapy of GLV-1h94 with 5-FC did not show any significant differences in replication behavior. Like the other vaccinia virus described before, the number of infectious particles stayed relatively constant during the whole observation period.

4.5 Organoids – finding the sweet spot between representativity and pragmatism?

In the beginning, major advances in human cancer research have been based on immortalized cell models, being exemplified by the generation of HeLa cancer cells in 1953[149]. Such two-dimensionally growing tumor cell lines are inexpensive and can be easily cultured and monitored in vitro; experiments are conveniently reproduced as popular cell lines have identical genetic properties all over the world.

Unfortunately, this also represents one of the major downsides of immortalized cancer cell lines: they lack the genetic and cellular heterogeneity found in primary tumors, as only robust cells survive during long-term cultivation.[150]

Another factor which plays into the poor recapitulation of actual patient tumors are culture conditions. As discussed earlier, the microenvironment of cells in vivo, including the extracellular matrix (ECM), strongly influences important factors such as cell morphology and gene expression. A monolayer cell culture is unable to sufficiently recreate this tumor microenvironment (TME) and hence misses a crucial part of tumor pathophysiology.[151,152]

Murine models, especially genetically engineered mouse models, are still a crucial part in drug development and basic research as they provide an outlook on fundamental insights into tumor biology and systemic consequences of drug application.[151,153] Unfortunately, findings in mouse models cannot be directly translated into therapy of human cancer patients, as tumorigenesis and systemic aspects differ profoundly. Additionally, using these models is quite time-consuming, costly and cannot provide a high-throughput screening as in vitro models could.[154,155]

Patient-derived tumor xenografts (PDTX), in which patients' tumors are transplanted into immunodeficient mice, represent a translational model for individual drug research. Although this model allows the maintenance of tumor architecture and stromal composition, PDTX have their disadvantages as well. Similar to other models, PDTX also fail to reproduce tumor heterogeneity, as only a small section of the primary tumor is implanted[156,157] and observations made by Morgan et al. suggest that clonal selection takes place, as less than half of mutations found in the primary tumor could be detected in PDTX tumor tissues.[157,158] Additionally, human stroma which is implanted and originally depicted as an advantage for TME similarity was found to be replaced quickly by host stromal cells.[157,159,160]

Taking all these considerations into account, patient derived tumor organoids (PDTO) could represent a model which comprises both the aspiration for a highly representative approach (conservation of tumor heterogeneity)[157,161] as well as the possibility of high-throughput screenings and thus represents a promising

model in the search for more efficient pre-clinical testing, especially when focusing on oncolytic viruses.

4.6 Clinical perspectives: a route to the practical “virogram”

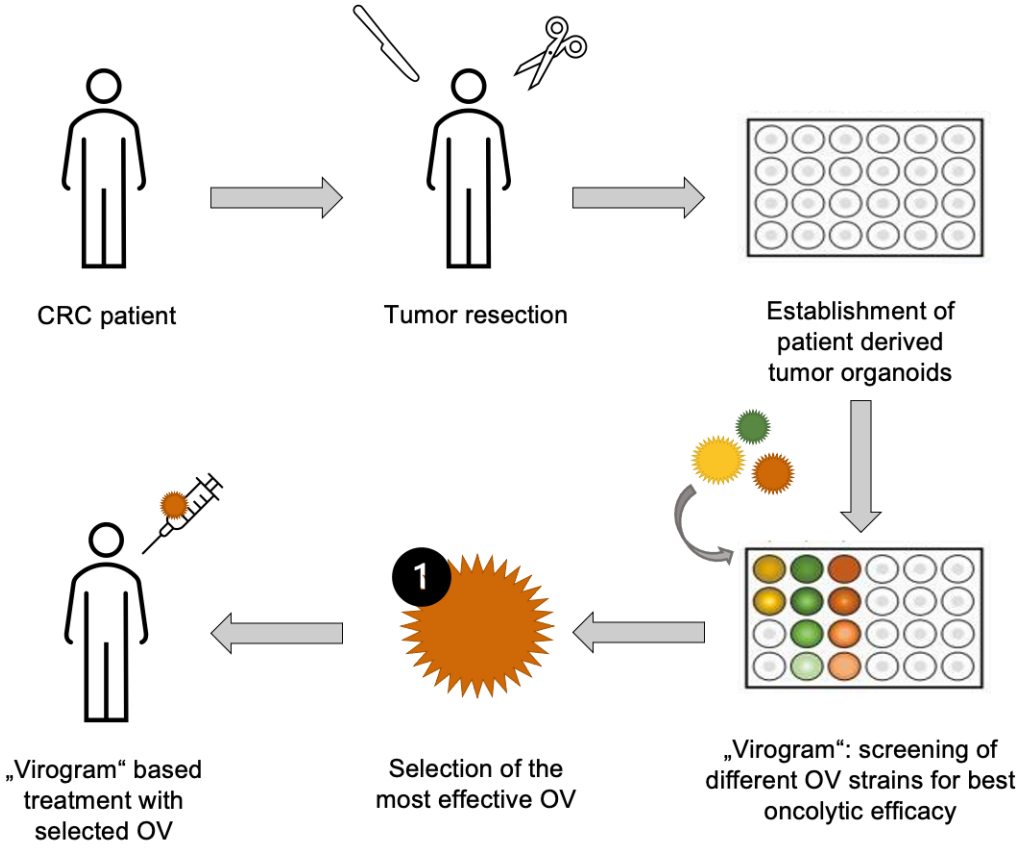

Figure 68: Practical steps for the route to the personalized “virogram” (CRC = Colorectal Carcinoma, OV = oncolytic virus); figure adapted from [162].

The final goal of this thesis was to create a personalized “virogram” to evaluate the optimal OV for each and every cancer patient. To reach this goal in a clinical context, different factors have to be taken into account when thinking about a broader application and an even more representative approach. These factors are discussed below.

4.6.1 Optimizing culture conditions to gain a bigger patient collective

The exact components of the organoid medium and their use in the context of cell growth and maintenance have already been described in the introduction. They were based on findings of Sato et al. in the search for the optimal culture medium for colon organoids. In 2011, Sato et al. further examined culture conditions not only for organoids derived from healthy colon tissue, but also colon adenocarcinoma. They found out that neither R-spondin nor Noggin was necessary for tumor growth. Notably, in most tumor organoids EGF was dispensable too, but not in all.[163] In 2015, a paper of the research group around Clevers showcased the attempt to establish a CRC organoid biobank. Here, they took advantage of the Wnt-dependency of normal colonic epithelium and hence selectively cultured tumor organoids (which in 90 % of the cases show an aberrant activation of the Wnt-pathway) by depriving the culture medium of Wnt-3a.[164]

Another aspect to take into consideration when thinking about optimizing culture conditions to ultimately expand the patient collective is the prevention of contamination. As CRC resectates originate from the non-sterile environment of the colon, contamination with bacteria or fungi is a common problem in organoid culture. Therefore, older protocols provide an antimicrobial approach: before processing, tumor specimens were washed with phosphate buffered saline (PBS) supplemented with penicillin/streptomycin (P/S). Marinucci et al. studied different combinations of PBS, P/S and Primocin washing in CRC resectates before further processing. Primocin is an antimicrobial and antifungal agent offering protection against both gram-positive as well as gram-negative bacteria, mycoplasma and fungi. Interestingly, tumor resectates that were washed with Primocin in any combination or on its own showed no contamination at all. CRC specimens which were washed with P/S on the other hand seemed to even hinder organoid establishment and growth.[165] **To sum it up,** a washing protocol with Primocin might help in the establishment of organoids from patient derived specimens.

4.6.2 Safety aspects: comparing tumoroids with “healthy” organoids

As OVs used in this thesis were only tested on PDTOs, an important aspect regarding applicability in the clinical context has to be taken into consideration: treating organoids generated from healthy tissue as well to make sure cytotoxicity applies primarily to cancer cells and not to healthy cells.

There are several studies which investigate the possibility of culturing tumor organoids as well as organoids from healthy tissue adjacent to the tumor. Van de Wetering et al. managed to generate a living biobank not only of CRC derived tumor organoids but also of organoids derived from adjacent healthy tissue. They proceeded to perform high-throughput screenings of PDTOs and were able to detect individual differences in therapy response.[164] Generating patient derived organoids from adjacent healthy tissue of resectates plays especially a crucial role in the scope of virotherapy, as a potential infection of healthy tissue has to be ruled out when trying to find an effective, but safe therapy.

4.6.3 Co-culturing organoids as a possible method to create a more realistic TME

The heterogenous composition of the TME and its importance regarding tumor development as well as maintenance and hence therapeutical approaches has been discussed earlier. To emulate this TME in vitro, there have already been several attempts in co-culturing tumor organoids with different cell types found in the TME.

As pointed out earlier, a crucial part of TME are tumor surrounding stromal cells, specifically cancer associated fibroblasts (CAFs). To this date, there are only two published studies investigating the consequences of co-culturing CRC PDTOs with CAFs. Luo et al. found that CAFs which were co-cultured with CRC PDTOs under established culture conditions presented a poor viability. In contrast to that, when co-culturing both CAFs and PDTOs in basal organoid medium without any supplements or antimicrobial additions, PDTOs showed extensive growth. This may be most likely due to CAFs excreting growth factors on their own.[166] Naruse

et al. even found that genes with malignant functions, which were downregulated in CRC PDTOs in mono-culture but highly expressed in the original CRC specimens, were expressed again when co-culturing PDTOs with patient-derived CAFs.[167] Both of these findings suggest the relevance of CAFs in the context of TME.

Another important cell type regarding TME are immune cells, more specifically tumor infiltrating lymphocytes (TIL), especially considering immunotherapy. Neal et al. managed to co-culture PDTOs not only with stromal cells, but with TIL embedded in the stroma as well. They successfully demonstrated immune-checkpoint inhibition with the observation of TIL activation and expansion.[168]

Another approach in creating a more realistic model of the TME in the context of CRC organoids is the co-culture with enteric nerve cells. The intestine possesses its own nervous system, the enteric nerve system (ENS), which is not only crucial for the digestive process but also functions as a regulator of intestinal epithelial stem cells and therefore possibly also has an impact on the development of neoplasia.[169] Westphalen et al. managed to co-culture nerve cells with intestinal organoids first.[170] After that, the study of Pastuła et al., who co-cultured cardiac organoids with enteric nerve cells suggested their impact on Wnt-signaling.[171] Dysregulation of this pathway leads to the development of intestinal cancer and therefore has to be taken into account when recapitulating organoid TME.

4.6.4 The route to application: thoughts on possible administration modalities

To date, the only OV approved by both FDA and EMA is T-VEC for the clinical treatment of unresectable, advanced melanoma (metastatic stage IIIB/C–IV M1a). Administration takes place intratumorally, aiming to trigger not only a local, but also a systemic anti-tumoral immune response.[172] This local administration is easily done in patients with melanoma, as the primary tumor is located externally on the skin. In the case of oncolytic melanoma therapy, the virus is administered repeatedly[173] and efficacy can also extend to satellite lesions which haven't been

injected with the virus.[174] But when thinking about the clinical applicability of OVs for treatment of CRCs, we don't have the luxury of an external application.

One possibility for a local application could be by endoscopic administration. As endoscopic equipment and techniques have massively improved in recent years with injection of e.g., hemostatic drugs even during critical bleeding events, an administration via a specific endoscopic application device seems feasible. When thinking of this approach, first and foremost safety considerations need to be addressed. Endoscopic equipment and application techniques need to be customized to prevent possible infectious events for health care stuff as well as patients. A phase I study by Chang et al. already explored this possibility by injecting T-VEC endoscopically into advanced pancreatic cancer, making use of an endoscopic ultrasound (EUS) as well.[175]

Another possible local application modality could be direct administration during surgery. In the context of our final goal of an individualized "virogram" this is only possible if a tumor sample is taken beforehand e.g. via endoscopic biopsy. The problem that becomes apparent here is whether the tumor sample taken is enough for culturing. Ganesh et al. were able to generate 65 rectal tumoroids from 58 patients in 83 derivation attempts (77 % success rate), i.e. using tissue obtained by endoscopic biopsy forceps.[176] Whether this is feasible with colon carcinomas as well has to be further investigated.

Finally, a systemic application modality via intravenous application is also tested in different tumor entities at the moment. Intravenous administration has several advantages: standardization of processes and drug dosage, simplified handling and better access.[173] This could possibly facilitate a more widespread approach and improve feasibility even in smaller clinics.

Unfortunately, when taking the systemic route, one is faced with problems like neutralizing antiviral antibodies[173,177–179] and other host mechanisms to evade viral infection. Several clinical trials regarding oncolytic virotherapy for colorectal cancer via IV application have been conducted in the past including phase I trials for Newcastle disease virus[173,180–182], reovirus[173,183–185], adenovirus[186] and vac-

cinia virus[173,187,188] as well as two phase II trials for CRC patients with liver metastasis, using hepatic artery infusion of the adenovirus *Onyx-015*[173,189,190]. This application route is still under investigation but could possibly present an option for OV administration in the future, especially in the context of CRC virotherapy.

5 Summary

As demographic change, especially in the western world, is marked by an ever-decreasing birth rate as well as an ever-growing life expectancy, our society becomes increasingly “old”. As a result, cancer incidence, one of them being colorectal cancer (CRC), increases and consequently becomes even more relevant for public health in the future. As we learn more about the molecular mechanisms behind cancer, we have to acknowledge that this disease has a rather heterogenous, even a very individual pathogenesis. Consequently, a “one size fits all”-approach regarding an effective therapy falls short.

To achieve this goal of personalized medicine, on the one hand, a representative as well as practical tumor cell model has to be employed. Organoids, especially patient derived tumor organoids (PDTOs) could be a promising tumor cell model as they harbor individual molecular properties of each patient and grow in a three-dimensional manner, in contrast to conventional cell models.

Furthermore, immunotherapy seems to be a promising approach for cancer therapy. This includes virotherapy, which makes use of the oncolytic properties of viruses, which are further enhanced through genetic engineering. These oncolytic viruses selectively infect neoplastic cells, replicate within them and finally destroy them. This destruction and subsequent release of cell components leads to an immunogenic systemic anti-tumor response. All of this is achieved while also sparing normal cells, which makes this therapy approach even more elegant.

The aim of this thesis was to utilize PDTOs as a novel tumor cell model to create individualized “virograms”, determining the best oncolytic virus for each patient and thus creating a personalized approach regarding clinical usage.

Firstly, it could be shown, that infection as well as replication of oncolytic viruses is possible in CRC-PDTOs. This has to date not been tested before and shows, that further experiments regarding oncolytic virotherapy for CRCs can be conducted using PDTOs in the future.

Furthermore, a personalized “virogram” for each PDTO was created, using a wide range of different oncolytic viruses. Interestingly, all PDTOs tested were most

susceptible to combination therapy of suicide-gene enhanced oncolytic viruses and the pro-drug 5-FC, showing significant viability reductions. Nonetheless, they also showed a heterogenous susceptibility regarding the other OVs. So in summary, PDTOs showed a difference in tumor cell viability reduction between different OVs but were still most susceptible when confronted with 5-FU.

When thinking about applying this in the clinical setting, more experiments regarding safety concerns, a more efficient culture approach as well as in vivo efficiency are needed. Nonetheless, taking all the aforementioned considerations into account, oncolytic virotherapy, especially when tested with the usage of PDTOs, seems to be a promising approach for cancer therapy in the future.

6 Zusammenfassung

Da der demografische Wandel, insbesondere in der westlichen Welt, durch eine immer niedrigere Geburtenrate und eine immer höhere Lebenserwartung gekennzeichnet ist, wird unsere Gesellschaft immer „älter“. Infolgedessen nimmt die Häufigkeit von Krebserkrankungen, darunter auch Darmkrebs, zu und wird somit in Zukunft noch entscheidender für die öffentliche Gesundheit. In dem Maße, wie wir mehr über die molekularen Mechanismen von Krebs erfahren, müssen wir anerkennen, dass diese Krankheit eine recht heterogene, ja sogar sehr individuelle Pathogenese aufweist. Folglich greift ein einheitlicher Ansatz für eine wirksame antitumorale Therapie zu kurz.

Um das Ziel einer personalisierten Onkologie zu erreichen, muss einerseits ein repräsentatives und andererseits ein praktikables Zellmodell verwendet werden. Organoide, insbesondere „patient derived tumor organoids“ (PDTOs), könnten ein vielversprechendes Zellmodell sein, da sie im Gegensatz zu konventionellen Zellmodellen individuelle molekulare Eigenschaften des jeweiligen Patienten aufweisen und dreidimensional wachsen können.

Außerdem scheint die Immuntherapie ein vielversprechender Ansatz für die Krebstherapie zu sein. Dazu gehört ebenso die Virotherapie, welche sich die onkolytischen Eigenschaften von Viren zunutze macht, die durch Genmodifikation noch zusätzlich verstärkt werden. Diese onkolytischen Viren infizieren selektiv neoplastische Zellen, vermehren sich in ihnen und lysieren sie schließlich. Diese Lyse und die daraus resultierende Freisetzung von Zellbestandteilen führt zu einer immunogenen systemischen Anti-Tumor-Reaktion. All dies geschieht unter Schonung der normalen Zellen, was diesen biologischen Therapieansatz noch eleganter macht.

Das Ziel dieser Arbeit war es, PDTOs als Zellmodell zu verwenden, um individualisierte „Virogramme“ zu erstellen, das effizienteste onkolytische Virus für jeden Patienten zu bestimmen und so einen personalisierten Ansatz für den klinischen Einsatz der Virotherapie zu schaffen.

Zunächst konnte gezeigt werden, dass sowohl die Infektion als auch die Replikation von onkolytischen Viren in CRC-PDTOs möglich ist. Dies wurde bisher noch

nicht getestet und zeigt, dass weitere Experimente zur onkolytischen Virotherapie für CRCs in Zukunft mit PDTOs durchgeführt werden können.

Darüber konnte für jedes PDTO ein personalisiertes „Virogram“ erstellen werden, indem eine große Auswahl an verschiedenen onkolytischen Viren zum Einsatz kam. Interessanterweise reagierten alle getesteten PDTOs am empfindlichsten auf eine Kombinationstherapie aus Suizidgen-verstärkten onkolytischen Viren und der Pro-Drug 5-FC und zeigten eine deutliche Verringerung des Zellüberlebens. Allerdings präsentierten sie auch eine heterogene Anfälligkeit gegenüber den anderen OVs.

Zusammenfassend lässt sich also sagen, dass PDTOs einen Unterschied in der Verringerung der Zellviabilität zwischen den verschiedenen OVs zeigten, aber immer noch am empfindlichsten waren, wenn sie nach intrazellulärer Konvertierung von 5-FC mit dem Chemotherapeutikum 5-FU konfrontiert wurden.

Für die klinische Anwendung sind weitere Experimente in Bezug auf Sicherheitsaspekte, einen effizienteren Kulturansatz und die in-vivo-Effizienz erforderlich. Nichtsdestotrotz scheint die onkolytische Virotherapie unter Berücksichtigung aller oben genannten Überlegungen ein vielversprechender Ansatz für die zukünftige Krebsforschung zu sein, insbesondere wenn sie mit PDTOs prä-interventionell getestet wird.

7 Appendix

7.1 Abbreviations

5-FC	5-fluorocytosine
5-FU	5-fluorouracil
5-FUMP	5-fluorouridine monophosphate
ACL	Anocutaneous line
alk	Activin like kinase
APC	Adenomatous polyposis coli
ASC	Adult stem cells
ATCC®	American Type Culture Collection
ATU	Additional transcription unit
BCO	Brain cortical organoids
BMP	Bone morphogenic protein
BRAF	Proto-oncogene B-Raf
CAF	Cancer associated fibroblast
CDX	Caudal-type homeobox 2
CIN	Chromosomal instability
CIMP	CpG-island methylator phenotype
CNS	Central nervous system
CRC	Colorectal Carcinoma
DC	Dendritic cell
DGC	Differentiated glioma cell
dMMR	Deficient mismatch repair system
DNA	Desoxyribonucleotide acid
ds	Double stranded
DSMZ	Deutsche Sammlung von Mikroorganismen und Zellkulturen
ECM	Extracellular matrix
EGF	Epidermal growth factor
eGFP	enhanced green fluorescent protein
EGFR	Epidermal growth factor receptor
EHS	Engelbreth-Holm Swarm tumor
ENS	Enteric nerve system

ESC	Embryonic stem cells
EUS	Endoscopic ultrasound
FAP	Familial Adenomatous Polyposis
fcu-1	Fusion suicide gene
FDA	Food and Drug Administration
GBM	Glioblastoma
GFP	Green fluorescent protein
GM-CSF	Granulocyte-Macrophage-Colony-Stimulating factor
GSC	Glioblastoma stem cell
gusA	β-glucuronidase (β-gluc)
HDI	High development index
HNPCC	Hereditary Non-Polyposis Colorectal Cancer
hpi	Hours post infection
hpt	Hours post treatment
HSV-1	Herpes simplex virus Type 1
ICI	Immune checkpoint inhibitor
IDS	International Documentation System
iPSC	Induced pluripotent stem cells
ISC	Intestinal stem cells
KRAS	Kirsten Rat sarcoma virus
lacZ	β-galactosidase (β-gal)
LIVP	Lister strain from the Institute for Research on Viral Preparations
LOH	Loss of heterozygosity
MeV	Measles virus
MLH1	MutL homolog 1
MMR	Mismatch repair system
MOI	Multiplicity of infection
MSH2/3/6	MutS homolog 2/3/6
MSI	Microsatellite instability
MSI-H	Microsatellite instability-high
MSI-L	Microsatellite instability-low

MSS	Microsatellite stable
NRAS	Neuroblastoma RAS viral oncogene homolog
OV	Oncolytic virus
PBS	Phosphate buffered saline
PDO	Patient-derived organoid
PDTO	Patient-derived tumor organoid
PDTX	Patient-derived tumor xenografts
PEG	Polyethylene glycole
PFU	Plaque forming unit
PMS2	Postmeiotic Segregation Increased 2
PSC	Pluripotent stem cell
P_{SEL}	Synthetic early/late promoter
$P_{7.5}$	Early/late promoter
P_{11}	Late promoter
P/S	Penicillin/streptomycin
ROCK	Rho-associated kinase
rtfr	Reverse human transferrin receptor
ruc-GFP	Renilla luciferase – Aequorea green fluorescent protein
SCD	Super cytosine deaminase
SD	Standard deviation
SGT	Suicide gene therapy
SOX	also: SRY; (sex determining region Y)-box 2
TIL	Tumor infiltrating lymphocytes
TME	Tumor microenvironment
T-VEC	Talimogene laherparepvec
turboFP635	far-red fluorescent protein turbo FP635
UICC	Union international contre le cancer
VACV	Vaccinia virus
WNT	Wnt signaling pathway
ZIKV	Zika virus

7.2 List of figures

7.3 List of Tables

7.4 List of Formulas

8 References

1. **World Health Organization (WHO)/Europe (2023)** Demographic change, life expectancy fact-Sheet, World Health Organisation, [online] https://www.euro.who.int/__data/assets/pdf_file/0019/185311/Demographic-change,-life-expectancy-Fact-Sheet-Ger.pdf [abgerufen am 03.01.2023]
2. **The Global Cancer observatory (2021)** Population fact sheet on cancer worldwide, Global Cancer Organisation, [online], https://gco.iarc.fr/today/data/factsheets/populations/900-world-fact-sheets.pdf [abgerufen am 03.01.2023]
3. **Stewart, B.W. & Wild, C.P. (2014)** World Cancer Report 2014, [online] https://publications.iarc.fr/Non-Series-Publications/World-Cancer-Reports/World-Cancer-Report-2014 [abgerufen am 03.01.2023]

4. **Deutsche Gesellschaft für Gastroenterologie, Verdauungs- und Stoffwechselkrankheiten (DGVS)** S3-Leitlinie Kolorektales Karzinom Langversion 2.1 - Januar 2019, verfügbar unter: https://register.awmf.org/assets/guidelines/021-007OLl_S3_Kolorektales-Karzinom-KRK_2019-01.pdf" [abgerufen am 28.02.2023]

5. **Fielding, L. P. *et al.*** Clinicopathological staging for colorectal cancer: An International Documentation System (IDS) and an International Comprehensive Anatomical Terminology (ICAT). *J Gastroenterol Hepatol* **6**, 325–344 (1991).

6. **UICC/Sobin, L. H., Gospodarowicz, M. K. & Wittekind, C.** TNM Classification of Malignant Tumours, Seventh Edition - 2009, verfügbar unter: http://www.inen.sld.pe/portal/documentos/pdf/educacion/13072015_TNM%20Classification.pdf [abgerufen am 25.05.2022]

7. **NIHS Consensus Conference** Adjuvant Therapy for Patients With Colon and Rectal Cancer. *JAMA* **264**, 1444 (1990).

8. **Sung, H. *et al.*** Global Cancer Statistics 2020: GLOBOCAN Estimates of Incidence and Mortality Worldwide for 36 Cancers in 185 Countries. *CA: A Cancer Journal for Clinicians* **71**, 209–249 (2021).

9. **Zentrum für Krebsregisterdaten - Robert Koch Institut** (2018) Krebs - Darmkrebs [online] https://www.krebsdaten.de/Krebs/DE/Content/Krebsarten/Darmkrebs/darmkrebs_node.html;jsessionid=95095A32543ECFD84A1CB68C8BCE2E18.internet061 [abgerufen am 22.05.2022]

10. **Bray, F. & Soerjomataram, I.** *The Changing Global Burden of Cancer: Transitions in Human Development and Implications for Cancer Prevention and Control*. *Cancer: Disease Control Priorities*, Gelband H, Jha P, Sankaranarayanan R, et al. (Hrsg.), third edition, volume 3. Washington, DC: World Bank (2015).

11. **Fidler, M. M., Soerjomataram, I. & Bray, F.** A global view on cancer incidence and national levels of the human development index. *International Journal of Cancer* **139**, 2436–2446 (2016).

12. **Zentrum für Krebsregisterdaten & Gesellschaft der epidemiologischen Krebsregister in Deutschland e.V.** (2023) Krebs in Deutschland für

2019/2020, Kapitel 3.6 Darm [online] https://www.krebsdaten.de/Krebs/DE/Content/Publikationen/Krebs_in_Deutschland/kid_2023/kid_2023_c18_c20_darm.pdf?__blob= publicationFile [abgerufen am 23.05.2023]

13. **Onkopedia** (2024) Kolonkarzinom [online] https://www.onkopedia.com/de/onkopedia/guidelines/kolonkarzinom/@@guideline/html/index.html [abgerufen am 23.02.2024]

14. **Fearon, E. R. & Vogelstein, B.** A genetic model for colorectal tumorigenesis. *Cell* **61**, 759–767 (1990).

15. **Vogelstein, B. *et al.*** Genetic Alterations during Colorectal-Tumor Development. *N Engl J Med* **319**, 525–532 (1988).

16. **Pancione, M., Remo, A. & Colantuoni, V.** Genetic and Epigenetic Events Generate Multiple Pathways in Colorectal Cancer Progression. *Pathology Research International* **2012**, 1–11 (2012).

17. **Remo, A., Pancione, M., Zanella, C. & Vendraminelli, R.** Molecular pathology of colorectal carcinoma. A systematic review centred on the new role of the pathologist. *Pathologica* **104**, 432–441 (2012).

18. **Goel, A. *et al.*** The CpG Island Methylator Phenotype and Chromosomal Instability Are Inversely Correlated in Sporadic Colorectal Cancer. *Gastroenterology* **132**, 127–138 (2007).

19. **Schmitt, M. & Greten, F. R.** The inflammatory pathogenesis of colorectal cancer. *Nat Rev Immunol* **21**, 653–667 (2021).

20. **De Palma, F. *et al.*** The Molecular Hallmarks of the Serrated Pathway in Colorectal Cancer. *Cancers* **11**, 1017 (2019).

21. **Pino, M. S. & Chung, D. C.** The Chromosomal Instability Pathway in Colon Cancer. *Gastroenterology* **138**, 2059–2072 (2010).

22. **Geigl, J. B., Obenauf, A. C., Schwarzbraun, T. & Speicher, M. R.** Defining ‘chromosomal instability’. *Trends in Genetics* **24**, 64–69 (2008).

23. **Boland, C. R. & Goel, A.** Microsatellite Instability in Colorectal Cancer. *Gastroenterology* **138**, 2073-2087.e3 (2010).

24. **Rowan, A. J. *et al.*** *APC* mutations in sporadic colorectal tumors: A mutational “hotspot” and interdependence of the “two hits”. *Proc. Natl. Acad. Sci. U.S.A.* **97**, 3352–3357 (2000).

25. **de’ Angelis, G. L. *et al.*** Microsatellite instability in colorectal cancer. *Acta Bio Medica Atenei Parmensis* **89**, 97–101 (2018).

26. **Jiricny, J.** The multifaceted mismatch-repair system. *Nature Reviews Molecular Call Biology* **7**, 335-346 (2006).

27. **Boland, C.R & Goel, A.** Microsatellite Instability in Colorectal Cancer. Gastroenterology **138**, 2073–2087 (2010)

28. **Hegde, M., Ferber, M., Mao, R., Samowitz, W. & Ganguly, A.** ACMG technical standards and guidelines for genetic testing for inherited colorectal can-

cer (Lynch syndrome, familial adenomatous polyposis, and MYH-associated polyposis). *Genetics in Medicine* **16**, 101–116 (2014).

29. **Lynch, H. T., Snyder, C. L., Shaw, T. G., Heinen, C. D. & Hitchins, M. P.** Milestones of Lynch syndrome: 1895–2015. *Nat Rev Cancer* **15**, 181–194 (2015).

30. **Bleijs, M., van de Wetering, M., Clevers, H. & Drost, J.** Xenograft and organoid model systems in cancer research. *EMBO J* **38**, e101654 (2019).

31. **Bruni, D., Angell, H. K. & Galon, J.** The immune contexture and Immunoscore in cancer prognosis and therapeutic efficacy. *Nat Rev Cancer* **20**, 662–680 (2020).

32. **Cirri, P. & Chiarugi, P.** Cancer associated fibroblasts: the dark side of the coin. *Am J Cancer Res* **1**, 482–497 (2011).

33. **Weber, C. E. & Kuo, P. C.** The tumor microenvironment. *Surgical Oncology* **21**, 172–177 (2012).

34. **Shiga, K. *et al.*** Cancer-Associated Fibroblasts: Their Characteristics and Their Roles in Tumor Growth. *Cancers (Basel)* **7**, 2443–2458 (2015).

35. **Yamamura, Y. *et al.*** Akt–Girdin Signaling in Cancer-Associated Fibroblasts Contributes to Tumor Progression. *Cancer Research* **75**, 813–823 (2015).

36. **Hanahan, D. & Weinberg, R. A.** Hallmarks of cancer: the next generation. *Cell* **144**, 646–674 (2011).

37. **Arneth, B.** Tumor Microenvironment. *Medicina (Kaunas)* **56**, 15 (2019).

38. **Demir, I. E., Friess, H. & Ceyhan, G. O.** Nerve-cancer interactions in the stromal biology of pancreatic cancer. *Front Physiol* **3**, 97 (2012).

39. **Zhao, C.-M. *et al.*** Denervation suppresses gastric tumorigenesis. *Sci Transl Med* **6**, 250ra115 (2014).

40. **Ayala, G. E. *et al.*** Cancer-related axonogenesis and neurogenesis in prostate cancer. *Clin Cancer Res* **14**, 7593–7603 (2008).

41. **Larsson, J. & Scadden, D.** Nervous activity in a stem cell niche. *Cell* **124**, 253–255 (2006).

42. **Dai, H. *et al.*** Enhanced survival in perineural invasion of pancreatic cancer: an in vitro approach. *Hum Pathol* **38**, 299–307 (2007).

43. **Westphalen, C. B. *et al.*** Long-lived intestinal tuft cells serve as colon cancer-initiating cells. *J Clin Invest* **124**, 1283–1295 (2014).

44. **Mancino, M., Ametller, E., Gascón, P. & Almendro, V.** The neuronal influence on tumor progression. *Biochim Biophys Acta* **1816**, 105–118 (2011).

45. **Karsa, L. von *et al.*** European guidelines for quality assurance in colorectal cancer screening and diagnosis: overview and introduction to the full supplement publication. *Endoscopy* **45**, 51–59 (2013).

46. **Ribic, C. M. *et al.*** Tumor Microsatellite-Instability Status as a Predictor of Benefit from Fluorouracil-Based Adjuvant Chemotherapy for Colon Cancer. *N Engl J Med* **349**, 247–257 (2003).

47. **Cunningham, D. *et al.*** Colorectal cancer. *The Lancet* **375**, 1030–1047 (2010).

48. **Karapetis, C. S. *et al.*** K-ras Mutations and Benefit from Cetuximab in Advanced Colorectal Cancer. *N Engl J Med* **359**, 1757–1765 (2008).

49. **Pietrantonio, F. *et al.*** Predictive role of BRAF mutations in patients with advanced colorectal cancer receiving cetuximab and panitumumab: A meta-analysis. *European Journal of Cancer* **51**, 587–594 (2015).

50. **Tran, B. *et al.*** Impact of BRAF Mutation and Microsatellite Instability on the Pattern of Metastatic Spread and Prognosis in Metastatic Colorectal Cancer. *Cancer* **117**, 4623–4632 (2011).

51. **Ganesh, K. *et al.*** Immunotherapy in colorectal cancer: rationale, challenges and potential. *Nat Rev Gastroenterol Hepatol* **16**, 361–375 (2019).

52. **Fukuhara, H., Ino, Y. & Todo, T.** Oncolytic virus therapy: A new era of cancer treatment at dawn. *Cancer Sci* **107**, 1373–1379 (2016).

53. **Ferrucci, P. F., Pala, L., Conforti, F. & Cocorocchio, E.** Talimogene Laherparepvec (T-VEC): An Intralesional Cancer Immunotherapy for Advanced Melanoma. *Cancers* **13**, 1383 (2021).

54. **Dummer, R. *et al.*** Neoadjuvant talimogene laherparepvec plus surgery versus surgery alone for resectable stage IIIB–IVM1a melanoma: a randomized, open-label, phase 2 trial. *Nat Med* **27**, 1789–1796 (2021).

55. **Lee, A.** Nadofaragene Firadenovec: First Approval. *Drugs* **83**, 353–357 (2023).

56. **Kelly, E. & Russel, S. J.** History of Oncolytic Viruses: Genesis to Genetic Engineering. *Molecular Therapy* **15**, 651–659 (2007).

57. **Dock, G.** The influence of complicating diseases upon leukaemia. *The American Journal of Medical Sciences* **127**, (1904).

58. **Levaditi, C. & Nicolau, S.** Affinite u virus de la peste aviare pour les cellules neoplastiques (epithelioma) de la souris. *CR Soc Biol* **202**, 218–222 (1936).

59. **De Pace, N. G.** Sulla scomparsa di un enorme cancro vegetante del callo dell'utero senza cura chirurgica. *Ginecologia* **9**, 82–88 (1912).

60. **Levaditi, C. & Nicolau, S.** Sur le culture du virus vaccinal dans les neoplasmes epithelieux. *CR Soc Biol* 928 (1922).

61. **Hoster, H., Zanes, R. J. & von Haam, E.** Studies in Hodgkin's syndrome; the association of viral hepatitis and Hodgkin's disease; a preliminary report. *Cancer Research* **9**, 473–80 (1949).

62. **Onuigbo, W. I. B.** Historical trends in cancer surgery. *Med. Hist.* **6**, 154–161 (1962).

63. **Southam, C. & Moore, A.** Clinical studies of viruses as antineoplastic agents with particular reference to Egypt 101 virus. *Cancer* **5**, 1025–1034 (1952).

64. **Georgiades, J., Zielinski, T., Cicholska, A. & Jordan, E.** Research on the oncolytic effect of APC viruses in cancer of the cervix uteri. *Biuletyn Instytutu Medycyny Morskiej w Gdańsku* **10**, 49–57 (1959).

65. **Asada, T.** Treatment of human cancer with mumps virus. *Cancer* **34**, 1907–1928 (1974).

66. **Moore, A. E.** Viruses with Oncolytic Properties and Their Adaptation to Tumors. *Annals of the New York Academy of Sciences* **54**, 945–952 (1952).

67. **Martuza, R. L., Malick, A., Markert, J. M., Ruffner, K. L. & Coen, D. M.** Experimental Therapy of Human Glioma by Means of a Genetically Engineered Virus Mutant. *Science* **252**, 854–856 (1991).

68. **Russell, S. J. & Peng, K.-W.** Viruses as anticancer drugs. *Trends in Pharmacological Sciences* **28**, 326–333 (2007).

69. **Engeland, C. E. & Bell, J. C.** Principles of Oncolytic Virotherapy: Exploiting Hallmarks of Cancer and Turning Cold Tumors Hot. *Oncolytic Viruses*. Engeland, C. E. (Hrsg.), volume 2058. Springer New York, New York (2020).

70. **Pikor, L. A., Bell, J. C. & Diallo, J.-S.** Oncolytic Viruses: Exploiting Cancer's Deal with the Devil. *Trends in Cancer* **1**, 266–277 (2015).

71. **Kaufman, H. L., Kohlhapp, F. J. & Zloza, A.** Oncolytic viruses: a new class of immunotherapy drugs. *Nat Rev Drug Discov* **14**, 642–662 (2015).

72. **Russell, S. J., Peng, K.-W. & Bell, J. C.** Oncolytic virotherapy. *Nat Biotechnol* **30**, 658–670 (2012).

73. **Hanahan, D. & Weinberg, R. A.** Hallmarks of Cancer: The Next Generation D. *Cell* **144**, 646–674 (2011).

74. **Chen, D. S. & Mellman, I.** Elements of cancer immunity and the cancer–immune set point. *Nature* **541**, 321–330 (2017).

75. **Gajewski, T. F. *et al.*** Cancer immunotherapy strategies based on overcoming barriers within the tumor microenvironment. *Current Opinion in Immunology* **25**, 268–276 (2013).

76. **Gajewski, T. F.** The Next Hurdle in Cancer Immunotherapy: Overcoming the Non–T-Cell–Inflamed Tumor Microenvironment. *Seminars in Oncology* **42**, 663–671 (2015).

77. **Hegde, P. S., Karanikas, V. & Evers, S.** The Where, the When, and the How of Immune Monitoring for Cancer Immunotherapies in the Era of Checkpoint Inhibition. *Clinical Cancer Research* **22**, 1865–1874 (2016).

78. **Joyce, J. & Fearon, D.** T cell exclusion, immune privilege, and the tumor microenvironment. *Science* **348**, 74–80 (2015).

79. **Salmon, H. *et al.*** Matrix architecture defines the preferential localization and migration of T cells into the stroma of human lung tumors. *J. Clin. Invest.* **122**, 899–910 (2012).

80. **Russel, S. J. & Barber, G. N.** Oncolytic Viruses as Antigen-Agnostic Cancer Vaccines. *Cancer Cell* **33**, 599–605 (2018).

81. **Guo, Z. S. *et al.*** Oncolytic Immunotherapy: Conceptual Evolution, Current Strategies, and Future Perspectives. *Front. Immunol.* **8**, 555 (2017).

82. **Düzgünes, N.** Origins of Suicide Gene Therapy. *Suicide Gene Therapy: Methods and Protocols*. Düzgünes, N. (Hrsg.) volume 1895. Springer New York,

New York (2019).

83. **Moolten, F.** Tumor chemosensitivity conferred by inserted herpes thymidine kinase genes: paradigm for a prospective cancer control strategy. *Cancer Research* **46**, 5276–5281 (1986).

84. **Erbs, P. *et al.*** In vivo cancer gene therapy by adenovirus-mediated transfer of a bifunctional yeast cytosine deaminase/uracil phosphoribosyltransferase fusion gene. *Cancer Research* **60**, 3813–3822 (2000).

85. **Gross, S.** Biological Safety: Replication control of virotherapeutic vectors through cytostatics. (Eberhard Karls Universität Tübingen, Tübingen, 2018).

86. **Austin, E. A. & Huber, B. E.** A first step in the development of gene therapy for colorectal carcinoma: cloning, sequencing, and expression of Escherichia coli cytosine deaminase. *Mol Pharmacol* **43**, 380–387 (1993).

87. **Engeland, C. E. & Ungerechts, G.** Measles Virus as an Oncolytic Immunotherapy. (2021).

88. **Moss, W. J.** Measles. *The Lancet* **390**, 2490–2502 (2017).

89. **Guseva, S., Milles, S., Blackledge, M. & Ruigrok, R. W. H.** The Nucleoprotein and Phosphoprotein of Measles Virus. *Front. Microbiol.* **10**, 1832 (2019).

90. **Tolonen, N., Doglio, L., Schleich, S. & Locker, J. K.** Vaccinia Virus DNA Replication Occurs in Endoplasmic Reticulum-enclosed Cytoplasmic Mini-Nuclei. *MBoC* **12**, 2031–2046 (2001).

91. **Harrison, S. C. *et al.*** Discovery of antivirals against smallpox. *Proc Natl Acad Sci U S A* **101**, 11178–11192 (2004).

92. **Henderson, D. A. & Moss, B.** Smallpox and Vaccinia. *Vaccines. 3rd edition* Plotkin S. A. & Orenstein, W. A. (Hrsg.) volume 3. Saunders (1999).

93. **Carter, M. E. *et al.*** A Three-Dimensional Organoid Model of Primary Breast Cancer to Investigate the Effects of Oncolytic Virotherapy. *Frontiers in Molecular Biosciences* **9**, (2022).

94. **Wiedenmann, J. *et al.*** A far-red fluorescent protein with fast maturation and reduced oligomerization tendency from Entacmaea quadricolor (Anthozoa, Actinaria). *Proc Natl Acad Sci U S A* **99**, 11646–11651 (2002).

95. **Zhang, Q. *et al.*** The highly attenuated oncolytic recombinant vaccinia virus GLV-1h68: comparative genomic features and the contribution of F14.5L inactivation. *Mol Genet Genomics* **282**, 417–435 (2009).

96. **Zhang, Q. *et al.*** Eradication of Solid Human Breast Tumors in Nude Mice with an Intravenously Injected Light-Emitting Oncolytic Vaccinia Virus. *Cancer Research* **67**, 10038–10046 (2007).

97. **Berchtold, S. *et al.*** Assessing and Overcoming Resistance Phenomena against a Genetically Modified Vaccinia Virus in Selected Cancer Cell Lines. *IJMS* **21**, 7618 (2020).

98. **Kelly, K. J. *et al.*** Novel Oncolytic Agent GLV-1h68 Is Effective Against Malignant Pleural Mesothelioma. *Hum Gene Ther* **19**, 774–782 (2008).

99. **Zhang, Q. *et al.*** Eradication of Solid Human Breast Tumors in Nude Mice

with an Intravenously Injected Light-Emitting Oncolytic Vaccinia Virus. *Cancer Res* **67**, 10038–10046 (2007).

100. **Ahmad, I. & Wilson, D. W.** HSV-1 Cytoplasmic Envelopment and Egress. *IJMS* **21**, 5969 (2020).

101. **Liu, B. L. *et al.*** ICP34.5 deleted herpes simplex virus with enhanced oncolytic, immune stimulating, and anti-tumour properties. *Gene Ther* **10**, 292–303 (2003).

102. **Bommareddy, P. K., Patel, A., Hossain, S. & Kaufman, H. L.** Talimogene Laherparepvec (T-VEC) and Other Oncolytic Viruses for the Treatment of Melanoma. *Am J Clin Dermatol* **18**, 1–15 (2017).

103. **Andtbacka, R. H. *et al.*** Final planned overall survival (OS) from OPTiM, a randomized Phase III trial of talimogene laherparepvec (T-VEC) versus GM-CSF for the treatment of unresected stage IIIB/C/IV melanoma (NCT00769704). *Journal for ImmunoTherapy of Cancer* **2**, P263 (2014).

104. **Wilson, H. V.** A New Method by Which Sponges May Be Artificially Reared. *Science* **25**, 912–915 (1907).

105. **Smith, E. & Cochrane, W. J.** Cystic Organoid Teratoma. *Can Med Assoc J* **55**, 151–152 (1946).

106. **Dutta, D., Heo, I. & Clevers, H.** Disease Modeling in Stem Cell-Derived 3D Organoid Systems. *Trends in Molecular Medicine* **23**, 393–410 (2017).

107. **Clevers, H.** Modeling Development and Disease with Organoids. *Cell* **165**, 1586–1597 (2016).

108. **Lancaster, M. A. & Knoblich, J. A.** Organogenesis in a dish: Modeling development and disease using organoid technologies. *Science* **345**, 1247125 (2014).

109. **Steinberg, M. S.** The Problem of Adhesive Selectivity in Cellular Interactions. *Academic Press* 321–366 (1964).

110. **Rossi, G., Manfrin, A. & Lutolf, M. P.** Progress and potential in organoid research. *Nat Rev Genet* **19**, 671–687 (2018).

111. **Barcellos-Hoff, M. H., Aggeler, J., Ram, T. G. & Bissell, M. J.** Functional differentiation and alveolar morphogenesis of primary mammary cultures on reconstituted basement membrane. *Development* **105**, 223–235 (1989).

112. **Sato, T. *et al.*** Single Lgr5 stem cells build crypt-villus structures in vitro without a mesenchymal niche. *Nature* **459**, 262–265 (2009).

113. **Corrò, C., Novellasdemunt, L. & Li, V. S. W.** A brief history of organoids. *Am J Physiol Cell Physiol* **319**, C151–C165 (2020).

114. **Dedhia, P. H., Bertaux-Skeirik, N., Zavros, Y. & Spence, J. R.** Organoid Models of Human Gastrointestinal Development and Disease. *Gastroenterology* **150**, 1098–1112 (2016).

115. **Artegiani, B. & Clevers, H.** Use and application of 3D-organoid technology. *Human Molecular Genetics* **27**, R99–R107 (2018).

116. **Kleinman, H. K. & Martin, G. R.** Matrigel: Basement membrane matrix

with biological activity. *Seminars in Cancer Biology* **15**, 378–386 (2005).

117. **Sugimoto, S. & Sato, T.** Establishment of 3D Intestinal Organoid Cultures from Intestinal Stem Cells. *3D Cell Culture: Methods and Protocols*. Koledova, Z. (Hrsg.) volume 1612, Springer New York, New York, (2017).

118. **Sato, T. *et al.*** Long-term Expansion of Epithelial Organoids From Human Colon, Adenoma, Adenocarcinoma, and Barrett's Epithelium. *Gastroenterology* **141**, 1762–1772 (2011).

119. **Haramis, A.-P. G. *et al.*** De Novo Crypt Formation and Juvenile Polyposis on BMP Inhibition in Mouse Intestine. *Science* **303**, 1684–1686 (2004).

120. **Sato, T. *et al.*** Paneth cells constitute the niche for Lgr5 stem cells in intestinal crypts. *Nature* **469**, 415–418 (2011).

121. **Watanabe, K. *et al.*** A ROCK inhibitor permits survival of dissociated human embryonic stem cells. *Nat Biotechnol* **25**, 681–686 (2007).

122. **Del Bufalo, F. *et al.*** 3D modeling of human cancer: A PEG-fibrin hydrogel system to study the role of tumor microenvironment and recapitulate the in vivo effect of oncolytic adenovirus. *Biomaterials* **84**, 76–85 (2016).

123. **Zhu, Z. *et al.*** Zika virus has oncolytic activity against glioblastoma stem cells. *J Exp Med* **214**, 2843–2857 (2017).

124. **Zhu, Z. *et al.*** Zika Virus Targets Glioblastoma Stem Cells through a SOX2-Integrin αvβ5 Axis. *Cell Stem Cell* **26**, 187-204.e10 (2020).

125. **Ferreira, R. O. *et al.*** Effect of Serial Systemic and Intratumoral Injections of Oncolytic ZIKVBR in Mice Bearing Embryonal CNS Tumors. *Viruses* **13**, 2103 (2021).

126. **Fiorini, E. & Corbo, V.** Oncolytic virotherapy meets the human organoid technology for pancreatic cancers. *EBioMedicine* **57**, 102828 (2020).

127. **Rangsitratkul, C. *et al.*** Intravesical immunotherapy with a GM-CSF armed oncolytic vesicular stomatitis virus improves outcome in bladder cancer. *Mol Ther Oncolytics* **24**, 507–521 (2022).

128. **Hamdan, F. *et al.*** Novel oncolytic adenovirus expressing enhanced cross-hybrid IgGA Fc PD-L1 inhibitor activates multiple immune effector populations leading to enhanced tumor killing in vitro, in vivo and with patient-derived tumor organoids. *J Immunother Cancer* **9**, e003000 (2021).

129. **Harryvan, T. J. *et al.*** Gastrointestinal cancer-associated fibroblasts expressing Junctional Adhesion Molecule-A are amenable to infection by oncolytic reovirus. *Cancer Gene Ther* **29**, 1918–1929 (2022).

130. **Scheubeck, G. *et al.*** Starvation-Induced Differential Virotherapy Using an Oncolytic Measles Vaccine Virus. *Viruses* **11**, 614 (2019).

131. **Berchtold, S. *et al.*** Innate immune defense defines susceptibility of sarcoma cells to measles vaccine virus-based oncolysis. *J Virol* **87**, 3484–3501 (2013).

132. **Dias *et al.*** Targeted Delivery of FCU1 Suicide Gene to Tumor Cells by Oncolytic Adenovirus. *Molecular Therapy* **17**, S224 (2009)**.**

133. **Zhang, C. *et al.*** A recombinant Chinese measles virus vaccine strain rMV-Hu191 inhibits human colorectal cancer growth through inducing autophagy and apoptosis regulating by PI3K/AKT pathway. *Transl Oncol* **14**, 101091 (2021).

134. **Wang, N. *et al.*** A novel vaccinia virus enhances anti-tumor efficacy and promotes a long-term anti-tumor response in a murine model of colorectal cancer. *Mol Ther Oncolytics* **20**, 71–81 (2021).

135. **Ottolino-Perry, K. *et al.*** Oncolytic vaccinia virus synergizes with irinotecan in colorectal cancer. *Mol Oncol* **9**, 1539–1552 (2015).

136. **Eveno, C. *et al.*** Gene Therapy Using Therapeutic and Diagnostic Recombinant Oncolytic Vaccinia Virus GLV-1h153 for Management of Colorectal Peritoneal Carcinomatosis. *Surgery* **157**, 331–337 (2015).

137. **Yin, L. *et al.*** Antitumor effects of oncolytic herpes simplex virus type 2 against colorectal cancer in vitro and in vivo. *Ther Clin Risk Manag* **13**, 117–130 (2017).

138. **Reinblatt, M., Pin, R. H. & Fong, Y.** Carcinoembryonic antigen directed herpes viral oncolysis improves selectivity and activity in colorectal cancer. *Surgery* **136**, 579–584 (2004).

139. **Shayan, S. *et al.*** Cell type-specific response of colon cancer tumor cell lines to oncolytic HSV-1 virotherapy in hypoxia. *Cancer Cell Int* **22**, 164 (2022).

140. **Zhang, N. *et al.*** Construction of an IL12 and CXCL11 armed oncolytic herpes simplex virus using the CRISPR/Cas9 system for colon cancer treatment. *Virus Res* **323**, 198979 (2022).

141. **Kuroda, T., Rabkin, S. D. & Martuza, R. L.** Effective treatment of tumors with strong beta-catenin/T-cell factor activity by transcriptionally targeted oncolytic herpes simplex virus vector. *Cancer Res* **66**, 10127–10135 (2006).

142. **Zhang, W. *et al.*** Inhibition of colorectal cancer liver metastasis in BALB/c mice following intratumoral injection of oncolytic herpes simplex virus type 2 for the induction of specific antitumor immunity. *Oncol Lett* **17**, 815–822 (2019).

143. **Sato-Dahlman, M. *et al.*** CD133-targeted oncolytic adenovirus demonstrates anti-tumor effect in colorectal cancer. *Oncotarget* **8**, 76044–76056 (2017).

144. **Song, H., Zhong, L.-P., He, J., Huang, Y. & Zhao, Y.-X.** Application of Newcastle disease virus in the treatment of colorectal cancer. *World J Clin Cases* **7**, 2143–2154 (2019).

145. **Wang, B. *et al.*** A Novel Combination Therapy for Human Oxaliplatin-resistant Colorectal Cancer Using Oxaliplatin and Coxsackievirus A11. *Anticancer Res* **38**, 6121–6126 (2018).

146. **Liu, Z. *et al.*** Establishment and biological characteristics of oxaliplatin-resistant human colon cancer cell lines. *Chin J Cancer* **29**, 661–667 (2010).

147. **Usui, T. *et al.*** Establishment of a Novel Model for Anticancer Drug Resistance in Three-Dimensional Primary Culture of Tumor Microenvironment. *Stem Cells Int* **2016**, 7053872 (2016).

148. **Hu, J. C. C. *et al.*** A phase I study of OncoVEXGM-CSF, a second-generation oncolytic herpes simplex virus expressing granulocyte macrophage colony-

stimulating factor. *Clin Cancer Res* **12**, 6737–6747 (2006).

149. **Scherer, W. F., Syverton, J. T. and Gey, G. O.** Viral multiplication in a stable strain of human malignant epithelial cells (Strain HeLa) derived from an epidermoid carcinoma of the cervix. *The Journal of experimental medicine* **97**, 695-710 (1953).

150. **Masters, J. R. W.** Human cancer cell lines: fact and fantasy. *Nat Rev Mol Cell Biol* **1**, 233–236 (2000).

151. **Kretzschmar, K.** Cancer research using organoid technology. *J Mol Med* **99**, 501–515 (2021).

152. **Junttila, M. R. & de Sauvage, F. J.** Influence of tumour micro-environment heterogeneity on therapeutic response. *Nature* **501**, 346–354 (2013).

153. **Cheon, D.-J. & Orsulic, S.** Mouse models of cancer. *Annu Rev Pathol* **6**, 95–119 (2011).

154. **Tuveson, D. & Clevers, H.** Cancer modeling meets human organoid technology. *Science* **364**, 952–955 (2019).

155. **Drost, J. & Clevers, H.** Organoids in cancer research. *Nat Rev Cancer* **18**, 407–418 (2018).

156. **Kemper, K. *et al.*** Intra- and inter-tumor heterogeneity in a vemurafenib-resistant melanoma patient and derived xenografts. *EMBO Mol Med* **7**, 1104–1118 (2015).

157. **Bleijs, M., Wetering, M., Clevers, H. & Drost, J.** Xenograft and organoid model systems in cancer research. *EMBO J* **38**, (2019).

158. **Morgan, K. M., Riedlinger, G. M., Rosenfeld, J., Ganesan, S. & Pine, S. R.** Patient-Derived Xenograft Models of Non-Small Cell Lung Cancer and Their Potential Utility in Personalized Medicine. *Front Oncol* **7**, 2 (2017).

159. **Julien, S. *et al.*** Characterization of a large panel of patient-derived tumor xenografts representing the clinical heterogeneity of human colorectal cancer. *Clin Cancer Res* **18**, 5314–5328 (2012).

160. **Peng, S. *et al.*** Tumor grafts derived from patients with head and neck squamous carcinoma authentically maintain the molecular and histologic characteristics of human cancers. *J Transl Med* **11**, 198 (2013).

161. **Roerink, S. F. *et al.*** Intra-tumour diversification in colorectal cancer at the single-cell level. *Nature* **556**, 457–462 (2018).

162. **Kloker, L. D., Yurttas, C. & Lauer, U. M.** Three-dimensional tumor cell cultures employed in virotherapy research. *Oncolytic Virother* **7**, 79–93 (2018).

163. **Sato, T. *et al.*** Long-term expansion of epithelial organoids from human colon, adenoma, adenocarcinoma, and Barrett's epithelium. *Gastroenterology* **141**, 1762–1772 (2011).

164. **van de Wetering, M. *et al.*** Prospective derivation of a living organoid biobank of colorectal cancer patients. *Cell* **161**, 933–945 (2015).

165. **Marinucci, M. *et al.*** Standardizing Patient-Derived Organoid Generation Workflow to Avoid Microbial Contamination From Colorectal Cancer Tissues.

Front Oncol **11**, 781833 (2021).

166. **Luo, X. *et al.*** Hydrogel-based colorectal cancer organoid co-culture models. *Acta Biomater* **132**, 461–472 (2021).

167. **Naruse, M. *et al.*** Re-expression of REG family and DUOXs genes in CRC organoids by co-culturing with CAFs. *Sci Rep* **11**, 2077 (2021).

168. **Neal, J. T. *et al.*** Organoid Modeling of the Tumor Immune Microenvironment. *Cell* **175**, 1972-1988.e16 (2018).

169. **Demir, I. E., Friess, H. & Ceyhan, G. O.** Nerve-cancer interactions in the stromal biology of pancreatic cancer. *Front Physiol* **3**, 97 (2012).

170. **Westphalen, C. B. *et al.*** Long-lived intestinal tuft cells serve as colon cancer-initiating cells. *J Clin Invest* **124**, 1283–1295 (2014).

171. **Pastuła, A. *et al.*** Three-Dimensional Gastrointestinal Organoid Culture in Combination with Nerves or Fibroblasts: A Method to Characterize the Gastrointestinal Stem Cell Niche. *Stem Cells Int* **2016**, 3710836 (2016).

172. **Ferrucci, P. F., Pala, L., Conforti, F. & Cocorocchio, E.** Talimogene Laherparepvec (T-VEC): An Intralesional Cancer Immunotherapy for Advanced Melanoma. *Cancers* **13**, (2021).

173. **Cook, M. & Chauhan, A.** Clinical Application of Oncolytic Viruses: A Systematic Review. *IJMS* **21**, 7505 (2020).

174. **Rh, A. *et al.*** Cutaneous head and neck melanoma in OPTiM, a randomized phase 3 trial of talimogene laherparepvec versus granulocyte-macrophage colony-stimulating factor for the treatment of unresected stage IIIB/IIIC/IV melanoma. *Head & neck* **38**, (2016).

175. **Chang, K., Senzer, N., Binmoeller, K., Goldsweig, H. & Coffin, R.** Phase I dose-escalation study of talimogene laherparepvec (T-VEC) for advanced pancreatic cancer (ca). *Journal of Clinical Oncology* **30**, e14546–e14546 (2012).

176. **Ganesh, K. *et al.*** A rectal cancer organoid platform to study individual responses to chemoradiation. *Nat Med* **25**, 1607–1614 (2019).

177. **C, H. & R, C.** Achieving systemic delivery of oncolytic viruses. *Expert opinion on drug delivery* **16**, (2019).

178. **Breitbach, C. J. *et al.*** Intravenous delivery of a multi-mechanistic cancer-targeted oncolytic poxvirus in humans. *Nature* **477**, 99–102 (2011).

179. **Fisher, K. D. *et al.*** Polymer-coated adenovirus permits efficient retargeting and evades neutralising antibodies. *Gene Ther* **8**, 341–348 (2001).

180. **Laurie, S. A. *et al.*** A phase 1 clinical study of intravenous administration of PV701, an oncolytic virus, using two-step desensitization. *Clin Cancer Res* **12**, 2555–2562 (2006).

181. **Hotte, S. J. *et al.*** An optimized clinical regimen for the oncolytic virus PV701. *Clin Cancer Res* **13**, 977–985 (2007).

182. **Pecora, A. L. *et al.*** Phase I trial of intravenous administration of PV701, an oncolytic virus, in patients with advanced solid cancers. *J Clin Oncol* **20**, 2251–

2266 (2002).

183. **Vidal, L. *et al.*** A phase I study of intravenous oncolytic reovirus type 3 Dearing in patients with advanced cancer. *Clin Cancer Res* **14**, 7127–7137 (2008).

184. **Lolkema, M. P. *et al.*** A phase I study of the combination of intravenous reovirus type 3 Dearing and gemcitabine in patients with advanced cancer. *Clin Cancer Res* **17**, 581–588 (2011).

185. **Comins, C. *et al.*** REO-10: a phase I study of intravenous reovirus and docetaxel in patients with advanced cancer. *Clin Cancer Res* **16**, 5564–5572 (2010).

186. **Garcia-Carbonero, R. *et al.*** Phase 1 study of intravenous administration of the chimeric adenovirus enadenotucirev in patients undergoing primary tumor resection. *J Immunother Cancer* **5**, 71 (2017).

187. **Downs-Canner, S. *et al.*** Phase 1 Study of Intravenous Oncolytic Poxvirus (vvDD) in Patients With Advanced Solid Cancers. *Mol Ther* **24**, 1492–1501 (2016).

188. **Park, S. H. *et al.*** Phase 1b Trial of Biweekly Intravenous Pexa-Vec (JX-594), an Oncolytic and Immunotherapeutic Vaccinia Virus in Colorectal Cancer. *Mol Ther* **23**, 1532–1540 (2015).

189. **Reid, T. R., Freeman, S., Post, L., McCormick, F. & Sze, D. Y.** Effects of Onyx-015 among metastatic colorectal cancer patients that have failed prior treatment with 5-FU/leucovorin. *Cancer Gene Ther* **12**, 673–681 (2005).

190. **Reid, T. *et al.*** Hepatic arterial infusion of a replication-selective oncolytic adenovirus (dl1520): phase II viral, immunologic, and clinical endpoints. *Cancer Res* **62**, 6070–6079 (2002).

9 Erklärung zum Eigenanteil

Die Arbeit wurde in der Medizinischen Universitätsklinik, Abteilung für Innere Medizin VIII, in der Arbeitsgruppe „Virotherapie“ unter Betreuung von Herrn Prof. Dr. med. Ulrich M. Lauer durchgeführt.

Die Konzeption der Studie erfolgte in Zusammenarbeit mit Herrn Prof. Dr. Ulrich M. Lauer (Leiter der Forschungsgruppe “Virotherapie”) und Frau Dr. med. Susanne Berchtold (Laborleiterin).

Sämtliche Versuche wurden von mir eigenständig durchgeführt (nach Einarbeitung durch die Labormitarbeiterinnen Frau Dr. med. Susanne Berchtold und Frau Irina Smirnow (MTA))

Ich versichere, meine Promotionsarbeit selbstständig (nach Anleitung durch Frau Dr. S. Berchtold und Prof. U.M. Lauer) verfasst und keine weiteren, als die von mir angegebenen Quellen, verwendet zu haben.

Stuttgart, den 31.08.2024 _____

(Franziska von Schimonsky)

10 Acknowledgement

Nach dieser wissenschaftlichen Arbeit bin ich (natürlich neben dem Zugewinn an fachlichem Wissen) zumindest zu einer entscheidenden Erkenntnis gekommen: ohne die lieben Menschen in meinem Leben und in diesem Labor wäre diese Arbeit nicht möglich gewesen.

Als erstes möchte ich meinem Doktorvater, Prof. Dr. Ulrich M. Lauer, danken. Zuallererst dafür, dass er mir dieses Thema überlassen und mir das Vertrauen geschenkt hat, diese Arbeit zu verfassen. Und zum anderen für die Möglichkeit, in die wissenschaftliche Arbeit einzutauchen und es mit einem wundervollen Team zu erleben. Die persönliche Betreuung sowie die stetigen Hilfestellungen waren essenziell zum Gelingen dieser Arbeit.

Ganz besonderen Dank gilt meiner Betreuerin Dr. med. Susanne Berchtold, an die ich mich jederzeit wenden konnte und die meine Arbeit mit sehr viel Geduld und Durchhaltevermögen begleitet hat. Mit einer großen Menge Humor, Witz und Engagement hat sie gemeinsam mit mir diesen Weg beschritten, der sicher nicht immer ein einfacher war. Hierfür werde ich für immer dankbar sein.

Frau Irina Smirnow und Frau Andrea Schenk, den Herzen und Seelen dieses Labors, möchte ich ebenso ganz besonders danken. Sie haben mir die Arbeit mit Zellen nähergebracht und mit viel Geduld meine Missgeschicke und Fehler hingenommen. Ihre herzliche und liebe Art hat mich direkt als Teil des Teams zugehörig fühlen lassen, was mir meine Zeit im Labor sehr versüßt hat.

Natürlich wäre dieser Abschnitt nicht der gleiche gewesen ohne Herrn Dr. Markus Burkard, Herrn Prof. Dr. Dr. Sascha Venturelli und Herrn Dipl. Biochem. Christian Leischner. Sie haben mich immer wieder ermuntert, mich nicht allzu ernst zu nehmen und mir sowohl bei wissenschaftlichen als auch nicht-wissenschaftlichen Fragestellungen jederzeit geholfen.

Selbstverständlich möchte ich mich auch bei meinen Mit-Doktoranden bedanken, die mir nicht nur beistanden, sondern auch mit mir litten, feierten und tanzten. Vielen Dank an Stavros Sotiriadis, Joschka Gottesleben, Sebastian Gräter sowie Linus Kloker.

Bei Frau Prof. Dr. med. Knipper und allen weiteren Beteiligten des IZKF Promotionskollegs bedanke ich mich für das Engagement, die Motivation und Inspiration.

Neben dem Dank der Personen auf wissenschaftlicher Seite möchte ich nun zum Schluss den Personen meines persönlichen Umfelds danken. Eine Doktorarbeit ist nicht nur eine fachliche Anstrengung, sondern ganz besonders auch eine persönliche Herausforderung, gespickt von Zweifeln, Überforderung und Versagensängsten. Um dies alles bewältigen zu können, bedarf es ganz außerordentlicher Menschen. Ich möchte deswegen besonders meinen Eltern, Gisela und Lothar von Schimonsky, danken. Sie waren meine stetige Motivation und mein Antrieb, mein Rückhalt und meine Kraft. Ihre Unterstützung hat mich diese Arbeit und dieses Studium meistern lassen und ich werde Ihnen für immer für das Geschenk Ihrer Liebe dankbar sein.

Wenn ich an die Personen denke, die mich am meisten unterstützt und mir den Rücken gestärkt haben, dann darf meine beste Freundin, Carmen Tina Schablitzki, nicht fehlen. Ihre Freundschaft hat mir durch manche dunkle Stunde geholfen; ohne sie wäre meine Zeit in Tübingen nicht dieselbe gewesen. Ihre Unterstützung sowie ihr emotionaler Beistand waren mir einer der größten Stützen während meines Studiums und der Zeit der Doktorarbeit und ich wüsste nicht, wo ich heute ohne sie wäre.

Und zu guter Letzt möchte ich auch meinem Verlobten Dominik Vorholt danken, der die letzten Meter meiner Dissertation begleitet (und vorangetrieben) hat. Dank seiner Hilfe und seiner Ermutigungen konnte ich schlussendlich diese Arbeit beenden. Nun dürfen wir uns endlich beide „Doktor“ nennen!

Alles in allem: Ich danke Euch!